INFORMATION TO USERS

This material was produced from a microfilm copy of the original document. While the most advanced technological means to photograph and reproduce this document have been used, the quality is heavily dependent upon the quality of the original submitted.

The following explanation of techniques is provided to help you understand markings or patterns which may appear on this reproduction.

1. The sign or "target" for pages apparently lacking from the document photographed is "Missing Page(s)". If it was possible to obtain the missing page(s) or section, they are spliced into the film along with adjacent pages. This may have necessitated cutting thru an image and duplicating adjacent pages to insure you complete continuity.

2. When an image on the film is obliterated with a large round black mark, it is an indication that the photographer suspected that the copy may have moved during exposure and thus cause a blurred image. You will find a good image of the page in the adjacent frame.

3. When a map, drawing or chart, etc., was part of the material being photographed the photographer followed a definite method in "sectioning" the material. It is customary to begin photoing at the upper left hand corner of a large sheet and to continue photoing from left to right in equal sections with a small overlap. If necessary, sectioning is continued again – beginning below the first row and continuing on until complete.

4. The majority of users indicate that the textual content is of greatest value, however, a somewhat higher quality reproduction could be made from "photographs" if essential to the understanding of the dissertation. Silver prints of "photographs" may be ordered at additional charge by writing the Order Department, giving the catalog number, title, author and specific pages you wish reproduced.

5. PLEASE NOTE: Some pages may have indistinct print. Filmed as received.

University Microfilms International
300 North Zeeb Road
Ann Arbor, Michigan 48106 USA
St. John's Road, Tyler's Green
High Wycombe, Bucks, England HP10 8HR

77-12,757

RAMANATHAN, Nagaswamy, 1938-
A STUDY OF THERMAL INSTABILITY IN AN
ATMOSPHERE WITH ZONAL FLOW AND ROTATION.

The University of Oklahoma, Ph.D., 1976
Physics, atmospheric science

Name also appears as Ramanathan R. Nagaswamy.

Xerox University Microfilms, Ann Arbor, Michigan 48106

THE UNIVERSITY OF OKLAHOMA

GRADUATE COLLEGE

A STUDY OF THERMAL INSTABILITY IN AN ATMOSPHERE WITH ZONAL FLOW AND ROTATION

A DISSERTATION

SUBMITTED TO THE GRADUATE FACULTY

in partial fulfillment of the requirements for the

degree of

DOCTOR OF PHILOSOPHY

BY

NAGASWAMY RAMANATHAN

Norman, Oklahoma

1976

A STUDY OF THERMAL INSTABILITY IN AN ATMOSPHERE

WITH ZONAL FLOW AND ROTATION

APPROVED BY

J. L. Inman

S. B. Eliason

M. Rasmussen

Ray B. Arms

DISSERTATION COMMITTEE

ABSTRACT

In this study the problem of instability of a parallel flow with thermal convection as a primary mechanism in the formation of organized cloud patterns is considered. Viscous and Coriolis effects are included. The basic flow is taken to be antisymmetric and to possess curvature. This antisymmetric profile is chosen to correspond to a baroclinic Ekman profile and the shear in the basic flow decreases with height. The characteristics of the developed unstable modes are determined in terms of the properties of the basic state and the wave numbers of the superimposed three-dimensional perturbations. The hydrodynamic boundary conditions correspond to that of a free upper surface with a rigid lower boundary. The thermal boundary conditions are constant temperature and constant heat-flux at both boundaries. Linearized Boussinesq equations are used, and a finite-difference technique is employed to obtain solutions. The Coriolis influence on the developed modes is found to have a slightly destabilizing nature for small wave-lengths. At moderate and low shears the structures of the modes show a super-position of transverse-like and longitudinal-like modes. The modes travel with a speed greater than that of the basic flow averaged over the entire depth; they appear

to be a combination of stationary and low speed transitive type perturbations similar to those found in investigations of Couette flow. The preferred wavelength at high shears is of the order of 5-6 km. The influence of shear is found to be stabilizing irrespective of the nature of its distribution in the convective layer. The constant heat flux hypothesis may not be very suitable in atmospheric investigations with a zonal flow; its effect on the modes is stabilizing in nature.

ACKNOWLEDGEMENTS

The author wishes to express his deep gratitude to Dr. Rex L. Inman without whose patient help, guidance and encouragement this dissertation would never have been completed. Gratitude is also extended to Dr. M. L. Rasmussen, Dr. E. M. Wilkins, Dr. S. B. Eliason and Dr. J. S. Fein for their valuable suggestions and encouragement.

The author wishes to record his appreciation to Ms. Jo Ann Oberst for her excellent typing of this dissertation. Last but not least, thanks must go to my wife, Usha, for helping in every possible way.

TABLE OF CONTENTS

LIST OF TABLES

LIST OF FIGURES

NOMENCLATURE

C_p	Specific heat at constant pressure
C_r	Phase speed of the developed mode
D, D^2	$\frac{d}{dz}$, $\frac{d^2}{dz^2}$ nondimensional derivatives with respect to height
$\frac{d}{dt}$	Eulerian derivative $(\frac{\partial}{\partial t} + \vec{V}\cdot\vec{\nabla})$
f	Coriolis parameter
F	Dimensionless Coriolis parameter
g	Acceleration due to gravity
H	Dimensional depth of the convective layer
K_M	Coefficient of eddy viscosity
K_H	Coefficient of eddy conductivity
k	Nondimensional horizontal wave number $(= k_x^2 + k_y^2)$
k_x	Nondimensional wave number of the perturbation in the x direction
k_y	Nondimensional wave number of the perturbation in the y direction
n	Number of intervals used in finite-difference formulation
$\bar{P}$	Basic state pressure
p'	Perturbation pressure
Pr	Prandtl number
Q	Absolute temperature
R	Gas constant for dry air
Ra	Rayleigh number
Re	Reynolds number
Ri	Richardson number

$\bar{T}$	Basic state potential temperature
T_o	Potential temperature at the lower boundary
T^*	Imposed potential temperature difference between the two boundaries
T'	Perturbation potential temperature
$\bar{u},\bar{v},\bar{w}$	Basic state velocity in the x, y, and z directions, respectively
U_*	Free stream velocity - maximum velocity of the flow at the free boundary
u',v',w'	Perturbation velocities in the x, y, and z directions, respectively
U,V,W,Z,θ	Perturbation amplification factors for velocities, vorticity and potential temperature, respectively
$\vec{V}$	Three-dimensional velocity vector for the basic state
$\vec{X}$	Eigenvector of the perturbation variables
x,y,z	Cartesian coordinates in tangent plane
α	Coefficient of thermal expansion $(= \frac{1}{T_o})$
β	The difference of the environmental and dry adiabatic lapse rates
γ	Environmental lapse rate of temperature
Λ	Environmental lapse rate of potential temperature
Γ_d	Dry adiabatic lapse rate
$\varkappa$	R/C_p
∇	Del operator $(\vec{i}\frac{\partial}{\partial x} + \vec{j}\frac{\partial}{\partial y} + \vec{k}\frac{\partial}{\partial z})$
∇_H^2	Horizontal Laplacian operator $(\frac{\partial^2}{\partial x^2} + \frac{\partial^2}{\partial y^2})$
∇^2	Three dimensional Laplacian operator $(\nabla_H^2 + \frac{\partial^2}{\partial z^2})$
ρ_o	Mean density in the basic state at T_o
ρ'	Perturbation density
σ	Nondimensional complex wave frequency

σ_r	Nondimensional amplification rate of the perturbation
ζ	Perturbation vorticity
$\vec{\Omega}$	Angular velocity of earth

A STUDY OF THERMAL INSTABILITY IN AN ATMOSPHERE WITH ZONAL FLOW AND ROTATION

CHAPTER I

OUTLINE OF THE PRESENT STUDY AND OBJECTIVES

This study is concerned with the formation of organized convection in the planetary boundary layer (PBL) when a mean flow is present. This type of convection is important since the heat and momentum transfer through the atmospheric boundary layer can be strongly influenced by it. It is known that circulations may develop in stratified fluids because of buoyancy forces that arise through heating of the lower layers or cooling of upper layers. Under certain conditions the convection is organized into distinct cellular patterns known as Benard cells. Jefferys (1928) has suggested that the effect of a shearing current is to arrange these cells, which occur in initially motionless liquids, in bands oriented in the direction of the shear. In the atmosphere cellular clouds as well as cloud bands are observed; the cloud bands usually occur in flows with strong shear. Generally they are capped by an inversion layer. The resemblance between observed cloud

patterns and patterns produced in laboratory experiments, particularly in the presence of turbulence, has been questioned by Batchelor (1954). However, investigations show that linear wind shear and/or gradient of shear favor convective streeting. Thus, it is clear that the growth and maintenance of these organized patterns depends mainly on the basic flow, i.e., upon energy exchanges with the basic flow. Hence, it is necessary to specify a basic flow having lateral or vertical variations, since an invariant basic current cannot interact or exchange energy with imposed perturbations.

The PBL can be considered to be approximately the lower 1-2 km of the atmosphere. In the free atmosphere above, the basic flow is controlled by the pressure-gradient and Coriolis forces. Hence many of the developments in the free atmosphere can be studied by considering only the above two forces coupled with the vertical and/or the lateral variations of the basic flow. However, in the PBL created by the earth's surface, viscous effects are not negligible. They are dominant in the surface layer (<100m); in the Ekman layer, which covers the rest of the PBL, the flow is controlled by pressure, Coriolis, and viscous forces.

Thus, it is clear that in a study of the formation of organized convection in the PBL, viscous effects are to be considered in addition to a varying basic flow. Since organized cloud patterns generally appear when thermal strati-

fication is unstable, it is necessary to specify the temperature distribution at the outset. Realistic rolls are found to arise because of inviscid instability associated with the point of inflexion in the lateral component of the Ekman flow. However, for simplicity we consider the basic flow in the PBL to be vertical variant in the x-z plane. Boundary layer flows can be defined as flows which monotonically increase or decrease through the boundary layer. These can be approximated by plane parallel flow for the purpose of instability studies (Rosenhead, 1963, Chapter 9). Thus, as a first approximation we choose the basic flow to be a plane parallel flow. This effectively restricts the PBL to a layer of constant height.

The neglect of the meridional flow in the basic state may appear to be too stringent a condition. However, the inclusion of $\bar{v}$ in the basic state will only alter the shear direction. Riehl's (1965) observations indicate that, "The direction of the cloud streets usually lies along the direction of the shear of the wind." Based on this, some investigations have included $\bar{v}$ in the basic equations. This study is not concerned with the orientation of cloud bands with respect to the basic flow. The inclusion of $\bar{v}$ in the basic state can be done in this study by utilizing a polynomial approximation for $\bar{v}$ similar to that adopted for the zonal component of the Ekman profile. However, the usefulness of such a study may be highly restrictive since elegant

studies using the full Ekman profile exist in the literature. We are guided by a summary of the conclusions reached by Kuettener (1971); "convective cloud bands in the earth's atmosphere tend to form in strong flows heated from below with curved velocity profile of rather uniform direction." That is, the shear direction can be uniform. Thus, a study with plane parallel flow in the basic state is appropriate.

As this study is confined to parallel basic state flows only, i.e., only flow along the x-axis, the principal controlling factors in our study are shear and/or shear gradient, buoyancy, and viscosity. Thus, the instabilities that can arise in the present study are (1) thermal instability due to gravitational forces, (2) shear and/or shear gradient instabilities, and (3) the instability of parallel flows in which viscosity plays a role. These roughly correspond to the physically possible instabilities in the PBL. The Coriolis force, in general, is a stabilizing influence and its effect is to elongate the cells in the direction of rotation (Chandrasekar, 1953). We have included the Coriolis force even though the effect may be quite small.

The instabilities may be controlled by any one of the mechanisms mentioned above, individually, or by a combination or interaction under suitable circumstances. Such possibilities are commonly known and have been given attention in the field of meteorology, e.g., baroclinic-barotropic

combined shear. By such interaction the existing instabilities either may be modified or suppressed or an entirely new type of instability may arise. The interaction between the thermal mode of instability and the viscous instability which appears in high shear flows has been studied in the case of unstably stratified plane Poiseuille flow (Gage and Reid, 1968).

Basic flows possessing constant shear have been studied by Kuo (1963), Deardorff (1965), Gallagher and Mercer (1965), Asai (1964, 1970a), and Lipps (1971). Kuttener (1959) argued that Couette flows are unrealistic representations of flows in the atmosphere; he attributed the formation of cloud bands to curved velocity profiles with uniform wind direction. Basic flows with curvature (shear gradient) have been studied by Gage and Reid (1968), Asai (1970b), and Kuttener (1971). The above investigations have shown that variable shear flows, variable or constant, exert an inhibiting influence on thermal instability. However, the above investigations were either too complex or solutions were obtained that may not apply to the real atmospheric convection process, such as motionless atmosphere, etc. A simple investigation which takes into account both the variations of the shear and the shear gradient in the convective layer has not been attempted. By including the Coriolis force, the momentum, energy and vorticity equations are coupled and this

facilitates the inclusion of shear and shear gradient simultaneously into the system of equations solved. This investigation adopts this approach.

In this study the basic state velocity profile is taken to be a cubic polynomial, approximated from a baroclinic Ekman profile. No unique mathematical formulation has been derived to describe the wind flow in an unstable baroclinic boundary-layer, due to the difficulty of defining the boundary layer thickness. An assumption of an infinitely deep boundary layer would be physically unrealistic; hence, in this study the boundary-layer thickness is taken to be a constant defined by the height of the inversion layer which caps off the organized convection. In the deduced basic flow profile the essential features are retained; namely, the shear decreases with height, having its maximum at the ground as observed in the atmosphere. Moreover, the vorticity gradient is a function of height and is negative throughout the convective layer. Thus, the profile differs from those considered in previous investigations and appears to be in better agreement with observations. Fig. 1 shows the velocity profile (a) in the PBL which is taken to be 1 km in depth in this investigation. Barotropic (b), baroclinic (c) Ekman profiles together with a profile of constant shear flow (d) are also shown in Fig. 1 for comparison. The insert diagram shows an observed profile in the atmosphere associated with a cloud street formation (Kuttener, 1971).

The vorticity profile is given in Fig. 2. It is clear from the figures that the cubical profile is in better agreement with observations than a simple Couette flow. Hence, study of the stability of organized convection with the deduced profile and with realistic boundary conditions as defined later, is considered appropriate.

The initial potential temperature distribution is specified by $\bar{T} = T_o - \Lambda Z$, where T_o is the potential temperature at $z = 0$, the rigid lower boundary. The lapse rate, Λ, is assumed to be constant and numerical values are chosen such that the system is in a gravitationally unstable configuration.

It is known from observations that the cloud bands occur primarily over land areas in contrast to cellular patterns which are observed mostly over oceans. The reason for such preferential formation, apart from increased frictional effects due to the nature of the surface topography, seems to be connected with heat-transfer properties of bounding surfaces. Hence, attention to heat transfer at the bounding surfaces (known as thermal boundary conditions) is called for, since through these surfaces heat exchange takes place to and from the convective layer. Sparrow et al. (1964), have shown that the effect of constant transport of heat energy (constant heat flux) through the boundaries is to allow convection to occur at weaker gravitational instability. However, that study is restricted to initially motionless liquids. The controlling influence

of constant heat flux boundary conditions on the growth of perturbations in a flowing medium has not been explored.

Thus, the objectives of this investigation are, (1) to study the stability of thermal modes under the combined influence of shear/shear gradient and viscosity with rotation, (2) to determine the influence of constant heat flux boundary conditions on the stability of the organized convection, and (3) to study the possible interactions between the various mechanisms involved.

The present study, which uses the same mathematical formulation as Asai (1970), differs from his investigations in the sense that the zonal current has a decreasing vertical shear with height; also, a different set of thermal, hydrodynamic boundary conditions are specified. Even though the scale of circulations considered is very small, Coriolis effects are included so as to facilitate the introduction of shear directly into the system of relevant equations given in Chapter III. Particular attention is given to the stability of modes with constant heat flux boundary conditions. The hydrodynamic boundary conditions are taken to satisfy no slip at the lower boundary with a free surface at the top. As mentioned earlier, with these specifications, we can expect qualitative and quantitative changes in the stability characteristics of the modes allowed by the system. The nature of these unstable modes can be ascertained by studying the structure of the perturbation

variables in a vertical plane (x-z plane) parallel to the basic flow.

In this linear study the perturbation technique is used to linearize the governing equations and, assuming the perturbations are periodic in the zonal and meridional directions, the problem is reduced to an eigenvalue problem. Solutions are obtained by the finite difference method.

In this chapter, an outline of this study, with the objectives, is given. A resume of the different assumptions and simplifications made in this study is given in Chapter II. The description of the physical model, the formulation of the zonal profile, and the hydrodynamic and the thermal boundary conditions are given in Chapter III, Sections 3.1, 3.2 and 3.3, respectively. Section 3.4 is devoted to the mathematical formulation of the model. The designation of the experimental parameters and a discussion of the validity of the assumptions adopted in this study is given in Chapter IV. In Chapter V a recapitulation of the physics of this model is given. In the remaining subsections the results are discussed. The summary and conclusions reached in this study are given in Chapter VI.

CHAPTER II

LIMITATIONS OF THE STUDY

In this study the circumstances under which organized convection occurs in the PBL are examined in terms of the stability properties of the flow in the region. Suitable approximations and assumptions are made to keep the study simple and more manageable; however, essential features are retained. At appropriate places, particularly in the discussion of the choice of parameters, the significance of the assumptions is given. They are summarized here for convenience.

1. The thickness or depth of the PBL is specified a priori and is controlled by the height of the inversion layer which caps off convection. Variations in the height of the convective layer, due to uniform subsidence or lifting of the inversion base, are neglected.
2. The present model incorporates no effects of diabatic heating (e.g., release of latent heat) which might obscure the interpretation of the results.
3. When a mean wind is present there will be some turbulence before the onset of convection. The atmospheric

boundary layer contains various kinds of eddies and in general simultaneously exhibits both turbulent and laminar characteristics in varying degrees (Sutton, 1953). New perturbations are created by various thermal processes and the effect of the earth's topography. Their effect on thermal convection may be represented by replacing the molecular values by eddy viscosity values in the governing equations. Thus eddy values of the coefficient of viscosity and thermal conductivity are used.

4. Variations of eddy coefficients with respect to space and time are neglected. Thus, finer distinctions characterizing the nature of open or closed cells are neglected.

5. The earth's topography has been neglected for simplicity, since terrain features may introduce horizontal temperature gradients. Thus, in this study we are concerned only with thermal convection arising from unstable stratification over a larger uniform surface without specific horizontal anomalies.

6. Although unstable lapse rates occur diurnally these are transient in the sense that they are not maintained lapse rates and once convection has occurred the instability is removed. This instability is more of the Rayleigh-Taylor type, resulting in a field of plumes rather than the Rayleigh-Bernard type treated here (Krishnamurti, 1973). Hence, variation in lapse rate or variation in surface temperature due to diurnal heating has been neglected in this study.

7. Lateral variations of the basic current $(\frac{\partial \bar{u}}{\partial y})$ are neglected. This may not lead to a serious error as barotropic instabilities are mainly confined to very large wavelengths. In the Ekman layer the lateral variations are represented by the y-component of the flow. In this study we are confining ourselves to parallel flows with vertical variations only.

8. The perturbations remain infinitesmal throughout the study and interact only with the basic flow; thus non-linear effects are neglected. Because of mathematical simplifications due to linearization, the critical conditions of instability for small disturbances are readily obtained. The validity of the process of linearization for hydrodynamic stability studies has been well established (Lin, 1955).

9. Variations of density except when coupled with gravity are neglected. By the Boussinesq approximation compressible waves such as sound waves, which are of no meteorological significance, are filtered out.

10. Since no analytical techniques are available a numerical approach has been undertaken to obtain solutions, with the disadvantage that they may not be unique. In fact, many solutions can be obtained by a simple choice of the controlling parameters.

The above simplifications might appear excessive. However, in constructing a simple model we are left with the choice of judicious selection of crucial parameters. For

instance, an incompressible model can give realistic results in the study of many atmospheric phenomena even though the atmosphere is not incompressible.

CHAPTER III

PHYSICAL DESCRIPTION OF THE MODEL AND THE MATHEMATICAL FORMULATION

3.1. Physical Description

The configuration of the system is shown in Fig. 3. As is customary in the study of convection, it is assumed that the convective layer is bounded by two horizontal, flat surfaces separated by a distance H. The lower plate is assumed to be rigid and is taken to represent the earth's surface. The upper surface is chosen to coincide with the base of an inversion layer. Since variations with respect to height due to uniform subsidence or lifting have been neglected the inversion alyer can be considered to be stationary with respect to the convective layer below.

In the basic state the fluid in the convective layer is assumed to move with a velocity $\bar{u}$ along the x-direction; i.e., $\bar{u} = \bar{u}(z)$; $\bar{v} = 0$; $\bar{w} = 0$. Thus, in the basic state only vertical variations are considered. Such a time independent steady current always can be obtained from observations when the data are averaged over a suitable period of time. By neglecting all variations in the meridional (y) direction

we essentially consider a unidirectional flow in the basic state. The reason for this has already been discussed in Chapter I.

Empirical Deduction of the Velocity Profile

Now we discuss an empirical deduction of the basic state velocity profile assumed for this study. The mechanism of maintenance of such a profile in the atmosphere is not given. Two possibilities are available to choose the basic state profile: (a) use observed data, or (b) guess a profile that is close to the observations. The use of the observed profiles may not be suitable in idealized studies because in the atmosphere the precise nature of the controlling variables is not known. Moreover, the use of such profiles may mar the whole study or may create some irresolvable difficulties in the interpretation of the results. Hence, we choose the second alternative. Such use of guess profiles are common in stability studies. For example, observations indicate that cloud bands appear with curved velocity profiles. Hence, jet-shaped, parabolic profiles have been chosen for the basic state in previous investigations. As already mentioned, the growth of these disturbances is primarily controlled by the basic flow in the PBL. Hence, we choose the Ekman profile since this profile previously has been found to yield realistic results. It is necessary to note that, in the Ekman layer, the shear is

concentrated mainly in the lower portions of the layer and decreases with height. The Ekman profile is strictly valid only above the surface layer; i.e., at heights greater than 50 m. However, the error involved, in considering the phenomena we are interested in, is probably not significant.

Since in this study the lateral variation of the basic current has been neglected for simplicity, the relevant component is the x-component of the Ekman profile. For a baroclinic geostrophic wind this is given by $\bar{u} = u_g(1-e^{-az}\cos az) + B_1 z$, where a and B_1 are constants; a depends on latitude. Expanding e^{-az} and cos az, noting that these are bounded functions, and neglecting terms of higher order than the third power, we obtain

$$\bar{u} = u_g(az - \frac{a^3 z^3}{2}) + B_1 z \ .$$

Then our guess corresponding to this is a cubical expression for $\bar{u}$; thus $\bar{u} = u_*(Ax^3 + Bx + C)$ where A, B, and C are constants, $x = \frac{z}{H}$, and u_* is a characteristic velocity defined in Fig. 3. We take the bottom of the inversion layer to correspond to the top of the boundary layer; since the presence of a stable layer is not essential in this study we consider the developments in the convective layer itself. To determine A, B, and C we apply the boundary conditions $\bar{u} = 0$ at $z = 0$ or $x = 0$ (rigid boundary); this yields $C = 0$. Also, the condition $\bar{u} = u_*$ at $z = H$ or $x = 1$, gives

$$A + B = 1 \ . \qquad (1)$$

We now apply the condition $\frac{d\bar{u}}{dx} = 0$ at $z = H$ or $x = 1$. This condition represents continuity of the tangent at the boundary, so as to have no viscous stresses at the boundary. This is essentially the dynamic boundary condition. Applying this condition we obtain

$$3A + B = 0 \ . \tag{2}$$

From (1) and (2) we get $A = -\frac{1}{2}$, $B = \frac{3}{2}$. Thus our profile reduces to

$$\bar{u} = u_*(\frac{3}{2} x - \frac{1}{2} x^3) \ . \tag{3}$$

Neglecting the cubical term, we arrive at the profile for Couette flow. This profile satisfies all the required conditions and may be considered as a slight generalization of Couette flow. It is necessary to note that we have used a baroclinic Ekman profile for our guess. However, we do not propose any mechanism for the maintenance of the basic profile in the atmosphere. With this cubical profile to represent the basic state we investigate the problem.

The initial thermal stratification already has been specified as $\bar{T} = T_o - \Lambda Z$. In the basic state, the pressure gradient which balances the gravitational force may be written as

$$\frac{\partial \bar{P}}{\partial z} = - g \rho_0[1 - \alpha(\bar{T} - T_o)]$$

where ρ_o is the density of the medium at z, α is the coefficient of thermal expansion, and $\bar{P}$ is the pressure in the

basic state. The hydrodynamic and thermal boundary conditions are given in Sections 3.2 and 3.3. The relevant mathematical formulation appears in Section 3.4.

3.2. Hydrodynamic Boundary Conditions

Studies of this type differ in the nature of bounding surfaces, e.g., smooth, rigid, etc. Jeffreys (1928) has shown that critical values for the onset of stationary convection are a function of the boundary conditions. Furthermore, he has recommended that at least one of the boundaries should be free and the other rigid, to be more realistic in atmospheric studies. In this study the lower boundary is taken to be rigid and coincides with the earth's surface. By this specification no slip occurs, and all the velocity components, including perturbation quantities, vanish.

The base of the inversion layer which forms the upper boundary in this investigation is taken to be that of a 'free' surface; i.e., tangential viscous stresses vanish. However, this specification is not unique. It has been considered to act as a rigid lid to permit the build up of convective activity in most studies. The inversion layer either does not permit the development or acts as a damper until it is penetrated and 'explosive' development takes place (Dirks, 1969). The base of the inversion layer has been treated as an open boundary in some studies (Barnes, 1967). In recent studies (Krishnamurti, 1973) it has been treated as a 'porous' boundary and 'free' boundary conditions

have been used. The assumption of symmetrical (free or rigid) hydrodynamical boundary conditions at both surfaces does not appear to correspond to any realistic physical situation in the atmosphere. Thus, the dynamical boundary conditions chosen for this study are:

1. rigid lower boundary (no slip),
2. free upper boundary (slip occurs).

3.3. Thermal Boundary Conditions

These depend on whether or not the boundaries are conducting, insulated, or allow constant heat-flux. The assumption of insulating surfaces on either one of the boundaries is not realistic since the inversion layer gets destabilized in the course of time, and the earth's surface is neither a good conductor nor a perfect insulator. Furthermore this assumption would alter the temperature of the insulated surface drastically. As in free convection, the temperature and velocity distributions are interdependent; a change in surface temperature would alter the existing lapse rate and modify the velocity distribution in the convective layer. Since such alterations are not desirable in this study the assumption of insulated surfaces need not be considered.

Perfectly conducting surfaces maintained at constant temperatures have been considered in previous studies. With these boundary conditions temperature perturbations vanish at both surfaces. Thus, the assumption of fixed surface

temperature would mean they are in contact or they have infinite thermal conductivity and heat capacity. As the inversion base (upper boundary) is not insulated, there will be heat exchange on either side of the boundary. Because the heat-transfer coefficients are finite, the boundary temperature will not remain constant during the convection process. In fact, inversion base warming by radiation is known to occur and is an indicator of the existing lapse rate (Haltiner and Martin, 1957, p. 129). Since the earth's surface also is not a perfect conductor and the lapse rate is assumed to be a constant, the assumption of a fixed surface temperature is not realistic.

Because of the reasons stated above the assumption of constant heat-flux on both surfaces would be closer to physical reality. Thus, the thermal boundary condition may be stated as: constant heat-flux at both boundaries, irrespective of the convective perturbation temperature. Sparrow et al. (1964) have shown that the system is rendered more gravitationally unstable with this condition. The relevant equations together with a summary of the application of the boundary conditions are given in the next section.

3.4. Mathematical Formulation

The vector equation of motion, the mass continuity equation and the heat-conduction equation pertinent to the

problem at hand can be written as:

$$\rho \frac{d\vec{V}}{dt} = - \vec{\nabla} p - g \rho \vec{k} + K_M \rho(\nabla \cdot \nabla)\vec{V} - \rho \ (2\vec{\Omega} \times \vec{V}) \ , \tag{4a}$$

$$\frac{d\rho}{dt} = - \rho \vec{\nabla} \cdot \vec{V} \ , \tag{4b}$$

$$\frac{dQ}{dt} = K_H \nabla^2 Q \ . \tag{4c}$$

Where $\frac{d}{dt} = \frac{\partial}{\partial t} + \vec{V} \cdot \vec{\nabla}$ and $\vec{V}$ is the three-dimensional velocity vector. Also, in the above equations ρ denotes the density, p the pressure, Q the temperature, and K_M and K_H are the coefficients of eddy viscosity and eddy conductivity, respectively. The molecular coefficients of viscosity and conductivity are neglected in comparison with their eddy counterparts which are also considered isotropic constants. The remaining symbols carry their usual meaning and the nomenclature of the various symbols is given at the beginning. The Coriolis term is included and the horizontal accelerations arising from the centrifugal force ($\Omega^2 R$ terms) are combined with the gravitational acceleration.

The vector equation of motion is general enough to permit all kinds of motions from very short acoustic waves to planetary scale Rossby waves. Thus, it is necessary to simplify the above equations relevant to the phenomena considered. In this investigation, very short acoustic waves and other three-dimensional compressible waves are of no direct concern and may be considered as noise. We eliminate

these waves by applying the Boussinesq approximation. Thus, considering the variations of density due to thermal expansion only insofar as they affect buoyant forces, we can replace ρ which occurs with g in the above equations by:

$$\rho = \rho_o(1 - \alpha \Delta T) \ , \tag{5}$$

where α is the coefficient of thermal expansion, ρ is the density corresponding to a mean potential temperature T and ΔT is the deviation of potential temperature from T_o, i.e., $\Delta T = T - T_o$. Treating ρ elsewhere in the equations as a constant equal to ρ_o, we can rewrite the vector equation of motion as:

$$\frac{d\vec{V}}{dt} = -\frac{1}{\rho_o}\vec{\nabla} p - g(1 - \alpha \Delta T)\ \vec{k} + K_M(\nabla\cdot\nabla)\vec{V} - (2\vec{\Omega} \times \vec{V}) \tag{6}$$

and the mass continuity equation reduces to:

$$\vec{\nabla}\cdot\vec{V} = 0 \ . \tag{7}$$

With the tangent plane approximation the equations of motion in cartesian coordinates can be written as:

$$\frac{du}{dt} - fv = -\frac{1}{\rho_o}\frac{\partial p}{\partial x} + K_M \nabla^2 u \ , \tag{8a}$$

$$\frac{dv}{dt} + fu = -\frac{1}{\rho_o}\frac{\partial p}{\partial y} + K_M \nabla^2 v \ , \tag{8b}$$

$$\frac{dw}{dt} = -\frac{1}{\rho_o}\frac{\partial p}{\partial z} - g(1 - \alpha \Delta T) + K_M \nabla^2 w. \tag{8c}$$

The continuity and energy equation in cartesian coordinates can be written as:

$$\frac{\partial u}{\partial x} + \frac{\partial v}{\partial y} + \frac{\partial w}{\partial z} = 0 \ , \tag{8d}$$

$$\frac{dT}{dt} = K_H \nabla^2 T \ . \tag{8e}$$

where $\frac{d}{dt} = \frac{\partial}{\partial t} + u \frac{\partial}{\partial x} + v \frac{\partial}{\partial y} + w \frac{\partial}{\partial z}$, $\nabla^2 = \frac{\partial^2}{\partial x^2} + \frac{\partial^2}{\partial y^2} + \frac{\partial^2}{\partial z^2}$

and u, v, and w are the velocities in the x, y, and z directions, respectively. The above nonlinear system of equations apply to the basic state and the perturbations.

The basic state variables for the PBL ($z \leq 1$ km) can be written as

$$\bar{u} = U_*\{\frac{3}{2}\frac{z}{H} - \frac{1}{2}(\frac{z}{H})^3\} \qquad (0 \leq z \leq H)$$

$$\bar{v} = 0$$

$$\bar{w} = 0$$

$$\bar{T} = T_o - \Lambda z \qquad (0 \leq z \leq H)$$

$$\bar{P} = \bar{P}\ (x,y,z)$$

$$\bar{\rho} = \rho_o(z)\ (1 - \alpha(\bar{T} - T_o))$$

$$T^* = \Lambda H$$

where the symbols are defined in the summary of the nomenclature utilized. The symbol T represents potential temperature and Λ is the environmental lapse rate of potential temperature. If Λ were zero the boundary layer would be in an adiabatic state corresponding to an isothermal state in liquids.

From the above definitions we obtain $\frac{\partial}{\partial y}, \frac{\partial}{\partial x}\ (\bar{u},\bar{v},\bar{w},\bar{T}) = 0$ $\frac{\partial \bar{u}}{\partial z} \neq 0$, $\frac{\partial^2 \bar{u}}{\partial z^2} \neq 0$, $\frac{\partial \bar{T}}{\partial z} = -\Lambda$, and $\frac{\partial^2 \bar{T}}{\partial z^2} = 0$. The processes which establish a uniform heating of the lower surface so as to

eliminate horizontal inhomogenities in potential temperature and maintain a linear temperature profile in the convective layer (PBL) are not modelled here.

The relation between absolute temperature Q and potential temperature T can be written as

$$Q = T \left(\frac{p}{1000}\right)^{\varkappa}$$

where $\varkappa = R/C_p = 0.286$, R is the gas constant for dry air, and C_p is the specific heat at constant pressure. By differentiating the above relation we obtain

$$\frac{dT}{dz} = \frac{T}{Q}\left\{\frac{\partial Q}{\partial z} + \Gamma_d\right\} .$$

The difference between T and Q is very small at least up to 1 km in the atmosphere, the region of interest in this study. Thus, for practical purposes $\bar{T} = \bar{Q}$. Without any great loss in accuracy we obtain $\Lambda \cong (\gamma - \Gamma_d)$, where γ is the environmental lapse rate of absolute temperature and Γ_d is the dry adiabatic lapse rate. Similarly, since $\frac{\partial \bar{T}}{\partial x} = \frac{\partial \bar{T}}{\partial y} = 0$ because of uniform heating of the surface we can write without any great loss in accuracy $\frac{\partial \bar{Q}}{\partial x} = \frac{\partial \bar{Q}}{\partial y} = 0$. That is $\bar{Q} = \bar{Q}(z)$ only. The density variations along the x and y directions $(\frac{\partial \bar{\rho}}{\partial x}, \frac{\partial \bar{\rho}}{\partial y})$ can be calculated using $\bar{P} = \bar{\rho} R \bar{Q}$ and the equations of motion for the basic state which specifies the variations of $\bar{P}$ along the three space directions. The equations of motion can be written as

$$-\frac{1}{\rho_o}\frac{\partial \bar{p}}{\partial x} + K_M \frac{d^2\bar{u}}{dz^2} = 0 , \qquad (9a)$$

$$-\frac{1}{\rho_o}\frac{\partial \bar{p}}{\partial y} - f\bar{u} = 0 , \qquad (9b)$$

$$\frac{\partial \bar{p}}{\partial z} = -g\,\rho_o(1 - \alpha(\bar{T} - T_o)) . \qquad (9c)$$

Using appropriate values for the constants

($K_M = 10^5$ cm^2/sec, $U_* = 10^3$ cm/sec, $H = 10^5$ cm

$\frac{\partial^2 \bar{u}}{dz^2} = 3 \times 10^{-10}$ cm^{-1} sec^{-1}, $\rho_o = 10^{-3}$ gm/cm^3

$\bar{Q} = 300^oK$, $R = 2.86 \times 10^6$ erg gm^{-1} $^oK^{-1}$) ,

we can obtain from the above equations

$$\frac{\partial \bar{p}}{\partial x} \sim 10^{-14} \text{ gm cm}^{-4}, \text{ and } \frac{\partial \bar{p}}{\partial y} \sim 10^{-13} \text{ gm cm}^{-4} .$$

These are negligible compared with the absolute variation of density along the vertical which is of the order of 10^{-10}. However, the relative variation (relative to an isothermal state) is of the order of 10^{-13}. A rigorous calculation taking into account the variation of $\frac{\partial \bar{p}}{\partial x}$, $\frac{\partial \bar{p}}{\partial y}$ will yield identical results. By the Boussinesq approximation we neglect the variations of density along the horizontal directions. In common with many other investigations we shall consider the average density along the vertical in the isothermal state and treat it as a constant. In cellular convection problems the relative variation of density is considered. Thus, $\bar{\rho} = \rho_o(1 - \alpha(\bar{T} - T_o))$.

Considering the second equation of motion it might appear that geostrophic balance is achieved in the PBL. However, the y-component of the velocity vector is zero and is not geostrophic.

All dependent variables are written as follows:

$u = \bar{u} + u'$, $v = v'$, $w = w'$, $p = \bar{p} + p'$, and $T = \bar{T} + T'$

where the primed quantities are assumed to be small in comparison with the mean state variables. By substitution of the expanded terms into the system of equations (8) and neglecting terms involving products of perturbation quantities one can obtain the linearized equations for the total motion, i.e., basic flow plus perturbations. The perturbation equations can be obtained from these equations by subtracting the basic state equations defined by (9). In the following equations basic flow variables are denoted with a bar (-) and the perturbation quantities are expressed by the same symbols but without a bar. We obtain the following equations for the perturbations:

$$\frac{\partial u}{\partial t} + \bar{u}\frac{\partial u}{\partial x} + w\frac{\partial \bar{u}}{\partial z} - f v = -\frac{1}{\rho_0}\frac{\partial p}{\partial x} + K_M \nabla^2 u , \qquad (10a)$$

$$\frac{\partial v}{\partial t} + \bar{u}\frac{\partial v}{\partial x} + f u = -\frac{1}{\rho_0}\frac{\partial p}{\partial y} + K_M \nabla^2 v , \qquad (10b)$$

$$\frac{\partial w}{\partial t} + \bar{u}\frac{\partial w}{\partial x} = -\frac{1}{\rho_0}\frac{\partial p}{\partial z} + g\,\alpha\Delta T + K_M \nabla^2 w, \qquad (10c)$$

$$\frac{\partial u}{\partial x} + \frac{\partial v}{\partial y} + \frac{\partial w}{\partial z} = 0 , \qquad (10d)$$

$$\frac{\partial T}{\partial t} + \bar{u}\frac{\partial T}{\partial x} + w\frac{d\bar{T}}{dz} = K_M \nabla^2 T . \qquad (10e)$$

Eliminating u, v, and p from Eq. 10a, b, c, and making use of Eq. (10d) and remembering $\bar{u} = \bar{u}(z)$, we obtain:

$$\left(\frac{\partial}{\partial t} + \bar{u}\frac{\partial}{\partial x} - K_M \nabla^2\right) \nabla^2 w - \frac{d^2\bar{u}}{dz^2}\frac{\partial w}{\partial x} + f\frac{\partial \zeta}{\partial z} = g\,\alpha\,\nabla_H^2 T \qquad (11)$$

where $\nabla_H^2 = \frac{\partial^2}{\partial x^2} + \frac{\partial^2}{\partial y^2}$.

The energy equation may be written as:

$$(\frac{\partial}{\partial t} + \bar{u} \frac{\partial}{\partial x} - K_H \nabla^2)\ T + w \frac{d\bar{T}}{dz} = 0 \ . \tag{12}$$

The vorticity equation derived from (10a) and (10b) may be written as:

$$(\frac{\partial}{\partial t} + \bar{u} \frac{\partial}{\partial x} - K_M \nabla^2)\ \zeta - \frac{d\bar{u}}{dz} \frac{\partial w}{\partial y} - f \frac{\partial w}{\partial z} = 0 \tag{13}$$

where $\zeta = \frac{\partial v}{\partial x} - \frac{\partial u}{\partial y}$ (14)

is the vertical component of relative vorticity. Since we can write:

$$\nabla_H^2\ u = - \frac{\partial \zeta}{\partial y} - \frac{\partial^2 w}{\partial x \partial z} \tag{15}$$

$$\nabla_H^2\ v = \frac{\partial \zeta}{\partial x} - \frac{\partial^2 w}{\partial y \partial z} \tag{16}$$

the horizontal components of motion also can be obtained. With the Coriolis force taken into account, the set (11), (12), and (13) are coupled and form three simultaneous equations in w, T and ζ. Thus, to obtain the desired solutions these equations must be solved simultaneously. Eqs. (11) - (16) are still dimensional. As is customary in boundary layer flows, the above equations are nondimensionalized choosing the depth of the boundary layer (H) as the characteristic length {L}, the free stream velocity $\{U_*\}$ as the characteristic velocity, the imposed temperature difference T^* as the charac-

teristic temperature {T} and the characteristic time {t} defined as the ratio of characteristic length to characteristic velocity. In mathematical symbols they are defined as:

$$\{L\} = H \ ,$$

$$\{T\} = T^* \ ,$$

$$\{t\} = H/U_* \ .$$

We arrive at the following dimensionless equations in place of (11) - (16).

$$\zeta = \frac{\partial v}{\partial x} - \frac{\partial u}{\partial y} \tag{14}$$

$$\nabla_H^2 \, u = - \frac{\partial \zeta}{\partial y} - \frac{\partial^2 w}{\partial x \partial z} \tag{15}$$

$$\nabla_H^2 \, v = \frac{\partial \zeta}{\partial x} - \frac{\partial^2 w}{\partial y \partial z} \tag{16}$$

$$\left(\frac{\partial}{\partial t} + \bar{u} \frac{\partial}{\partial x} - Re^{-1} \nabla^2\right) \nabla^2 w - \frac{d^2 \bar{u}}{dz^2} \frac{\partial w}{\partial x} + F \frac{\partial \zeta}{\partial z} - Ri \, \nabla_H^2 \, T = 0 \ , \tag{17}$$

$$\left(\frac{\partial}{\partial t} + \bar{u} \frac{\partial}{\partial x} - Pr^{-1} \, Re^{-1} \nabla^2\right) T + w \frac{d\bar{T}}{dz} = 0 \ , \tag{18}$$

$$\left(\frac{\partial}{\partial t} + \bar{u} \frac{\partial}{\partial x} - Re^{-1} \nabla^2\right) \zeta - \frac{\partial w}{\partial y} \frac{d\bar{u}}{dz} - F \frac{\partial w}{\partial z} = 0 \ , \tag{19}$$

where

$$Pr = \frac{K_M}{K_H} \ ,$$

$$Re = \frac{H \, U_*}{K_M} \ ,$$

$$Ri = \frac{g \, \alpha \, H \, T^*}{U_*^2} \ ,$$

and

$$Ra = \frac{g \, \alpha \, H^3 \, T^*}{K_M \, K_H} \ .$$

(14), (15), and (16) remain identical to their dimensional counterparts. It is necessary to note that a relationship, $Ra = Pr\ Re^2\ Ri$, exists among the four dimensionless parameters. Since we are concerned here with unstable stratification, the temperature at the lower boundary is higher than the upper boundary and Ri as defined here has a sign opposite from the conventional one. Perturbations are assumed to be of the form

$$\begin{Bmatrix} u \\ v \\ w \\ \zeta \\ T \end{Bmatrix} = \begin{Bmatrix} U(z) \\ V(z) \\ W(z) \\ Z(z) \\ \theta(z) \end{Bmatrix} e^{\{i\ (k_x\ x + k_y\ y)\ +\ \sigma\ t\}} \qquad (20)$$

where k_x, k_y are the wave numbers in the x and y directions, respectively, U(z), V(z), W(z), Z(z), and $\theta(z)$ are the amplitude factors dependent on height and σ is the complex wave frequency ($\sigma = \sigma_r + i\ \sigma_i$). A discussion on these factors is given in Chapter 4.

Inserting Eq. (20) into (17), (18), and (19) we obtain:

$$\{\sigma + \bar{u}\ i\ k_x - Re^{-1}\ (D^2 - k^2)\}\ (D^2 - k^2) - \frac{d^2\bar{u}}{dz^2}\ i\ k_x\ W + F\ \frac{dZ}{dz} + Ri\ k^2\ \theta = 0\ , \qquad (21)$$

$$\{\sigma + i\ k_x\ \bar{u} - Pr^{-1}\ Re^{-1}\ (D^2 - k^2)\}\ \theta - W = 0\ , \qquad (22)$$

$$\{\sigma + i\ k_x\ \bar{u} - Re^{-1}\ (D^2 - k^2)\}\ Z - i\ k_y\ W\ \frac{d\bar{u}}{dz} - F\ \frac{dW}{dz} = 0\ , \qquad (23)$$

$$k^2 U = i k_y Z + i k_x DW , \tag{24}$$

$$k^2 V = - i k_x Z + i k_y DW , \tag{25}$$

where $D = \frac{d}{dz}$, $D^2 = \frac{d^2}{dz^2}$, and $k^2 = k_x^2 + k_y^2$. Since a constant lapse rate of temperature is assumed, $- \frac{d\bar{T}}{dz}$ is taken to be unity in Eq. (22). Eqs. (21) - (25) are used to determine the stability characteristics of the flow.

In seeking solutions of these equations we apply the boundary conditions explained in the previous section. As the convective layer is bounded between the fixed surfaces (the inversion base and the earth's surface), there can be no motion normal to them. The boundary conditions are applied at z = 0 and 1 as the equations were nondimensionalized with respect to H.

Thus, W = 0 at z = 0 and z = 1. (26)

At the rigid boundary no slip occurs; the components of velocity, u and v, at right angles to the vertical, vanish identically on this surface. From the equation of continuity we arrive at:

$$\frac{\partial W}{\partial z} = 0 \; ; \quad A = 0 \text{ at } z = 0 \quad \text{(rigid boundary)} . \tag{27}$$

At the free surface tangential viscous stresses vanish; hence,

$$\frac{\partial^2 W}{\partial z^2} = 0 \; ; \; \frac{\partial Z}{\partial z} = 0 \text{ at } z = 1 \quad \text{(free surface)} . \tag{28}$$

The thermal boundary condition for constant heat flux becomes:

$$D\,\theta = 0 \quad (D = \frac{d}{dz}) \text{ at } z = 0 \text{ and } z = 1 \,. \qquad (29)$$

For perfectly conducting (constant temperature) boundaries:

$$\theta = 0 \text{ at } z = 0 \text{ and } z = 1 \,. \qquad (30)$$

Numerical Procedure

Eqs. (21), (22), and (23) are now ordinary differential equations with variable coefficients. These may be transformed into a set of algebraic equations by using finite differences. Dividing the convective layer into n strips of equal thickness, the vertical derivative of W, for example, at the k^{th} level can be approximated by centered differences (centered differences are adopted to reduce the truncation error):

$$\left(\frac{dW}{dz}\right)_k = \frac{n}{2}\,(W_{k+1} - W_{k-1}) \,,$$

$$\left(\frac{d^2W}{dz^2}\right)_k = n^2\,(W_{k+1} + W_{k-1} - 2\,W_k) \,.$$

The formulation with finite differences is quite straight forward and hence it is not given in detail.

Eqs. (21), (22), and (23) can be written using centered differencing as shown below:

$$Re^{-1}\,n^4\,W_{k+2} - \beta_k\,W_{k+1} + \gamma_k\,W_k - \beta_k\,W_{k-1} + Re^{-1}\,n^4\,W_{k-2}$$

$$- F\,\frac{n}{2}\,Z_{k+1} + F\,\frac{n}{2}\,Z_{k-1} - Ri\,k_H^2\,\theta_k$$

$$- \sigma\,\{n^2\,W_{k+1} - (2n^2 + k_H^2)\,W_k + n^2\,W_{k-1}\} = 0 \qquad (21a)$$

$$W_k + Pr^{-1} Re^{-1} n^2 \theta_{k+1} - \alpha_k \theta_k + n^2 Pr^{-1} Re^{-1} \theta_{k-1} - \sigma \theta_k = 0 \tag{22a}$$

$$F \frac{n}{2} W_{k+1} + i k_y \left(\frac{d\bar{u}}{dz}\right)_k W_k - F \frac{n}{2} W_{k-1} + Re^{-1} n^2 Z_{k+1} - \lambda_k Z_k + Re^{-1} n^2 Z_{k-1} - \sigma Z_k = 0 \tag{23a}$$

where

$$\beta_k = Re^{-1} (4n^4 + 2k_H^2 n^2) + \bar{u} i k_x n^2 ,$$

$$\gamma_k = Re^{-1} (6n^4 + 4k_H^2 n^2 + k_H^4) + \bar{u} i k_x (2n^2 + k_H^2) + i k_x \left(\frac{d^2\bar{u}}{dz^2}\right)_k ,$$

$$\alpha_k = (2n^2 + k_H^2) Pr^{-1} Re^{-1} + \bar{u} i k_x ,$$

$$\lambda_k = (2n^2 + k_H^2) Re^{-1} + \bar{u} i k_x ,$$

and

$$k_H^2 = k_x^2 + k_y^2 \text{ (Horizontal wave number)} .$$

Boundary conditions are similarly transformed into finite-difference form.

Vertical Velocity

$W_o = W_n = 0$, $\quad W = 0$ at $z = 0$ and $z = 1$,

$W_{n+1} + W_{n-1} = 0$, $\quad \frac{d^2W}{dz^2} = 0$ at $z = 1$,

$W_1 - W_{-1} = 0$, $\quad \frac{dW}{dz} = 0$ at $z = 0$.

Vorticity

$$Z_o = 0 \qquad \text{at } z = 0,$$

$$Z_{n+1} - Z_{n-1} = 0, \qquad \frac{\partial Z}{\partial z} = 0 \text{ at } z = 1.$$

Temperature

Constant Heat Flux:

$$\theta_1 - \theta_{-1} = 0 \text{ at } z = 0, \quad \frac{d\theta}{dz} = 0 \text{ at } z = 0,$$

$$\theta_{n+1} - \theta_{n-1} = 0 \text{ at } z = 1, \quad \frac{d\theta}{dz} = 0 \text{ at } z = 1.$$

Constant Temp:

$$\theta_o = \theta_n = 0 \qquad \text{at } z = 0 \text{ and } z = 1.$$

In the above formulation the lower boundary is located at k = 0 and the upper boundary at k = n. $(-1)^{th}$, $(n+1)^{th}$ strips are located at a distance of (1/n) from the bottom and top boundaries, respectively.

With constant temperature boundary conditions (21a), (22a), and (23a) yield 3n-2 linear equations in 3n-2 unknown variables of W, θ and Z. With constant heat flux boundary conditions we obtain 3n linear equations in 3n unknown variables of W, θ and Z. The additional two equations arise as θ does not vanish at the boundaries, i.e., only the derivative vanishes. The above linear equations can be cast in matrix form as $(A - \sigma B)\ \vec{X} = 0$ where $\vec{X}$ is an eigenvector containing variables W, θ and Z. The complex matrix [A] is of

the order (3n-2 x 3n-2) or (3n x 3n) depending upon the thermal boundary conditions imposed. The matrix elements in [A] are arranged corresponding to the arrangement of perturbation variables in the vector $\vec{X}$. The arrangement of matrix elements in [B] is similar to that of [A]. The arrangement in $\vec{X}$ is done as below:

Constant temperature boundaries:		Constant heat flux boundaries:	
$\vec{X}$ (1, ... n-1)	--→ W	$\vec{X}$ (1, ... n-1)	--→ W
$\vec{X}$ (n, ... 2n-2)	--→ θ	$\vec{X}$ (n, ... 2n)	--→ θ
$\vec{X}$ (2n-1, ... 3n-2)	--→ Z	$\vec{X}$ (2n+1, ... 3n)	--→ Z

where the arguments (1, ... n-1) etc., specify the sequential arrangement of the perturbation variables in the vector $\vec{X}$.

The necessary and sufficient condition that the system of Eqs. (21a), (22a), and (23a) possess a nonzero solution for the perturbations variables; i.e., nonzero vector $\vec{X}$ is that the matrix $(A - \sigma B)$ be singular. If [B] is non singular we can rewrite the above condition as

$$|B^{-1} A - \sigma I| = 0$$

where [I] is the unit matrix and $[B^{-1}]$ is the inverse of [B]. From the above equation it is clear that the σ's are the eigenvalues of the matrix $[B^{-1}A]$. The values of σ which permit the above condition to be fulfilled are, of course, dependent upon the nature of the matrix $[B^{-1}A]$ which in turn depends upon the nature of the problem such as the prescribed static stability,

shear, wavelength of the imposed perturbations, etc. These eigenvalues which may be complex, i.e., $\sigma = \sigma_r + i\,\sigma_i$, determine the stability characteristics of the flow.

If $\sigma_r > 0$ the amplitude of the perturbations will increase exponentially with time and the current is said to be unstable. If $\sigma_r < 0$ the amplitude will decrease with time and the current is said to stable. If $\sigma_r = 0$ the basic flow does not interact with the imposed perturbation and is said to be neutral. The σ_i's determine the phase speeds of the modes and they are used in conjunction with σ_r to determine the nature of the modes.

The eigenvalues may then be used to obtain the eigenvector $\vec{X}$ which provides the amplitude of the perturbations. The horizontal component of the velocity, U and V, are obtained from the amplitude of the vorticity using Eqs. (24) and (25). The amplitudes and phase angles of the perturbations are used to determine their structures.

In this study the stability characteristics, as indicated by the eigenvalues, are of primary interest. The structures are obtained for chosen eigenvalues to ascertain the nature of the perturbations. A series of computations was made for a number of different wavelengths of the imposed perturbations with prescribed shear in the basic current. The results are discussed in Chapter V. The relevant parameters chosen for this study with their physical significance are discussed in Chapter IV.

CHAPTER IV

DESIGNATION OF THE EXPERIMENTAL PARAMETERS

In this chapter we discuss the physical significance and the range of values of the various parameters involved in this investigation. The validity of the assumptions which were summarized in Chapter II are discussed in detail.

In the previous chapter, we reduced the linearized partial differential equations to ordinary differential equations by assuming that solutions exist, for the imposed perturbations, in separable functions of x, y, z and t, such as $W = W(z)\, e^{\{i(k_x x + k_y y) + \sigma t\}}$. A special case can be obtained by imposing the condition that the perturbations remain neutral ($\sigma_r = 0$) throughout the period of study. The solutions obtained in this special case, known as mariginal state solutions, separates the stable from unstable states. It is not the objective of this investigation to seek solutions which determine the criteria for the onset of convection. In this study the imposed perturbations are allowed to grow or decay exchanging energy only with the basic flow of the convective layer. Therefore, we do not equate σ_r to zero. The stability characteristics of the

flow are determined from the magnitudes of the real and imaginary parts of σ. These are the eigensolutions of the problem.

The functional form of W(z) varies according to the nature of the bounding surfaces. The imposed hydrodynamic and thermal boundary conditions essentially specify the nature of bounding surfaces. These boundary conditions are determined by the nature of the physical problem to be solved. If the bounding surfaces are free, W(z) can be readily expressed in a closed analytical form (Rayleigh case). However, increasing difficulties are encountered when one attempts to obtain analytical solutions for W(z) when a different set of hydrodynamic and/or thermal boundary conditions (symmetrical or asymmetrical) are specified or when additional forces are considered. Additional complexities arise if we allow the imposed perturbations to grow or decay while exchanging energy with the basic flow. The present investigation contains all the above mentioned problems and normal modes are not easily determined analytically under these conditions. In the absence of an analytical solution, it has become an accepted practice to obtain numerical solutions. The present study is one of that kind and the obtained results form a solution valid in the range of parameters specified. A clear understanding of the governing parameters involved is necessary for a judicious choice of a value or values for those parameters as the results

are dependent upon these specifications. Thus, a discussion of the parameters is in order before the results are presented.

The nature of the bounding surfaces, hydrodynamic and thermal boundary conditions, which control the amplification of the perturbations has already been discussed.

At first it is necessary to indicate the layer for which the parameters are specified, i.e., the convective layer or the stable layer formed above the convective layer. Organized convection such as cellular cloud formations or horizontal roll vortices (bands) are observed to form beneath an inversion layer of height 1-2 km. However, the presence of a stable layer is not a necessary condition for the development of perturbations. Both hollow and solid type of cells occur in the absence of a stable layer (Mitchell, 1967). The formation of clouds serves only as an indicator of the developed disturbances and appear if enough moisture is present for condensation. Thermoconvective eddies arranged in regular patterns occur, even in clear air (Konrad, 1968).
Thus, the above two conditions (namely, the presence of a stable layer and the formation of visible clouds) are sufficient but not necessary conditions. The stable layer above the convective layer may cause secondary effects such as increasing the width of the cells but it does not supply energy for the development of the pattern itself. It is not the intent of this paper to find the proper width to

height ratio of the developed patterns as observed in the atmosphere. It is a desired objective of this paper to find the preferential scale of the most unstable wavelength of the imposed perturbations, under the condition of vertical shear in the basic current. The stable layer can modify this wavelength through non-isotropic diffusion and by subsidence, etc. Since the stable layer affects the developing perturbations very little it is superfluous in this study. The perturbations are imposed on the basic current of the convective layer. The equations given in the previous chapter apply to the convective layer. Thus, the region of interest in this study is the convective layer itself and the parameters are specified for this layer. The convective layer is assumed to correspond to the PBL and has a fixed depth. The flow in the PBL is assumed to be parallel flow.

It may be appropriate at this juncture to point out the differences between 'cells' and 'bands' or 'strips' as these terms are often used in this paper. In hydrodynamic stability studies the organized convection 'bands' or 'cells' are recognized as the ultimate products of the imposed perturbations. Thus, the identification and specification of these disturbances is done in terms of wavelength or wave numbers of imposed perturbations and not by any physical dimensions. The geometry of the modes (square, etc.) is specified in advance through the wave numbers selected for the x- and y-directions. If the imposed perturbations,

such as those specified in this investigation, are three-dimensional the resulting disturbances are referred to as 'cells'. Thus, cells are three dimensional and are specified by wavelengths in two perpendicular directions. In particular, if equal wavelengths are specified in the x- and y-directions the resulting mode is a 'square' cell. The height of the cell is equal to the depth of the convective layer. Hence, a governing parameter in this study is the height of the convective layer itself.

In a motionless or steady-current atmosphere, cells can appear in regular polygonal patterns. However, in a varying current such as prescribed in this investigation, distorted polygons would result. Such distorted patterns often occur in the atmosphere and are frequently observed by meteorological satellites. In this study, we limit ourselves to simple geometric forms such as 'square' or 'rectangular' cells.

In a shearing current the cloud elements often align themselves in rows with clear spaces between them. These cloud bands form in two-dimensional cells. The spacing between the cloud streets or rows is the roll horizontal wavelength. Cloud rows formed with their axes parallel to the mean wind are called longitudinal bands. These have infinite wavelength in the direction of the mean wind. On the other hand, transverse bands have infinite wavelength across the mean wind. In calculations, either of these two

dimensional strips are obtained by specifying an infinite wavelength in the appropriate direction.

The basic state velocity specifies the shear in the system. Thus, the critical parameters in this investigation are the depth of the convective layer (H), the basic state velocity ($\bar{U}$), and the wave numbers of the perturbations in the x- and y-directions (k_x, k_y). The transport of heat and momentum is specified by eddy coefficients (K_H, K_M) while the Coriolis parameter (f) specifies the magnitude of the earth's vorticity. All of the above parameters have dimensions.

In the previous chapter the governing equations were rendered dimensionless using the free stream velocity (U_*), the depth of the convective layer (H), and the imposed temperature difference between the bounding surfaces of the convective layer (T^*). Thus, we obtain four dimensionless parameters; these are the Rayleigh number (Ra), the Reynolds number (Re), the Richardson number (Ri), and the Prandtl number (Pr). The dimensionless wave numbers are denoted by the same symbols as utilized for the dimensional wave numbers.

Specification of Parameteric Values

The Coriolis parameter f is specified as 10^{-4} sec^{-1}, which corresponds to mid-latitudes. The Prandtl number (Pr) in the case of atmospheric convection is the ratio of the eddy, rather than molecular, coefficients of viscosity and conductivity. Thus, we define Pr as the ratio of K_M to K_H.

Even though the values of eddy coefficients of viscosity and conductivity both vary with the scale of the circulations involved, i.e., with the depth of the convective layer, their ratio is generally considered to be near unity. Thus, a value of unity for the Prandtl number can be considered as an appropriate choice even though it may be strictly valid only in neutral conditions. Observational values differ considerably from unity especially under unstable conditions. A couple of tests have been made with Pr = 0.53; these will be discussed in the next section. The depth of the convective layer (H) is assumed to be 1 km in agreement with observations. If the remaining parameters (Ra, Ri and Re) are specified properly the relevant equations can be solved to find the growth rate of the imposed perturbations for the specified wave numbers.

The principal parameters of the problem are the Reynold's number (Re) associated with the basic flow and the Rayleigh number (Ra) associated with the mean temperature gradient. When Re = 0, i.e., no zonal flow, we know that instability sets in with respect to arbitrary three dimensional disturbances at a critical Rayleigh number of 1108, in the absence of rotation under the assumed boundary conditions. When Ra = 0, instability can arise as a result of viscosity acting as destabilizing factor.

In this investigation the imposed temperature difference between the top and bottom boundaries of the convective

layer is specified by the Rayleigh number. Since an unstable stratification is specified the temperature of the lower boundary is higher than that at the free surface upper boundary. Since we are not interested in determining the critical Rayleigh number (i.e., the Rayleigh number which when exceeded only can give rise to unstable modes) the Rayleigh number is specified for each calculation.

The imposed temperature difference T^* can be written as $(\gamma - \Gamma_d)H$ where γ is the environmental lapse rate and Γ_d is the dry adiabatic lapse rate. The quantity $\beta = \gamma - \Gamma_d$ is a small amount which must be added to the dry adiabatic before convection can begin. A static atmospheric layer with a lapse rate equal to the dry adiabatic is analogous to the isothermal liquid layer assumed in theoretical studies.

Some difficulty is encountered in selecting a proper value for the Rayleigh number. The difficulty arises mainly due to two factors; (1) selecting proper values for the eddy coefficients and (2) specifying suitable lapse rate. These are discussed below.

Eddy Coefficients

A considerable amount of literature exists which deals with the specification of eddy values and their variations with height for different stability conditions in the atmosphere. Many semi-empirical formulae are derived but the applicability of these formulae is not universal. Observa-

tional studies have not yielded any conclusive results on the variation of eddy values. However, as expected by intuition, the eddy values for conduction in unstable situations are considerably larger than in neutral and stable conditions. Numerical values may vary as much as three orders of magnitude. Based on Cedar Hill data, Wong and Brundidge (1966) have deduced negative values for eddy conduction coefficients. However, we shall assume in this study that both eddy coefficients remain positive.

There is no general agreement on the spatial variations of these coefficients either. Many investigations, assuming anisotropy of eddy diffusion coefficients, have been undertaken to explain the height to width ratio of cellular cloud patterns observed in the atmosphere. Ray (1965) has shown, irrespective of hydrodynamic boundary conditions, "In general a horizontal transfer coefficient of any kind that is large compared with vertical coefficients will flatten the cells". In other words, the desired cell width to height ratio can be obtained by a suitable combination of spatial change of the eddy coefficients. Since the determination of cell height to width ratio in the marginal state is not our main concern in this study, further attention will not be given to investigations carried out for this purpose. The above investigations show the elusive nature of eddies and the considerable ambiguity that can arise in the choice of a value for these coefficients.

Thus, in choosing eddy coefficients of diffusion K_H or K_M we must be guided more by intuition rather than by a knowledge of the fundamental physics of the process. In this investigation the eddy diffusion coefficients are assumed to be isotropic constants because of a lack of any proper estimate. Moreover, we are not attempting to determine the sense of circulation of the cells. Thus, variation of diffusion coefficients with height are not considered. Simple scale considerations may yield better estimates of the values of these exchange coefficients.

In a simple dimensional approach the exchange coefficients are usually equated to the product of a characteristic length and a characteristic velocity. For example, K_x may be written in our model as $K_x = U_* H$, where U_* is the characteristic velocity and H is the characteristic length. This yields a value of 10^5 cm^2 sec^{-1} for K_M, assuming U_* is equal to 1 cm sec^{-1}. Since we have assumed that the eddy coefficients are equal and isotropic we arrive at an estimate for K_H and K_M equal to 10^5 cm^2 sec^{-1}. Although these are probably conservative estimates they are in agreement with Kuttener's (1971) values.

Specification of Lapse Rate

The temperature gradient necessary to produce these organized patterns is very small. The assumption of a fixed lapse rate in the convective layer is only an idealization,

particularly in the presence of various other nonlinear processes such as entrainment, etc. Since atmospheric convection is modelled here it is appropriate to consider deviations from the dry adiabat lapse rate; β denotes the deviation from the dry adiabatic value.

Jeffreys (1928) has obtained a critical Rayleigh number 0(1000) and a critical temperature gradient $0(10^{-11}$ deg $cm^{-1})$ using eddy coefficients equal to 10^5 cm^2 sec^{-1}. Sasaki (1970) stated, "The Rayleigh number of the convective layer may be in the range of 10^2 to 10^3 if β is about 10^{-3} deg m^{-1} and κ and ν (eddy coefficients) are 10^2 to 10^3 m^2 sec^{-1}. Since the convective layer is fully turbulent and the stratification is nearly neutral, the above estimates are realistic". In other words, the eddy coefficients should be of the order of 10^6 cm^2 sec^{-1} - 10^7 cm^2 sec^{-1} and $\beta = 10^{-5}$ deg cm^{-1}. However, this estimate is not unique. Kuttener (1971) has pointed out, "We are therefore justified to assume that the vertical potential temperature gradient θ' (β in our notation) is smaller than 0.5 deg km^{-1}. Keeping in mind that this should be an average value throughout the convective layer, including areas of ascending and descending motion, θ' is probably quite small." In other words, β should be less than 0.5×10^{-5} deg cm^{-1}. Kuttener has used eddy coefficient values equal to 10^5 cm^2 sec^{-1} and has obtained a critical Rayleigh number of 10^3.

With the same boundary conditions as utilized in this investigation Agee and Chen (1973) have obtained a critical Rayleigh number of 500 for a 1 km deep convective layer; a simple calculation yields $\beta = 10^{-8}$ deg cm^{-1}. This specifies the minimum lapse rate required for the start of convection. From the above results, it is clear that the range of β differs considerably with the suggested values for the eddy coefficients. This is not surprising due to the elusive nature of eddies. The eddies may change in shape and vary in size and they are not a property of the atmosphere itself, unlike molecular coefficients whose values are known and whose variation with temperature can be explicitly calculated. In this investigation β is assumed to have the value $\sim 10^{-7}$ deg cm^{-1} which is probably closer to the values used by Agee and Chen. This choice for β is mainly due to coincidence of the boundary conditions with their investigation. Since the Rayleigh number is proportional to $\frac{\beta}{K_H K_M}$ many values of K_H, K_M, and β will yield the same ratio. A value for β close to zero is considered appropriate, since super adiabatic temperature gradients would be difficult to maintain in the atmosphere in the presence of eddy motions. Moreover, in the second part of this investigation, we will assume that there is a constant flow of heat energy through both boundaries. This assumption is most appropriate if β is small. Thus, a value for $\beta \sim 10^{-7}$ deg cm^{-1} and $Ra = 10^4$ with eddy coefficients 10^5 cm^2 sec^{-1} is considered a good choice.

The other two parameters that remain to be specified are the Richardson number and the Reynolds number. Since Ra and Pr are already specified these parameters are not independent. They are related by the relationship $Ra = Pr\ Ri\ Re^2$. The Richardson number is the ratio of static stability to vertical wind shear and by definition it is independent of both viscosity and thermal conductivity. Since the proper values for eddy coefficients are not known with any certainty, we choose Ri as an independent parameter in our model. Thus, in this investigation the Richardson number serves as a measure of the baroclinity of the flow since the static stability is already specified by the Rayleigh number. Tabulated results are given in terms of Ri as was done by Asai (1970a) in his Couette flow investigation.

If the maximum velocity at the top of the convective layer U_* is calculated, with values of Ri that are used in this investigation, U_* may appear to be too small. This is due to the choice of Rayleigh number which in turn depends upon the lapse rate and the eddy coefficients. If bigger Rayleigh numbers, corresponding to larger lapse rates or smaller eddy coefficients, are chosen with the same Richardson number, U_* will increase. For example, if Ri is equal to 1, U_* has values 100 and 316 cm sec^{-1} for Ra equal to 10^4 and 10^5, respectively. Thus, U_* increases or decreases depending upon the specification of the Rayleigh number. This does not affect the results since only nondimensionalized

equations with nondimensionalized parameters are used in this investigation. Thus, neither the preferred scale (wavelength) of convection or the preferred mode of convection will change. However, a specification of larger Ra will yield instabilities of higher modes which are of no significance in this linear study. Moreover, the range of wavelengths of unstable modes will extend on either side of the mode of primary interest. However, we determine the preferred scale at which the instability is greatest; thus, it is of no consequence. As discussed before the reason for choosing a value of 10^4 for the Rayleigh number is that, in this study unstable modes with wavelengths less than cumulus scale (~ 1 km) are of no significance. We are interested in mesoscale cellular convection. It should be noted that each cell consists of numerous cloud elements and does not consist of a single cumulus cloud.

The only parameters which are varied during the investigation are the wave numbers of imposed perturbations (k_x and k_y) and the vertical shear (Ri) of the basic flow. The variation of k_x or k_y or both specifies the geometry of the cells and the wavelength of the imposed perturbations. As a result of varying Ri, we vary the vertical shear or baroclinity of the basic flow. The remaining parameters, Ra which specifies the static stability of the layer, H the depth of the convective layer, f, Pr and the coefficients of eddy diffusion are kept constant throughout the calculations unless otherwise specified. The preferred wavelength is determined from

the eigensolutions.

In this investigation the horizontal wavelength of the imposed perturbations ($k = \sqrt{k_x^2 + k_y^2}$) is varied from 1 to 30 km. For the range of Ri (2 to 0.2) considered, longer wavelengths are stable. The vertical resolution of the grid used in the calculations is about 80 m. Further details are given in the discussion of the results in the next chapter.

In the first part of the investigation both bounding surfaces are kept at constant temperature and in the second part of the investigation constant heat flux boundary conditions are assumed. Thus, the influence of thermal boundary conditions on the growth of normal modes are determined. The parameters used in the second part of this investigation are identical to those used in the first part.

CHAPTER V

RESULTS AND DISCUSSION

Before viewing the results, let us elaborate on the physical picture described by this convective model. In general, cloud patterns in the form of strips or cells with mesoscale wavelengths (10-100 km) form over land and/or oceanic areas; the shorter waves form over land areas where the ground temperature is warmer than the air temperature. The apparent similarity between convective patterns obtained in laboratory fluids heated from below and this observation suggests that a sufficient condition for the appearance of the patterns in the atmosphere is surface heating and gravitationally unstable configuration. Thus, these patterns are identified as a part of the convection process in the atmosphere. Convection is one of the most complicated processes particularly over land areas. In the atmosphere convection manifests through a variety of physical phenomena such as thermals,rising plumes, etc. The rising buoyant thermals and plumes sometimes penetrate the low-level inversion layer and reach up to the level of the tropopause. These cases are of no direct concern to our study although they are an

important class of convection processes termed as 'penetrative convection'. The organized patterns of interest in this study, are identified with 'cellular or stationary convection'. This denotes a slow motion in which the entire fluid in the convective layer circulates, corresponding to a slow overturning of liquid under a low rate of heat supply. Considering the size of the medium these patterns are recognized as localized effects, even though the physical dimensions may be of the order of 50-100 km. The net effect of convection in the atmosphere is to neutralize the heat imbalance created by surface heating and to attain a gravitationally stable configuration. In the real atmosphere many other factors such as cold and warm air advection in the convection region, radiation, and topography can influence this kind of motion. For simplicity, these factors are neglected in this study. In the laboratory the transport of heat and momentum, necessary for steady convection, is governed by molecular vicosity and conductivity. In the atmosphere eddies transport heat and momentum. In this study, the dissipative effects of eddies are represented through the Prandtl number.

The proper identification of the exact support mechanisms for the occurrence of these patterns in the atmosphere is quite complex. In this study, buoyancy is assumed to be the principal support mechanism. The processes which establish the necessary constant lapse rate throughout the convective layer are not modelled. Supposedly, there is a

uniform heating of the earth's surface which maintains the necessary temperature gradient. In this investigation, we specify the Rayleigh number a priori; the lapse rate necessary for the onset of convection is kept constant throughout the period of investigation. Thus, the unstable modes are necessarily buoyancy supported even though their growth rate can be modified by viscosity, shear and/or shear gradient and rotation.

In the present formulation we concentrate on the effect of vertical shear on the formation of 'square' modes and bands (transverse and longitudinal) under different thermal boundary conditions and we determine the preferred scale of unstable modes. Thus, the crucial parameters in this study are vertical shear and buoyancy. The vertical shear is specified by the Richardson number.

To accomplish the stated goal a simple velocity profile is deduced as an approximation to the zonal component of the Ekman profile and this is taken to represent the zonal flow in the convective layer. Customary to these type of investigations the mechanism for the maintenance of the basic state profile is not specified. The region of interest in this study is the convective layer itself and not the stable layer formed above.

Since dimensionless equations are used in this investigation the tabulated results are expressed in terms of dimensionless parameters such as the Rayleigh number, Richardson

number, Prandtl number, and wave numbers of the imposed perturbations. The magnitude and the range of these parameters has already been discussed in the previous chapter. The characteristic values are presented in terms of the dimensionless complex frequency σ. The real part of the frequency σ_r denotes the amplification rate while the imaginary part σ_i denotes the frequency of the normal modes. Positive values of σ_r denotes amplification. The wave speeds of the developed modes are given by the $c_r = -\frac{\sigma_i}{k_x}$. Computations with stable roots are denoted by bars in the tabulated results. Weak stable modes are included in the tabulated results for proper interpretation. The parameters used in the calculations are given in Table 1. The nomenclature of the variables that appear in the governing equations and results are given at the beginning.

5.1. Convergence

In order to obtain satisfactory numerical solutions it is necessary to divide the convective layer into n layers such that convergence is attained; i.e., an increase in the number of intervals does not significantly alter the final results. We now discuss the basis for choosing a suitable number of intervals n to solve the present problem. Table 2 shows the variation of amplification rate with n for Ra = 10^4 and Ri = 1.0 under different thermal boundary conditions. These results show convergence at n = 12 at both wavelengths

tested. A further increase in the number of intervals produces no significant change in the results. Thus, we have selected n = 12 in this study. In this investigation this requires a matrix size ($B^{-1}A$, complex) of (34 X 34) or (36 X 36), depending upon the thermal boundary conditions, which gives 34 or 36 eigenvalues.

In Table 2 is shown the single unstable wave which appears both for short and long wavelengths, irrespective of thermal boundary conditions. It is also clear that the amplification rate with constant heat flux boundaries is considerably less than that determined with conducting boundaries. As the results shown in Table 2 do not agree with results obtained by previous investigators, it is necessary to check whether this is caused by rotation or by shear or by computational errors.

Table 1. The following constant values are used in the calculations for the specified parameters unless, otherwise stated explicitly in the subsequent tables.

$f = 10^{-4}\ sec^{-1}$	$Pr = 1.0$
$H = 1\ km$	$Ra = 10^{4}$
$K_M = 10^{5}\ cm^{2}\ sec^{-1}$	$Ri = 1.0$
$K_H = 10^{5}\ cm^{2}\ sec^{-1}$	$T_o = 300^{\circ}A$

Table 3 shows the critical Rayleigh numbers obtained with and without rotation in the absence of shear in the basic state. It is of interest to inquire how the results shown in

Table 2. Convergence test for complex eigenvalues (σ) for Ri = 1.0, Ra = 10^4, with rotation as a function of the number of intervals (n) and horizontal wave number (k) with different thermal boundary conditions specified for the bounding surfaces, (a) conducting (constant temperature) boundaries, (b) constant heat flux boundaries. The number of intervals (n) for all calculations presented from Table 3 onwards is for n = 12. In this as well as in subsequent tables the results are expressed in dimensionless quantities and $k_y = k_x$ (square mode) is specified unless otherwise indicated.

		(a)		(b)	
k	n	σ_r	C_r	σ_r	C_r
1.414	6	0.180	0.668	0.166	0.695
	11	0.174	0.677	0.162	0.710
	12	0.174	0.678	0.162	0.711
	13	0.174	0.678	0.162	0.711
3.5	6	0.147	0.741	0.094	0.765
	11	0.158	0.734	0.081	0.76
	12	0.158	0.734	0.081	0.76
	13	0.158	0.734	0.081	0.76
4.24	12	0.092	0.773	0.032	0.809
	13	0.092	0.773	0.031	0.810

Table 3 compare with the previous investigations. The result, obtained without rotation, agrees well with Southwell's (1940) values. However, with rotation the critical Rayleigh number increases to 1180, i.e., by about 8%. The increase in critical Rayleigh number with rotation is expected as appreciable changes (~ 10%) in the critical Rayleigh number can be caused by the rotational influences of the order of those found in the atmosphere. Frenzen and Nagakawa (1955) have obtained, with free surface boundary conditions, a 10% increase in the critical Rayleigh number with an absolute vorticity of 10^{-4} sec^{-1} in a 1 km deep convective layer. In the present investigation the absolute vorticity of the flow is 10^{-4} sec^{-1} since we have assumed a Coriolis parameter of magnitude 10^{-4} sec^{-1}. Thus, our results show a correct magnitude of increase in accordance with Frenzen's (1955) calculations with conducting boundaries. With no slip-constant heat flux boundaries Sasaki (1970) has obtained a critical Rayleigh number of about 800 which corresponds to a horizontal wave number of 2.5. In this study the results show a critical Rayleigh number of about 660 with the same thermal boundary conditions. This discrepancy is due to our asymmetric boundary conditions. With rotation the critical Rayleigh number increases to 740. This increase is in accordance with Frezen's (1955) calculations. Thus, the results presented in Table 3 provide an excellent base for checking the programming and suggest that the differences are real. In the range of wavelengths considered (< 5 km) the

Table 3. Determination of critical Rayleigh number with no shear in the basic current with and without rotation for the specified wave number under different thermal boundary conditions, (a) conducting boundaries (b) constant heat flux boundaries. Note that the critical Rayleigh number (Ra) for the case with the rotation is higher than that obtained with no rotation case irrespective of thermal boundary conditions.

		With Rotation		Without Rotation	
k	Ra	σ_r	c_r	σ_r	c_r
Conducting boundaries:					
2.68	1108	-0.061	0.66	0.003	0.635
	1158	-0.015	0.66		
	1180	0.001	0.66		
	1208	0.03	0.66		
Constant heat flux boundaries:					
2.68	660	-	-	0.001	0.687
	700	-0.039	0.677	0.024	0.687
	740	0.002	0.677		
	770	0.032	0.677		
	840	0.101	0.677		
	1100	0.350	0.677		

Coriolis force cannot be a major stabilizing influence on the developing modes. Hence, we conclude that the difference in results is caused by the shear. This is in accordance with the results of previous investigations that show that the shear has a stabilizing influence on convective modes. A closer inspection of the results in Table 3 shows that in the absence of a basic current (no shear), convection occurs at weaker gravitational stability with constant heat flux boundaries. This is shown in the results by an increase in the amplification rate for the same Rayleigh number. Thus, the results shown in Table 2 do not contradict the results of the previous investigations but supplement them with shear cases.

As we have mentioned earlier only a single unstable wave is found under the assumed boundary conditions. It is necessary to find out whether this is caused by the distribution of shear in the basic flow or by the imposed boundary conditions. In the case of Couette flow with symmetrical boundaries (both free or rigid) it has been found that two unstable waves traveling with equal speed in opposite directions relative to the mean velocity of the flow appear at short wavelengths. Table 4 summarizes the results obtained with Couette flow and the cubical profile at three different wavelengths. To eliminate the possibility of stabilization of any weak waves by the rotation the results are obtained without rotation. From the results it is clear that the

Table 4. Comparison of growth characteristics of the unstable mode with conducting boundaries and no rotation, for different specifications of basic state profile as a function of wave number and vertical shear.

		Couette		Cubical	
Ri	k	σ_r	C_r	σ_r	C_r
1.0	2.83	.213	.559	.228	.697
	4.24	-.018	.634	.085	.772
	1.414	.156	.556	.170	.675

distribution of shear is not the cause of the appearance of a single unstable wave since a similar result is obtained with the constant shear profile. By this we conclude that the hydrodynamic boundary conditions play a significant part in the stability of the flow. Comparing the results we find that the unstable mode which developed with constant shear distribution in the convective layer travels with a velocity close to the velocity found midway between the two boundaries, while the phase speed of the unstable mode obtained with the cubical profile appears to move with a velocity greater than the velocity averaged over the entire layer. The amplification rate is slightly larger than that obtained with a Couette flow. The above results confirm that the cubical profile can produce significantly different results than those obtained in the other investigations under the assumed boundary conditions. From Table 5 onwards the results shown are with the cubical polynomial profile, unless specifically stated otherwise.

As we have obtained two sets of results with different thermal boundary conditions it is convenient to discuss them separately. First, we shall discuss the results obtained with conducting boundaries. In the second part the results with constant heat-flux boundary conditions are discussed. Comparison of the two sets of results are given at the end.

Since three dimensional cells as well as two dimensional bands appear frequently in the PBL the discussion is first

centered on square modes. This also enables us to compare our results with the results of previous investigations. It might have been noticed that we obtained a convergence criterion only for square modes. Without any great loss of accuracy we can use this criterion for all cases discussed in this paper irrespective of the geometry of the cell.

5.2. Without Rotation

This is the simplest possible case with zonal flow. Table 5 gives the unstable modes without rotation as a function of wave number and shear. Since our interest is with rotation, computations were done only for two shear cases. In both the shear cases (Ri = 1.0 and Ri = 2.0) we found only a single unstable mode in the considered range of wavelengths of imposed perturbations. The flow is stable outside this range. Since this is a parallel flow, viscous unstable waves can arise. However, with the prescribed shears no such unstable mode was found. This is also confirmed by a variation of the stratification parameter, Ra. The growth rate of the unstable mode varies significantly, thereby proving they are of thermal origin. The effect of shear is to stabilize the modes as the shear increases. Increased shear in the basic flow also increases the phase speed of the modes. These are pictorially presented in Fig. 4 and 4a, respectively. Fig. 4 shows the variation of σ_r with horizontal wave number for two different values of Ri. It is

Table 5. Stability characteristics of the unstable mode without rotation as a function of wave number (k) and Ri with conducting boundaries. In this and in subsequent tables computations which yield stable roots are denoted by bars (-) and blanks denote no computations were performed in that range. Weak stable modes are denoted with a minus sign. The cubical polynomial profile is specified for the basic state unless otherwise stated.

	Ri = 2.0		Ri = 1.0	
k	σ_r	c_r	σ_r	c_r
0.5	-.005	0.675	-	-
1.0	.163	0.675	0.100	0.675
1.414			0.170	0.675
1.5	.302	0.675	0.183	0.675
2.0	.402	0.675	0.230	0.68
2.5	.460	0.677	0.243	0.685
2.83	.474	0.683	0.228	0.697
4.0	.376	0.71		
4.24			0.085	0.772
5.0	.200	0.75	0.016	0.800
5.5			-0.036	0.820
6.0	.035	0.795	-	-
6.25	-.010	0.801	-	-

clear that in the range of shears considered the maximum unstable mode appears in the large cumulus wavelength (~ 2 km). With a decrease of shear the preferred mode shifts towards lower wavelengths; for a very low shear the most unstable mode probably appears only in the small cumulus range (~ 100 m). However, with an increase of the baroclinicity of the flow the preferred mode can occur at increased wavelengths. Thus, it is evident that the vertical shear in the basic current can play a crucial role in the development of the organized pattern. For small shears only disturbances in the range of cumulus scale are excited. These results will be compared with rotation cases later in this chapter.

5.2.1. Constant Heat Flux Boundaries

Results are obtained for two shear cases as was done for the tests with conducting boundaries. Sasaki (1970) has shown that, without rotation, the wavelength most amplified is a function of the heat-flux through the boundaries; also, usually mesoscale wavelengths are amplified with constant heat flux boundaries. With free surface boundary conditions and with reasonable values of those parameters associated with cellular patterns the wavelength most amplified was found to be of the order of 10 km. However, with rigid boundaries only 6-km waves were found to be most amplified because of the reduction of the apparent depth in the case of non slip condition. It must be remembered that Sasaki's results are for a motionless basic state.

The results obtained with shear in the basic flow are given in Table 6 and Fig. 5 for Ri = 2.0 and Ri = 1.8. It is clear from Fig. 5 that with shear in the basic current the preferred mode of perturbation lies at the cumulus scale (~ 2.5 km). Fig. 5 and 5a show similar characteristics to those obtained in the conducting boundary cases. Hence, the discussion is not repeated here. Some discrepancy is expected due to the different hydrodynamic boundary conditions. From the trend shown by the growth rate at low shears the preferred wavelength would still only be at the large cumulus scale. However, as the shear is increased the preferred wavelength would also be larger. For example, for Ri = 2.0 the preferred wavelength is approximately 2.4 km and for Ri = 1.8 the preferred wavelength increases slightly to about 2.5 km. Since we have chosen a lapse rate quite close to the dry adiabatic value, the estimates with zonal current seems to be realistic but low compared to Sasaki's estimates.

It is of interest to compare our results with different thermal boundary conditions and determine if this condition has any effect on the preferred wavelength of the thermal mode.

5.2.2. Comparison of Growth Rates Under Different Thermal Boundary Conditions

Fig. 6 shows a comparison of results obtained under different thermal boundary conditions for Ri = 2.0. The relevant data are taken from Tables 5 and 6. It is clear

Table 6. The variation of growth characteristics of the unstable mode with constant heat flux boundaries and no rotation (f = 0) as a function of Ri and k.

	Ri = 2.0		Ri = 1.8	
k	σ_r	c_r	σ_r	c_r
0.25	.009	0.65	0.006	0.65
0.5	.050	0.704	0.044	0.71
1.0	.183	0.707	0.168	0.71
1.41	.287	0.707		
2.0	.396	0.706	0.364	0.707
3.0	.449	0.707	0.404	0.71
4.0	.325	0.735	0.268	0.74
5.0	.153	0.77	0.118	0.775
5.5	.084	0.81	0.055	0.82
6.0	.009	0.825		

from the figure that constant heat flux boundaries shift the preferred (most unstable) perturbation to higher wavelengths with a slightly decreased growth rate. Moreover, with constant heat-flux boundaries perturbations with longer wavelength become more unstable as is shown by the increased growth rate in Fig. 6 at low wave numbers. Thus, it is clear, at least under the conditions assumed in this study, that shear is the principal controlling factor as compared to the thermal boundary conditions. A comparison of phase speeds shows the waves move with higher speeds than in the case of perfectly conducting boundaries; this may be seen in Table 6. Since the growth rate can be taken as an indicator of the intensity of the convection, with constant heat flux boundaries, longer wavelength modes appear to be more intensified. The onset of convection appears to be in mesoscale wavelengths in both cases irrespective of shear. However, the most amplified wave only is of the order of 2 - 3 km. The reduction in growth rate may be due to larger frictional loss of heat due to the increased phase speed of the perturbations, particularly at low wave numbers. However, it appears that the additional buoyant energy is utilized in increasing the kinetic energy of the perturbations. Such transformations are feasible only with a zonal flow.

5.3. With Rotation

In this section we begin a discussion of the stability characteristics of perturbations superimposed on flow including

rotation with conducting boundaries. The structure of the obtained modes are described. A comparison is made with the results obtained for the non-rotating cases. The same sequence is repeated with constant flux boundary conditions. In the final part stability characteristics under different thermal boundary conditions are discussed. All discussion is for square cells.

Table 7 gives the growth rate of the unstable modes as a function of the baroclinicity of the flow at different wave numbers. Since only square cells are considered, the first column of the table refers to the horizontal wave number which is 1.414 times the wave number in either the x- or y-direction ($k = \sqrt{k_x^2 + k_y^2}$). The remaining columns refer to the results with a prescribed baroclinic shear which is expressed in terms of Richardson number. Large values of Ri correspond to lower baroclinicity and vice versa.

With the assumed boundary conditions we can expect inertial modes arising out of the destabilizing influence of viscosity at high shears. A search was made at very low Richardson numbers; i.e., very large shears with an increased number of intervals (n = 25). However, no unstable modes were detected. The flow seems to attain stability similar to that of Couette flow beyond a certain shear. However, a few stable modes with very low phase speed (~ .004) appear. A further investigation has shown these modes are not an inertial type originated by viscous forces. We shall dispose

Table 7. Stability characteristics of unstable modes with rotation as a function of Ri and k for conducting boundaries. Note that the mode stabilizes with increase in vertical shear (decrease in Ri) for the same wave number.

	Ri = 2.0		Ri = 1.8		Ri = 1.5		Ri = 1.0		Ri = .8		Ri = .5		Ri = .25	
k	σ_r	c_r	σ_r	c_r	σ_r	c_r	σ_r	c_r	σ_r	c_r	σ_r	c_r	σ_r	c_r
.25							-.034	.717						
.5	-.003	.644			-.002	.652							-.007	.689
1.0	.159	.667	.149	.669	.134	.670	.103	.674	.087	.676	.056	.68	.014	.693
1.41							.174	.678			.088	.686		
1.5	.3	.673	.26	.673			.186	.678	.150	.68			.002	.706
2.0	.402	.676	.374	.677	.328	.678	.235	.683	.188	.684	.092	.697	-	-
2.83							.232	.7						
3.0	.475	.687	.434	.689	.364	.693			.144	.719	.027	.752		
4.0	.378	.711	.328	.717	.247	.729			.061	.776	-.019	.806		
4.24							.092	.773						
5.0	.203	.758	.168	.763	.115	.778	.023	.803						
5.5	.122	.774			.049	.796								
5.66							-.048	.822						
6.0	.039	.795			-.002	.802								
6.5	-.053	.808												

of them since they are inconsequential to this study. Probably, these waves only can be detected with a different numerical scheme or by recasting the basic equations in appropriate fashion.

Thus, the reported unstable modes are necessarily of thermal origin modified by shear, rotation and viscosity. The influence of rotation can be expected to be very small. No attempt is made in this study to determine the influence of eddy viscosity alone on the unstable modes. It is not suitable in this investigation as we use eddy coefficients which we have assumed to be constant and isotropic. The nature of the eddy coefficients has been discussed in Chapter 6. One can get as many equally valid solutions as there are definitions for eddy coefficients. However, it is clear that the viscous influence exists in these normal modes as is shown by the dependency of wave speed of the unstable modes on wavelength (Table 7). Fig. 7 is a pictorial presentation of the results shown in Table 7. Another representation of the stability characteristics is given in Fig. 8. The variation of amplification rate with horizontal wave number k for different values of Ri is shown.

Figs. 7 and 8 look very similar to those for Couette flow obtained by Asai (1970a). This is to be expected since the profile of the zonal flow assumed in this study clearly lies between a Couette or constant shear profile and a variable shear profile. Neglect of the cubical term in the profile

used in this investigation immediately gives a Couette profile. It is also necessary to note that this profile lies just on the border line between profiles with no point of inflexion which are stable according to the frictionless theory and profiles with a point of inflexion which are unstable. The point of inflexion of the cubical profile is at the lower boundary. The discussion of the nature of the profile and of selected boundary conditions is given in Chapter 3.

By the special nature of this profile, we can expect results which have both the properties of a Couette profile and of a variable shear profile. Hence, in the discussion of the results, a comparison with the results obtained with Couette flow and with variable shear flow is considered appropriate. However, a direct one-to-one correspondence between the published results and the results obtained in this study is not feasible. This is due to the different boundary conditions applied in this study as well as to the nature of the zonal profile. For instance, we have seen that with asymmetrical hydrodynamic boundary conditions a single unstable mode appears both in short and in long wavelengths. On the other hand, with rigid or free boundary conditions and a constant shear profile with same stratification parameter (Ra) two unstable modes appear in the short wavelength range. Thus, the published results serve only as a guide in this study. Since the results in this study resemble those obtained with a constant shear profile (Couette flow) the

same terminology, following Kuo (1963), will be used to denote short wavelength disturbances as transitive and long wavelength disturbances as stationary, even though such nomenclature may not be strictly valid here. From Figs. 7 and 8, it is clear that there is a preferred wavelength of the perturbations at which there is maximum instability, as is shown by the maximum growth rate. The wavelength of maximum instability decreases as the Richardson number increases; the maximum unstable wavelength decreases from 6 km to 2 km. It is worthy to note that with the increase of the vertical shear of the flow the wave most amplified is closer to a mesoscale wavelength but at low shears the maximum unstable mode corresponds to a cumulus scale wavelength. Moreover, the range of unstable wavelengths decreases with increase in shear of the basic current. It is clear that there is a threshold limit for the onset of instability, below which the whole current becomes stable. In this investigation this limit is quite close to Ri = 0.2. In other words, the wave number of maximum instability does not decrease without limit as the shear is increased. Considering the many simplifications that are made in this study, it is certain that mesoscale wavelength disturbances can arise in the atmosphere by the action of vertical shear alone. However, the growth rates are quite small. Since realistic boundary conditions along with a shear profile closely resembling that found in the atmosphere, have been utilized

the interpretations given here may be correct. It is evident from Fig. 8 that vertical shear of the basic flow exerts an inhibiting influence on the growth of disturbances for all wavelengths. It is also interesting to note that, the longest unstable wavelength (12 km) remains practically the same irrespective of the shear in the basic flow. Thus, it appears, at least under the conditions assumed in this study, in the atmosphere the maximum wavelength at which gravitational convection can occur is at mesoscale range (~ 10 km). Many other factors such as subsidence, etc., may increase this limit. Considering Fig. 7, one can see from the neutral curve that there are two cut-off values for instability; one is at a small wave number and the other is at a large wave number. The shortest wavelength, below which the current becomes stable, corresponds to cumulus wavelengths. The values obtained appear to be quite reasonable.

We now proceed to analyze the properties of the unstable modes. Since we obtain a single unstable mode in this study, this mode may be considered as the lowest eigenmode which is of significance in a linear study. Higher modes may appear with a larger lapse rate or higher Rayleigh number but these are of importance only when we consider the interaction between the perturbations themselves. Since this is a linear study, consideration need not be given to higher modes. In stability studies, such as this investigation, a consideration of phase speed of the unstable modes may be fruitful in

the identification of the origin of the waves; it also may give one an idea about the influence of other mechanisms present in the system. Fig. 9 shows the phase speed variation of the unstable mode as a function of horizontal wave number and shear of the flow. The relevant data is taken from Table 7. At all wavelengths of disturbances the phase speed of the modes is greater than the velocity of the basic flow averaged over the entire depth of the boundary layer (~ 0.6). Table 4 shows a similar result for a Couette flow profile. Thus, it is clear that with asymmetric boundary conditions the unstable mode travels with a phase speed greater than the velocity of the basic flow averaged over the entire depth of the layer.

From Fig. 9 we see the maximum wave speed of the unstable mode is about 0.8 for Ri = 1.0 or Ri = 2.0 and about 0.75 for Ri = 0.5 (all wave speeds are nondimensional). The dependency of the wave speed on the wave number of the perturbations arises as a result of dispersive action of eddies. A similar result is obtained with Couette flow with symmetrical boundary conditions for transitive perturbations. Such perturbations probably exist in this study. This is inferred by the large wave speed attained by the unstable mode at high wave numbers. However, it is not evident from Fig. 9 since no distinct separation of longer stationary unstable perturbations from the short transitive perturbations exists. Figs. 7 and 8 also show a smooth transition similar to that

which may be expected with a variable shear flow. Thus, it is not clear whether the perturbations are a single kind or are two distinct types as in the case of Couette flow. Moreover, it appears from Fig. 9 that the wave speed is a function of wave number in the entire range studied. This is clearly seen in the curve marked Ri = 0.5.

As rotation is a stabilizing influence it cannot change the wave speed by itself. Thus, we proceed to consider the growth rate of perturbations. Usually, transitive perturbations are distinguished from stationary perturbations by the variation of their growth rate with wave number. The former has a slow growth rate almost independent of wave number while the growth rate of the latter varies considerably, (Kuo, 1963; Asai, 1970a). From an inspection of growth rates for Ri = 2.0 in Table 7 it is evident that at high wave numbers the variation is not less than 50% of that found for large wavelengths. For example, the growth rate change between k = 1.0 and k = 1.5 is about 0.141. A comparable growth rate is obtained between k = 5.0 and k = 5.5; i.e., .081 at the same shear (see Table 7). Since at higher wavelengths there is variation of phase speed with wave number and at short wavelengths there is a comparable growth rate, it appears that we cannot delimit the instability domain in two separate regions. Moreover, there appears to be a very smooth transition (Fig. 9) inferred by the absence of bend or kink in the plotted results. We may be correct to infer

that the unstable mode is a combination of a convective disturbance and of a gravity-wave type disturbance. Thus, we can expect the structure of the mode at both wavelengths to be a combination of both.

Structure of Unstable Mode

Figs. 10a, 10b, 11a and 11b show profiles of w and θ perturbations at two different wavelengths. The ordinate in the figures is the nondimensional height of the convective layer. From the figures it is clear that at both short and long wavelengths (k = 4.24 and 1.414) vertical velocity perturbations (w) attain two maxima in the convective layer. The principal maximum of vertical velocity in the long wavelength perturbations (k = 1.414) seem to be above the center of the convective layer. The principal maximum of the perturbations in short wavelength (k = 4.24) appears close to the rigid surface, i.e., below the center of the layer. A comparison of magnitudes reveals that short wavelength perturbations have a smaller vertical velocity than long wavelength perturbations even though there is no noticable difference in the magnitude of the temperature perturbations. From the above figures it may be seen that the principal maxima of w and θ for either wavelength do not coincide. This appears more pronounced in short wavelength perturbations (Figs. 11a and 11b). The vertical transport of horizontal momentum and sensible heat flux is shown in Figs. 10c, 10d, 11c and 11d, respectively. Figs. 10c and 11c show there is a net transport of negative momentum when averaged over

the entire layer but the net transfer in the short wavelength perturbation is small. A similar conclusion about sensible heat may be drawn by comparing 10d and 11d; the only difference is that the transport of heat is upward instead of downwards. Figs. 12a, 12b, 12c, 12d, 13a, 13b, 13c, and 13d refer to similar profiles with specification of a lower shear (Ri = 10.0) and a higher shear (Ri = 0.5) in the basic current, respectively. Fig. 13d shows that the net transport of heat averaged over the entire layer seems to be small. This is due to the presence of high shear (Ri = 0.5) in the basic current, which produces stability in the layer. For higher shears the buoyancy effects probably are negligible; mechanical effects predominate in this case. A typical structure of the unstable mode for a long wavelength perturbation is shown in Fig. 14a and 14b on a moderate shear (Ri = 1.0). In these figures the ordinate is the height of the convective layer and the abcissa is a full wavelength perturbation in the x-direction. The principal maximum of w and θ are denoted in the figures. The considerable elongation is due to Coriolis force and the inclination is caused by the basic current whose flow is in the positive x-direction. In the lower half of the layer both w and θ perturbations are inclined opposite to the direction of the basic current. It is not clear whether this is due to a boundary effect or due to the special nature of the flow. It appears to be the latter since boundary effects are

observed very close to the boundary only. The profiles of sensible heat-flux and momentum-flux are not of the same sign throughout the convective layer. This may be due to the asymmetrical boundary conditions.

Comparison With No Rotation

The results with no rotation have been presented in a previous section. The results obtained with no rotation are listed with the rotation cases in Table 8 for two different shears Ri = 2.0 and Ri = 1.0, respectively. It is evident from Table 8, at Ri = 2.0, that waves longer than 5 km (k = 1.5) are stabilized by the rotation. Slight destabilization of waves below 2 km is noticed in this shear. However, in case of larger shear, Ri = 1.0, it can be seen that waves below 6 km are destabilized. We have noticed the dependency of wave speed on wavelength arises as a result of the dispersive action of viscosity. It appears that the slight destabilization may be connected with viscous influence. However, the order of magnitude is very small.

Till now, we have considered the results for square modes with conducting thermal boundary conditions. In the next section we discuss the results obtained with constant heat-flux thermal boundary conditions.

5.4. Constant Heat-Flux Boundary Conditions

The results with constant heat-flux boundary conditions are given in Table 9. The first column refers to horizontal

Table 8. Comparison of stability characteristics of unstable modes with conducting boundaries between rotation and no rotation (f = 0) cases for different values of Ri and k. Slight destabilization of the mode may be noticed with increase in wave number for the specified values of Ri.

	Ri = 2.0				Ri = 1.0			
	Rotation		No Rotation		Rotation		No Rotation	
k	σ_r	c_r	σ_r	c_r	σ_r	c_r	σ_r	c_r
.5	-.003	.644	-.005	.675				
1.0	.159	.667	.163	.675	.103	.674	.100	.675
1.41					.174	.678	.170	.675
1.5	.3	.673	.302	.675	.186	.678	.183	.675
2.0	.402	.676	.402	.675	.235	.683	.230	.68
2.5	.46	.680	.460	.677			.243	.685
2.83					.232	.700	.228	.700
4.0	.378	.711	.376	.71				
4.24					.092	.773	.085	.772
5.0	.203	.758	.200	.75	.023	.803	.016	.800
6.0	.039	.795	.035	.795				

Table 9. Amplification rate and phase speed of unstable modes with rotation for different values of Ri and wave numbers (constant heat flux boundaries).

	Ri = 2.0		Ri = 1.8		Ri = 1.5		Ri = 1.0		Ri = .8		Ri = .5		Ri = .25	
k	σ_r	C_r	σ_r	C_r	σ_r	C_r	σ_r	C_r	σ_r	C_r	σ_r	C_r	σ_r	C_r
.25	.005	.622	.003	.622			-.008	.644	-.012	.661	-.015	.705		
.5	.042	.680	.037	.68	.029	.692	.014	.714	.009	.72			-.011	.748
1.0	.177	.703	.163	.707	.142	.71	.100	.718	.080	.721	.042	.725	-.008	.72
1.41	.284	.701					.162	.711			.064	.714		
1.5													-.034	.71
2.0	.395	.7	.365	.702	.314	.703	.213	.708			.053	.716		
2.83							.189	.718						
3.0	.451	.708	.406	.71	.331	.713			.069	.734	-.084	.797		
4.0	.330	.73	.274	.74	.184	.757								
4.24							.032	.809						
5.0	.159	.79	.124	.8	.071	.812	-.023	.838						
5.5	.089	.81	.060	.82	.015	.831								

wave number while the remaining columns denote the results obtained with the prescribed shear in the basic current.

Fig. 15 is the graphical presentation of the results of Table 9. The variation of amplification rate with wave number at different Ri is shown in Fig. 16. These figures are similar to the conducting boundary results presented in Figs. 7 and 8.

As with conducting boundaries, from Fig. 15 it can be seen that the neutral curve shows two cut-off values of instability; one is at a small wave number and the other at a large wave number. From Fig. 16 we notice the wavelength of greatest instability increases as Ri decreases. In general, with the constant heat flux boundary condition the wavelength of greatest instability is slightly larger than that obtained with conducting boundaries (compare Figs. 8 and 16). The zonal current becomes stable at Ri = 0.25, which is a lower shear than with conducting boundaries. A single unstable mode, taken as the lowest eigenmode, appears in all shears. The highest wavelength with constant flux boundaries that develops instability decreases as the shear increases in the basic current. This is in contrast with the result obtained with conducting boundaries. In Fig. 8 one can note that, irrespective of the shear in the basic current, the highest wavelength an unstable mode can attain is ~ 12 km. However, in Fig. 16 one can see that this wavelength changes with shear (see L. H. S of the figure), thereby showing that the

conducting boundary is more suitable for studying atmospheric motions than are constant heat flux boundaries. The slight increase in the growth rates obtained at large wavelengths is nullified by a decrease in wavelength as shear increases. The advantage gained in the increase of wavelength of the preferred perturbation is also nullified by the decrease in the growth rate. Thus, the constant heat flux hypothesis becomes of academic interest only, considering the zonal motion in the atmosphere. The characteristics of the unstable mode such as, wave speed, type, etc., remain the same; this has already been discussed for the constant temperature boundaries.

The vertical profiles of w and θ perturbations together with profiles of the vertical transport of horizontal momentum and heat flux are given in Figs. 17 and 18. Typical structures of w and θ perturbations for a short wavelength ($k = 4.24$) are shown in Figs. 19 a and 19b. These may be contrasted with conducting boundary results as shown in Figs. 14a and 14b.

Comparison With No Rotation

A comparison of the results (rotation versus no rotation) is given in Table 10 for two different shears ($Ri = 2.0$ and $Ri = 1.8$).

It is clear, that with rotation very slight stabilization is noticed at longer wavelengths (> 5 km). The slight

Table 10. Comparison of stability characteristics of unstable modes with constant heat flux boundaries between rotation and no rotation (f = 0) cases as a function of Ri and k. Notice the trend of destabilization of the modes with increase in wave number for a specified value of Ri; this is similar to results obtained with conducting boundaries (Table 8).

	Ri = 2.0				Ri = 1.8			
	Rotation		No Rotation		Rotation		No Rotation	
k	σ_r	C_r	σ_r	C_r	σ_r	C_r	σ_r	C_r
.25	.005	.622	.009	.65	.003	.622	.006	.65
.5	.042	.680	.050	.704	.037	.68	.044	.71
1.0	.177	.703	.183	.707	.163	.707	.168	.71
1.41	.284	.701	.287	.707				
2.0	.395	.7	.396	.706	.365	.702	.364	.707
3.0	.451	.708	.449	.707	.406	.71	.404	.71
4.0	.330	.73	.325	.735	.274	.74	.268	.74
5.0	.159	.79	.153	.77	.124	.8	.118	.775
5.5	.089	.81	.084	.81	.060	.82	.055	.82

destabilization occurs here also with Coriolis force but as with conducting boundaries the magnitude is negligible. Thus, it can be safely concluded that the rotation plays no significant role in the stability of modes, irrespective of the thermal boundary condition. This result is expected, as the scale of circulation involved is very small. However, it is clear this small destabilization is connected to viscous forces only.

5.5. Comparison Between Two Thermal Boundary Conditions

Table 11 shows a comparison of growth rates and wave speeds of unstable modes with different thermal boundary conditions at two different Ri. Irrespective of the shear present in the zonal flow it is seen from Table 11 that the amplification rate of the unstable modes is less than in the conducting boundary results.

While discussing convergence of the numerical solution we have shown that the results are of real nature but we have not explained how the amplification rate decreases when constant flux boundary conditions are utilized. The results of previous investigators have shown that conducting boundaries provide a stronger constraint against perturbations of the temperature profile than does the condition on the temperature derivative at the surface. Thus, the constant flux hypothesis allows convection to occur at weaker gravitational instability. The above results apply to the motionless media.

Table 11. Variation of stability characteristics of the unstable modes with rotation under different thermal boundary conditions, (a) constant temperature, (b) constant heat flux boundaries, for different values of Ri and k. It may be seen that the modes are more unstable with conducting boundaries than with constant heat flux boundaries, irrespective of the value of Ri and k.

	Ri = 2.0				Ri = 1.0			
	(a)		(b)		(a)		(b)	
k	σ_r	c_r	σ_r	c_r	σ_r	c_r	σ_r	c_r
.5	-.003	.644	.042	.680				
1.0	.159	.667	.177	.703	.103	.674	.100	.718
1.41					.174	.678	.162	.711
2.0	.402	.676	.395	.7	.235	.683	.213	.708
2.83					.232	.7	.189	.718
3.0	.475	.687	.451	.708				
4.0	.378	.711	.330	.73				
4.24					.092	.773	.032	.809
5.0	.203	.758	.159	.79	.023	.803	-.023	.838
5.5	.122	.774	.089	.81				

However, results of this study show that in the presence of an initial zonal flow the constant flux hypothesis stabilizes the thermal modes. The growth of the modes are strongly influenced by the shear in the basic flow. Keeping aside the influence of rotation which is very small in the range of wavelengths considered (Table 8) the main factors which can affect the growth rate are thermal boundary conditions and shear in the basic flow since the hydrodynamic boundary conditions remain the same in the cases compared. By applying the constraint, $\frac{\partial \theta}{\partial z} = 0$ at both boundaries, we are forcing the convective temperature perturbation to occur with maximum or minimum amplitude at both surfaces. Thus, we can expect the vertical profile of the temperature perturbations in the convective layer, to be altered drastically by the constant flux hypothesis for the value of shear prescribed. A comparison of the vertical profile of temperature with a constant flux boundary and a conducting boundary are shown in Figs. 17b and 10b verifying the above statement.

It can be observed from Fig. 17b that nearly equal amplitude temperature perturbations are produced throughout the convective layer, except at the surfaces. Moreover, the amplitude of temperature perturbations are highly reduced compared with those obtained with conducting boundaries. It may be noted that the profiles are not normalized with respect to a particular level of the convective layer.

The buoyancy force $g \alpha T^*$ is independent of the shear

in the basic flow and remains the same in both cases as we do not alter the stratification parameter, Ra. In the absence of basic flow in the convective layer more buoyant energy is available since there is no decrease of the convective temperature perturbations due to conduction and hence the modes are more unstable. However, if an initial flow is present the perturbations interact with the basic flow. Thus, it is clear that a decrease in the amplification rate only is connected to the energy transfer mechanism. Comparing the phase speed of the unstable modes in Table 11 it is seen that the phase speeds C_r increases when constant flux boundary conditions are employed. Irrespective of thermal boundary conditions, the phase speed of unstable perturbations increase with increasing wave number within the range of velocity of the basic flow. Thus, it is clear that with the constant heat transfer boundary conditions, the excess buoyant energy mainly goes to increase the phase speed of perturbations rather than to increase the growth rate of perturbations. The question remains as to why the amplification rate drops off significantly when constant flux boundaries are utilized. The answer to this question is found by comparing the vertical profiles of transport of horizontal momentum which are shown in Figs. 10c and 17c. It is clear from the profiles that under constant heat flux boundary conditions there is more upward transport of momentum against the mean gradient of the flow.

Asai (1970) has shown such a transport increases the shear of the basic flow. Since the shear is a stabilizing influence the increase in shear stabilizes the flow much more than in the case of conducting boundaries. This is also revealed by the fact the flow, with constant heat-flux boundary conditions, stabilizes at a lower shear (Ri = 0.25) than that of constant temperature boundary conditions which stabilizes below Ri = 0.25.

From Figs. 17a and 10a or Figs. 18a and 11a the w profiles for both boundary conditions remains of the same order of magnitude. The profiles of sensible heat-flux given in Figs. 17d and 10d show there is less transport of heat in the convective layer under constant heat-transfer boundary conditions. The smaller vertical heat-flux is responsible for the increase in wavelength of the preferred perturbation. One may note that only with a very high shear (Ri = 0.25) does the wavelength of greatest instability come close to a mesoscale wavelength (5-6 km); but, for lower shears the wavelength of maximum instability corresponds to that of cumulus scale (~ 2 km). This result seems to contradict Sasaki's result (1970), who has shown that in motionless media, the 10-km wave has greatest amplification (lowest critical Rayleigh number) with free boundaries, and with rigid boundaries a 6-km wave has the maximum amplification. Our results point out that with no shear or very little shear the wavelength of maximum instability lies in the cumulus

scale range, irrespective of the thermal boundary conditions. With high shear the longest unstable wavelength is about 5 km which is close to mesoscale, but the growth rate is very small. Constant heat-flux with a zonal flow reduces the allowed growth rate of the preferred perturbation; thus, the remarks made in the last section apply. Since in the atmosphere there is an ever present zonal flow and associated vertical shear it appears certain that mesoscale convection patterns attain maximum growth due to conditions other than constant heat-flux at the boundaries and vertical shear. An increase in Rayleigh number or the degree of stratification alone may not be sufficient. Table 12, compares the results obtained with $Ra = 10^5$ and $Ra = 10^4$. Fig. 20 is a pictorial presentation of the above results. It is clear from Fig. 20 that the range of instabilities shifts towards higher wave number and the maximum unstable wavelength still corresponds to about 3 km. Neglecting the amplification rate it can be seen that the maxima occur at the same wave number for both $Ra = 10^5$ and $Ra = 10^4$. This is for conducting boundaries. A similar result is obtained with constant heat-flux boundaries as is shown in Table 13 and Fig. 20a. The secondary maximum which appears at a higher wave number in Fig. 20 at $Ra = 10^5$ is not of much significance in this study.

5.6. Changes With Geometry of Modes

Now we turn our attention to the study of instability with different specification of wave numbers in the x- and

Table 12. Effect of Rayleigh number on the stability of the modes as a function of wave number with conducting boundaries for Ri = 1.0. Notice the increase in the range of instability as well as the amplification rate (σ_r) of the unstable mode as Ra increases.

	$Ra = 10^5$		$Ra = 10^4$	
k	σ_r	c_r	σ_r	c_r
.25	.022	.65	-.034	.717
.5	.081	.677		
1.0	.181	.665	.103	.674
1.41			.174	.678
1.5			.186	.678
2.0	.262	.675	.235	.683
	*.045	.682		
2.83			.232	.7
3.0	.248	.773		
4.0	.277	.84		
4.24	.281	.834	.092	.773
5.0	.285	.856	.023	.803
5.66			-.048	.822
6.25	.270	.885		
7.0	.250	.895		
8.0	.212	.905		
9.0	.165	.915		

*Higher Mode

Table 13. Results similar to those shown in Table 12 but with constant heat flux boundaries and Ri = 2.0.

	$Ra = 10^5$		$Ra = 10^4$	
k	σ_r	C_r	σ_r	C_r
.25	.042	.69	.005	.622
.5			.042	.680
1.0	.295	.67	.177	.703
1.41			.284	.701
2.0	.521	.669	.395	.7
	*.083	.708		
3.0	.543	.699	.451	.708
	*.179	.669		
4.0			.330	.73
5.0	.519	.829	.159	.79
	*.069	.478		
5.5			.089	.81
7.0	.470	.883		

*Higher Mode

y-direction. Previous investigators have shown that a variable shear flow and a constant shear flow stabilize the transverse mode in varying degrees. However, the above investigations have been conducted with symmetric hydrodynamic boundary conditions (both rigid or both free surface). Since our study differs in the specification of hydrodynamic boundary conditions and in the specification of the zonal profile we can expect a slightly different result. However, the basic conclusion remains unchanged.

No special attention is needed to consider the rotational influences since the stabilizing influence has been found to be negligible in the scale of circulation considered here. Thus, no special computations were performed to determine the influence of rotation alone on the transverse or longitudinal bands. In determining the influence due to variable shear on the geometry of convective modes a horizontal wave number close to the maximum unstable wavelength for a particular shear has been chosen (Ri = 1.0). Here k has been chosen to have a value equal to 2.0 and Ri = 1.0. At this particular shear the maximum unstable wave number is 2.4. The reason for this is two fold. First, for the preferred wavelength there is maximum heat and momentum transport. Secondly, the retarding influences of viscosity and other forces are a minimum.

We have seen, while discussing the phase speeds of unstable square modes, that the modes are of a mixed type;

i.e., they are a combination of small scale gravity-type wave disturbances and long wave convective type disturbances, former of which are dependent upon vertical shear. It will be instructive to find out the effect on such mixed mode separately for longitudinal and transverse modes. Thus, in the ensuing discussion we will pay particular attention to the structure of unstable modes as well as to the profiles of vertical velocity and temperature. Since the change in the thermal boundary conditions has been found to have a stabilizing effect and there is a slight alteration of the phase speed of the unstable square modes, in the following discussion the results are presented according to the specification of the geometry of the modes (transverse or longitudinal). As mentioned earlier in Charper IV, the geometry of the modes can be defined by the specification of wave numbers in the x- and y-directions. In the present discussion the wave number ratio of $\frac{k_y}{k_x}$ determines the type of mode. If $\frac{k_y}{k_x} >> 1$ it is longitudinal and if $\frac{k_y}{k_x} << 1$ it is a transverse mode. Theoretically, $k_y = 0$ specifies a transverse mode and $k_x = 0$ specifies a longitudinal mode; but for our purposes it is enough if the ratio $\frac{k_y}{k_x}$ is small or large. Any further reduction in the ratio by specifying a smaller k_x or k_y has no effect on the stability of the modes. Thus, strictly speaking, we are considering only 'rectangular' modes instead of a 'square' mode.

5.6.1. Transverse Modes

Table 14 shows the results obtained with different specifications of the ratio $\frac{k_y}{k_x}$, all less than one, as a function of Ri. In the same table, the results obtained with constant heat flux boundary conditions are given for an easy comparison. The fourth row in Table 14 represents a square mode. A graphical presentation of the results in Table 14 is given in Figs. 21 and 22. An inspection of Table 14 shows that the growth rate σ_r and phase speed remain almost the same for values below of the ratio less than 0.1, thus justifying our assumption that in numerical calculations it is sufficient to take a finite ratio for these wave numbers instead of making them zero or infinite by the specification of k_x or k_y to be zero. It is easily seen that the transverse modes are more stable than the square modes; the stabilization arises due to influence of shear in the basic current.

A typical comparison with constant shear results shows as expected that the variable shear has less inhibiting influence on the development of modes, irrespective of the hydrodynamic and thermal boundary conditions. These results are shown separately in the Table 14 (last row).

Comparison of results with constant heat flux boundary conditions (column 3 and 4 in Table 14) shows that at lower shears (Ri = 5.0) the growth rate of the modes is practically unchanged. However, with an increase of vertical shear the

Table 14. Stability characteristics of unstable transverse modes with different thermal boundary conditions for different values of Ri and wave number ratio k_y/k_x. It may be noticed that with the increase of shear in the basic current, modes are more stable with constant heat-flux boundary conditions than with conducting boundaries. Comparison with couette flow results for the same Ri and ratio k_y/k_x shows the constant shear flow has a stronger suppressing influence on the growth of the thermal mode than does the cubical flow with curvature.

$\frac{k_y}{k_x}$	Ri	(a) σ_r	(a) C_r	(b) σ_r	(b) C_r
0.05	5.0	.649	.672	.648	.694
	2.0	.324	.679	.289	.704
	1.0	.122	.691	.065	.70
0.1	5.0	.650	.674	.650	.695
	2.0	.326	.68	.291	.705
	1.0	.124	.691	.067	.70
	0.5	-.07	.734		
0.5	5.0	.670	.714	.679	.734
	2.0	.357	.719	.333	.745
	1.0	.169	.73	.125	.748
1.0	5.0	.698	.673		
	2.0	.402	.676	.395	.7
	1.0	.235	.684	.213	.709
*0.1	2.0	.317	.558	.269	.58
	1.0	.104	.573		

(a) - conducting boundaries

(b) - constant heat-flux boundaries

* - Couette flow

modes appear more stable in constant heat-flux boundary conditions. The only stabilizing influence present in the system is the shear of this basic flow since we have seen already that the rotational influence is negligible. The viscous influence on these modes are not separately considered due to lack of proper estimation of the eddy coefficients. However, the viscous influence exists. From the above result it is clear that the additional buoyant energy available because of the constant heat flux assumption goes mainly to increase the shear of the horizontal flow.

A consideration of vertical profiles of perturbations, momentum flux, and sensible heat-flux would be appropriate at this juncture. Such a consideration may point out the mechanism by which the modes are stabilized by a change in thermal boundary conditions. Through an inspection of the vertical profiles of w and θ in Figs. 23a, 23b, 24a and 24b one can see that, with constant heat flux boundary conditions, the amplitude of the temperature perturbations is considerably decreased while the amplitude of the w perturbations remains almost the same as that for conducting boundaries. Thus, one can expect that the transport of heat from the bottom to the top of the convective layer with constant heat-flux boundaries to be less than that in this case of constant temperature boundaries. A comparison of the perturbation velocity components in the x- and y-directions as shown in Figs. 23c and 24c indicates that the perturbation kinetic energy is

considerably enhanced with constant heat flux boundary conditions. This can also be seen from the increase in the horizontal momentum transport. The decrease in amplitude of $\hat{\theta}$ suggests that potential energy is a primary source for unstable perturbations; this is characteristic of thermal type perturbations. A comparison of sensible heat flux ($w\hat{\theta}$) profiles shown in Figs. 23f and 24f shows that there is less heat transport with constant heat flux boundaries.

The profiles in Figs. 23e and 24e compare the transport of horizontal momentum. It is seen from the profiles that a greater amount of momentum is transported upwards (shown by the increase in amplitude in positive direction) against the gradient of the mean flow. As previously stated this has been shown by Asai (1970a) to be the mechanism which increases the shear of the horizontal flow.

A typical structure of transverse modes, for constant flux boundary conditions, is shown in Figs. 25a, 25b, 25c and 25d. It is clear from the structures that the horizontal component of the perturbation velocity as well as w are inclined in the midlevels in the direction of the flow. This type of inclination always results in a transport of momentum upwards. However, the maximum temperature perturbation occurs, not at the mid level of the convective layer, but closer to the free upper boundary. A similar structure (not shown) is obtained with conducting boundaries. From the structure it appears that this is connected with asymmetric

hydrodynamic boundary conditions. The y-component of the perturbation velocity (v) appears without any distortion and the phase shifts appear to be very regular. Since a systematic study of the energy exchange with respect to each component of the flow has not been considered here it is not known whether this is of general nature.

5.6.2. Longitudinal Modes

In this section we proceed to a consideration of longitudinal modes or bands. As mentioned earlier the bands or rolls are oriented in the direction of the basic flow in contrast with transverse bands, which are located across the direction of flow. We have already seen that transverse bands are more stabilized under constant heat flux boundary conditions by an increase in the shear of the flow or by transport of momentum against the gradient of the mean flow. As before we specify the geometry of the mode through the specification of the ratio of the wave number in the x- and y-directions. If $k_y > k_x$ longitudinal bands are specified; this limit is practically attained if $\frac{k_y}{k_x} > 10.0$. Table 15 summarizes the results obtained for the various specifications of the ratio $\frac{k_y}{k_x}$. The first row refers to square cells or modes whose ratio is exactly equal to one. For the same ratios the results obtained by the change of thermal boundary conditions are given in the third major column. The first column refers to the specified ratio. The second column refers to the shear of the flow expressed in terms of the dimensionless Richardson

Table 15. Variation of phase velocity (Cr) and amplification rate (σ_r) of unstable longitudinal modes with different thermal boundary conditions as a function of Ri and wave number ratio k_y/k_x. It may be noticed that the modes are more unstable with constant heat flux boundaries than with constant temperature boundaries, irrespective of the value of Ri, in contrast with the results obtained for transverse modes (Table 14).

$\frac{k_y}{k_x}$	Ri	(a) σ_r	(a) C_r	(b) σ_r	(b) C_r
1.0	5.0	.698	.673	.724	.69
	2.0	.402	.676	.395	.70
5.0	5.0	.737	.683	.795	.693
	2.0	.465	.683	.498	.693
	1.0	.327	.684	.347	.695
10.0	5.0	.738	.689	.799	.694
	2.0	.467	.689	.505	.7
	1.0	.331	.689	.356	.7
	0.5	.234	.689	.251	.7
20.0	2.0	.468	.71		
*10.0	2.0	.468	.523	.505	.544
	1.0	.331	.527		

(a) - conducting boundaries

(b) - constant heat flux boundaries

* - Couette flow

number. The conditions specified for the computations are given at the end of the table. The results found in Table 15 are plotted in the same graph which shows the transverse band results. A quick glance at the graphs (Figs. 21 and 22) immediately reveals that the growth rates are generally higher than those of the transverse bands for the same shear. Thus, we may conclude the longitudinal mode is the preferred type of convection under the conditions assumed in this study. Since specified zonal flow contains variable shear the amplification rates are not equal at higher values of $\frac{k_y}{k_x}$, irrespective of the shear. In Table 15 the last row refers to the results obtained for Couette flow. An inspection of the results shown in Table 15 reveals that the longitudinal modes are more stable with conducting boundaries than they are with constant heat flux thermal boundary conditions. Thus, it is clear that the system is more gravitationally unstable under constant heat flux conditions since there is no decrease of perturbation temperature by conduction. It may be seen from Table 15 that the phase speed of longitudinal modes is practically unaltered. An increase in the ratio of $\frac{k_y}{k_x}$ to more than 10.0 does not substantially alter the results.

A comparison of results obtained under the same conditions, with a Couette flow profile, shows that longitudinal modes are practically independent of the distribution

of the shear in the basic current. From the results it is obvious that the energy transfer in longitudinal perturbations is substantially different from that of transverse perturbations. It will be instructive to consider the structure of longitudinal perturbations and compare that structure for two different boundary conditions.

Structure of the Modes

The profiles of the perturbation vertical velocity (w), temperature (θ), horizontal transport of momentum (UW), and heat flux (θW) for conducting boundaries are shown in Figs. 26a, 26b, 26c and 26d, respectively, for Ri = 1.0. For comparison, the corresponding profiles with constant flux boundaries are given in Figs. 27a, 27b, 27c and 27d for the same shear. A noticeable difference observed in the w profiles with constant flux boundaries (Fig. 27a) is that the maximum amplitude is located in the upper half of the convective layer. An opposite feature is noted with conducting boundaries (Fig. 26a). Fig. 27b shows that the maximum amplitude of the temperature perturbations occurs at the surfaces (top and bottom) due to the imposed boundary conditions. In the convective layer itself the amplitudes are almost constant. The profiles of the perturbations are not normalized with respect to a particular level of the convective layer since asymmetric boundary conditions and an asymmetric wind profile is utilized. From Figs. 26c and 27c it is clear that the

longitudinal mode transports large negative momentum to the rigid surface, compared to transverse modes. However, with conducting boundaries the transfer of momentum is mainly confined to the lower half of the convective layer (Fig. 26c). The sensible heat flux, averaged over the entire layer, is upwards; with constant heat flux boundaries there is a tendency to transport more heat in the upper half of the convective layer (Fig. 27d). This may have some significance in heat exchange between the PBL and the synoptic flow above the boundary layer. We find from Fig. 26d that with conducting boundaries there is counter gradient heat transport at some levels; however, this is quite small. This may be due to the mechanical (shear) effect. This does not appear with constant flux boundaries since there is more buoyant energy available. The structure of the perturbations W, θ, and U for conducting boundaries is shown in Figs. 28a, 28b, and 28c. The ordinate is height of the convective layer and the abcissa is a full wavelength in the x-direction. A remarkable feature that is observed in the structure is the change in the orientation with respect to the mean flow in the middle of the layer. In the lower half of the layer both w and θ perturbations in Figs. 28a and 28b are oriented against the direction of the mean wind; but in the upper half of the layer their orientation is the same as the transverse mode, i.e., in the direction of the mean flow. The orientation of U-perturbations shown in Fig. 28c is exactly

opposite to that of the W, θ perturbations. In general the phase angle between the W and U perturbations is out of phase. However, W and θ perturbations are in phase with each other in the major portion of the convection layer. These described features probably account for the oscillatory nature in the vertical transport of heat and horizontal momentum shown in Figs. 26d and 26c, respectively.

From the structures shown in Fig. 28 it appears that the inertial influence is strong as it is with longitudinal modes with the same shear. Similar structures are observed at a lower shear, but not at a higher shear, e.g., at Ri = 2.0 such structures are observed but not at Ri = 0.5 (higher shear). This may be taken as indirect evidence, even though not proved by extensive examples, that transverse modes may appear along with longitudinal modes. Since the absolute vorticity of the current does not change sign in the convective layer there can be no inertial modes due to shear only. However, the destabilizing influence of viscous forces is present. In this study we have not found a viscous induced unstable wave. Since we have found that the modes are of thermal origin it appears that the transverse mode-like inclinations are caused by thermal modes only.

5.7. Changes With Prandtl Number

We have used constant isotropic eddy diffusion coefficients and in the absence of a proper estimate of these

coefficients we have assumed their ratio equal to one, which is strictly valid only in neutral conditions. In the computations we specify the effects of transport of heat and momentum through the Prandtl number. Thus, the Prandtl number is an essential parameter in this investigation and choice of this parameter specifies different ratios of eddy coefficients and thus different values of heat and momentum transport. As noted earlier in the discussion of eddy coefficients, observational studies indicate that the coefficient of eddy conduction is considerably greater than the eddy momentum coefficient under unstable conditions. It is desirable to see the effect of such a larger heat conduction coefficient on the stability of the modes. Here we use the following observed values of the eddy coefficients as given by Krishnamurti (1973)

$$K_M = 3.7 \times 10^5 \text{ cm}^2/\text{sec} \; ; \quad K_H = 7.0 \times 10^5 \text{ cm}^2/\text{sec} \; ;$$

these correspond to an eddy Prandtl number equal to 0.53. A lower value of the Prandtl number specifies an increased heat transport. Thus, we can expect an increased growth rate for the unstable modes. Typical results with the change of Prandtl number are shown in Table 16. It is clear, irrespective of the nature of the modes (square, longitudinal or transverse), that the growth rate of unstable modes increases considerably with the specification of higher coefficients of conduction. Since extensive computations were not done a

Table 16. Effect of decreasing Prandtl number on the stability of modes as a function of k, geometry of the modes, and thermal boundary conditions. In the calculations the longitudinal mode is specified by the wave number ratio $k_y/k_x = 1.0$ and the transverse mode by $k_y/k_x = 0.1$.

(a)				(b)			
k	Pr	σ_r	C_r	k	Pr	σ_r	C_r
1.41	0.53	0.282	.663	4.24	0.53	0.252	.974
	1.00	0.174	.678		1.00	0.032	.809
*2.0	0.53	0.466	.67	**2.0	0.53	0.276	.705
	1.0	0.331	.69		1.0	0.068	.70

(a) - conducting boundaries

(b) - constant heat flux boundaries

* - longitudinal mode

** - transverse mode

general conclusion on the nature of the modes and variation of the phase speeds with wave number of perturbations cannot be given. However, it appears that the short wave disturbances attain a phase speed equivalent to that of the free stream velocity. This computation also shows that the increase in the value of eddy coefficients does not give rise to new instabilities of unstable modes. This is to be expected since the zonal flow profile and the boundary conditions have not been altered.

CHAPTER VI

SUMMARY AND CONCLUSIONS

The numerical model developed in this investigation has dealt with thermal convection associated with organized cloud patterns which occur below a stable layer in the atmosphere. Since the stable layer does not directly contribute energy for the development of the patterns it has been neglected. In this investigation we have considered the influence of vertical shear on the development of the patterns and have determined the preferred scale of growth of these patterns. The necessary shear is specified by assuming a zonal flow with a variable shear in the convective layer.

The formulation differs from other investigations in the assumed boundary conditions and in the specification of the zonal profile. The convective layer of fixed depth extends infinitely along the x- and y-directions. In the basic state variations in y-direction have been neglected. Thus, the basic flow was made unidirectional for simplicity. A flat bottom topography was assumed. The effect of the earth's rotation was retained, thereby allowing the development of motion perpendicular to the x-z plane. Inclusion of the Coriolis force also allows us to include the shear and shear

gradient of the flow directly in the relevant equation.

In the first part of the investigation conducting boundaries were assumed. In the second part of the investigation we assume constant heat flux on the boundaries. Thus, the influence of thermal boundary conditions on the convection is determined.

The shape of the cells was specified to be 'square' or 'rectangular'. The problem is then studied by varying the shear in the flow for different specifications of the cell size.

Constant isotropic and equal eddy coefficients were used to represent dissipative effects in the convective layer. The basic state of the system is unstably stratified and is kept constant throughout the period of investigation. The wavelength of the imposed perturbation ranges from 1-20 km. Cases with and without rotation were investigated for different shears in the basic flow. The structure of the unstable perturbations was analyzed to determine the nature of the developed modes.

The following significant results were obtained in this investigation:

1. Corresponding to each wavelength there is found to be a single unstable mode whose stability decreases as the vertical shear is increased. The appearance of a single mode has been traced to the asymmetrical boundary conditions.
2. The unstable mode has its maximum growth rate which

corresponds to a single wavelength and this wavelength decreases with decrease of shear. The maximum unstable wavelength for large shear appears to be about 5 km while at lower shears this decreases to about 2 km.

3. With rotation the longer wavelength mode stabilizes; only a slight destabilization has been noticed in the lower wavelength range. The destabilization is traced to the influence of viscosity as no other destabilizing influence is present in the system. However, the quantitative influence of viscosity is not clear.

4. The phase speed of the unstable modes are slightly higher than the average velocity of flow, averaged throughout the convective layer. Considering amplification rate and structure these are recognized as mixed modes, i.e., a combination of gravity-type disturbances and long wave convective type modes. The structures also show a sharp turn in the middle of the layer, i.e., inclination in the direction of the basic current with moderate shear.

5. The influence of variable shear on the stabilization of the modes appears to be much less than that in constant shear flow. In other words, the cubical profile flow which has decreasing shear with height exerts a weaker influence on the stability of the modes than does Couette flow under the same conditions.

6. The influence of constant heat flux boundaries with shear in the basic flow appears to be very small. Only a slight increase in the wavelength of the most unstable mode

is noticed for all shears. In the absence of zonal flow the maximum amplified wavelength corresponds to about 2 km. This is in contradiction with Sasaki's (1970) results.

7. The finite-difference scheme is not sensitive enough to detect the viscous unstable mode which can appear in this system with high shears.

8. The amplification rate of unstable modes increases if smaller values of the Prandtl number are utilized. A larger Rayleigh's number, which in this investigation denotes a higher temperature difference between the boundaries does not alter the preferred scale of the perturbations. However, the range of the instability increases towards lower wavelengths.

9. Heat flux counter to the gradient of basic state temperature appeared in small portions of the convective layer, especially near the top. This appears to be due to the asymmetrical hydrodynamic boundary conditions utilized.

An appropriate extension of this study may be to include a nonlinear temperature distribution in the convective layer instead of the linear temperature distribution assumed here. This might simulate the real physical situation of ascending and descending currents observed in the atmosphere. Since in the atmosphere the cellular patterns appear in distorted shapes solutions may be tried by specifying shape factors for the perturbations other than the simple 'square' cell specified here. Of course, generalization to consider nonlinear effects remains a possibility.

REFERENCES

Agee, E. M. and T. S. Chen, 1973: A model for investigating eddy viscosity effects on mesoscale cellular convection. J. Atmos. Sci., 30, 180-188.

Asai, T., 1964: Cumulus convection in the atmosphere with vertical wind shear, numerical experiment. J. Meteor. Soc. Japan, 42, 245-249.

_____, 1970a: Three dimensional features of thermal convection in plane Couette flow. J. Meteo. Soc. Japan, 48, 18-29.

_____, 1970b: Stability of a plane parallel flow with variable shear and unstable stratification. J. Meteor. Soc. Japan, 48, 128-139.

Barnes, S. L., 1967: Effects of large scale subsidence on cellular convection in the atmosphere. A numerical experiment. Ph.D. Thesis, University of Oklahoma, pp. 109.

Batchelor, G. K., 1954: Heat convection and buoyancy effects in fluids. Quart. J. R. Met. Soc., 80, 339-358.

Chandrasekar, S., 1953: The instability of a layer of fluid heated from below and subject to Coriolis forces. Proc. Roy. Soc. A., 217, 306-327.

Deardorff, J. W., 1965: Gravitational instability between horizontal plates with shear. Phys. of Fluids, 8, 1027-1030.

Frenzen, P. and Y. Nagakawa, 1955: Experimental study of cellular convection. Tellus, 7, 1-21.

Gage, K. S. and W. H. Reid, 1967: The stability of thermally stratified plane Poiseuille flow. J. Fluid. Mech., 53, 21-32.

Gallagher, A. P. and A. Mcd. Mercer, 1965: On the behavior of small disturbances in plane Couette flow with temperature gradient. Proc. Roy. Soc. A., 286, 117-128.

Haltiner, G. J. and F. L. Martin, 1957: Dynamical and Physical Meteorology. New York, McGraw-Hill Book Co., pp. 470.

Jefferys, H., 1928: Some cases of instability in fluid motion. Proc. Roy. Soc. A., 118, 195-208.

Konrad, 1968: The alignment of clear air convective cells. Proc. Inst. Comp. Cloud Physics, Toronto, Canada 539-543.

Krishnamurti, R., 1973: On cellular cloud patterns, Part I. Mathematical Model Tech. Report, pp. 30.

Kuettener, J., 1959: The band structure of the atmosphere. Tellus, 11, 267-294.

_____, 1971: Cloud bands in the earth's atmosphere. Tellus, 23, 404-425.

Kuo, H. L., 1963: Perturbation of plane Couette flow in stratified fluid and the origin of cloud streets. Physics of Fluids, 6, 195-211.

Lin, C. C., 1955: The Theory of Hydrodynamic Stability. Cambridge University Press, pp. 155.

Lipps, F., 1971: Two dimensional numerical experiments in thermal convection with vertical shear. J. Atmos. Sci., 28, 3-18.

Mitchell, R. L., 1967: Some considerations of cellular cloud patterns in the atmosphere. M.S. Thesis, University of Oklahoma, 58 pp.

Pellew, A. and R. Southwell, 1950: On the maintained convective motion in a fluid heated from below. Proc. Roy. Soc. A., 176, 312-342.

Ray, D., 1965: Cellular convection with non isotropic eddys. Tellus, 17, 434-439.

Rayleigh Lord, 1916: On convective currents in a horizontal layer of fluid when high temperature is on the under side. Phil. Mag., 32, 529-546.

Riehl, H., 1965: Introduction to Atmosphere, McGraw Hill, pp. 345.

Rosenhead, L., ed., 1963: Laminar Boundary Layers. Clarendon Press, pp. 687.

Sasaki, Y., 1965: Formation of cellular patterns in the lower atmosphere. Final Report, U.S.W.C. Cwb-10863, 1-18.

_____, 1970: Influences of thermal boundary layer on atmospheric cellular convection. J. Meteor. Soc. Japan, 48, 492-502.

Sparrow, E. M., et al., 1964: Thermal instability in a horizontal fluid layer: Effect of boundary conditions and non-linear temp-profile. J. Fluid. Mech., 18, 513-538.

Sutton, O. G., 1953: Micrometeorology. New York, McGraw-Hill, pp. 333.

Wong and K. C. Brundidge, 1966: Vertical and temporal distributions of heat conductivity and flux. J. Atmos. Sci., 23, 167-178.

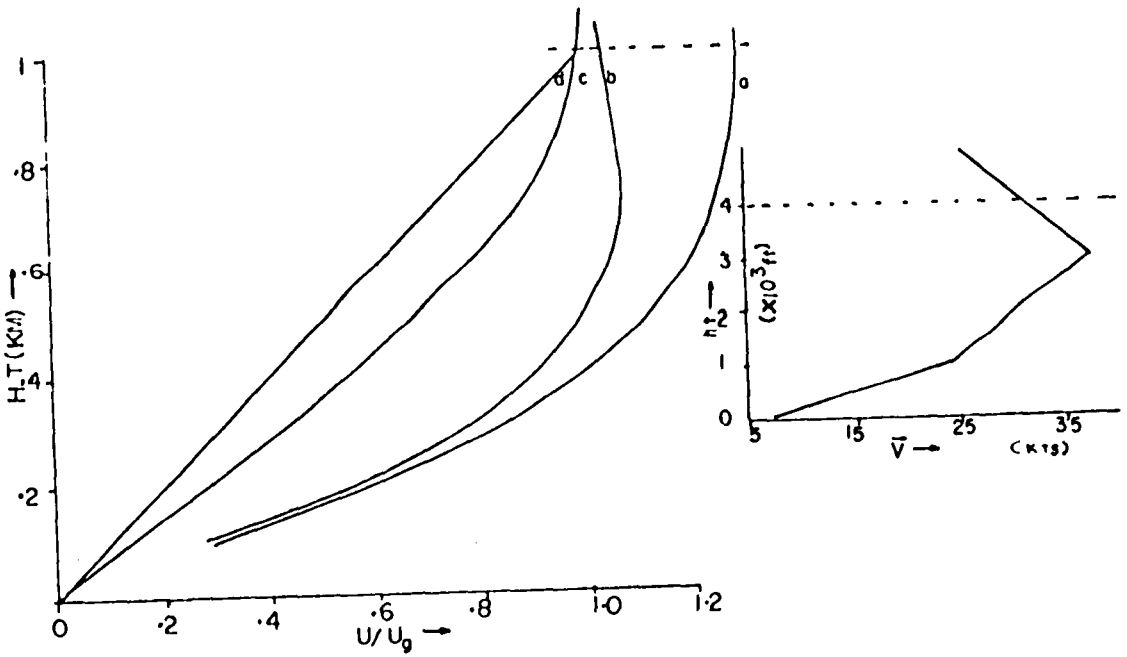

Fig. 1. Velocity profiles for (a) baroclinic Ekman flow, (b) barotropic Ekman Flow, (c) polynomial approximated flow, and (d) Couette flow. The ratio of the component to the geostrophic speed (Ug) is shown on the abscissa. In calculations for (a) and (b) $K = 5 \times 10^4$ cm^2/sec, $f = 10^{-4}$ sec^{-1} and $B_1 = 2.5 \times 10^{-3}$ sec^{-1}. The inset diagram shows an observed velocity profile with organized convection (taken from Kuttener 1971).

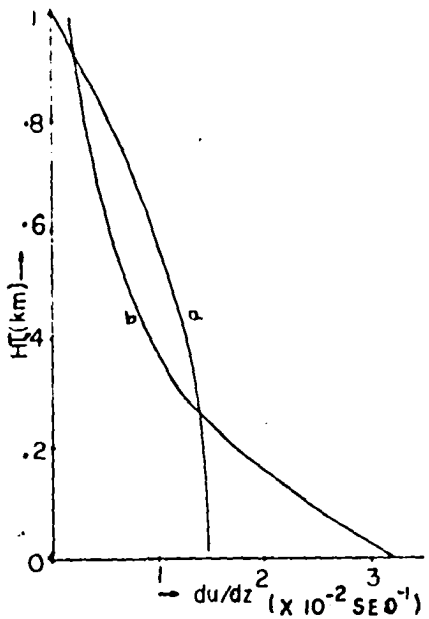

Fig. 2. The vorticity profiles associated with the basic flow approximated by (a) cubical polynomial and (b) x-component of baroclinic Ekman flow.

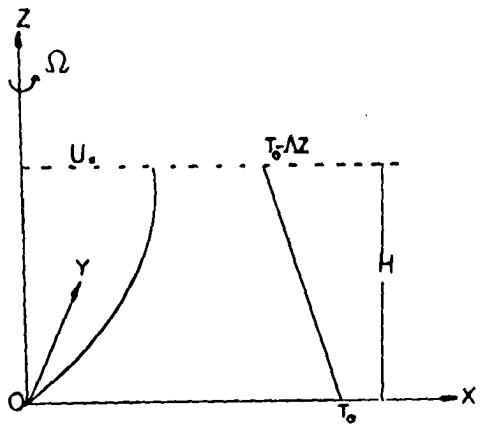

Fig. 3. Equilibrium configuration of the physical model. The curve and the inclined straight lines schematically represent the basic flow and temperature distribution, respectively.

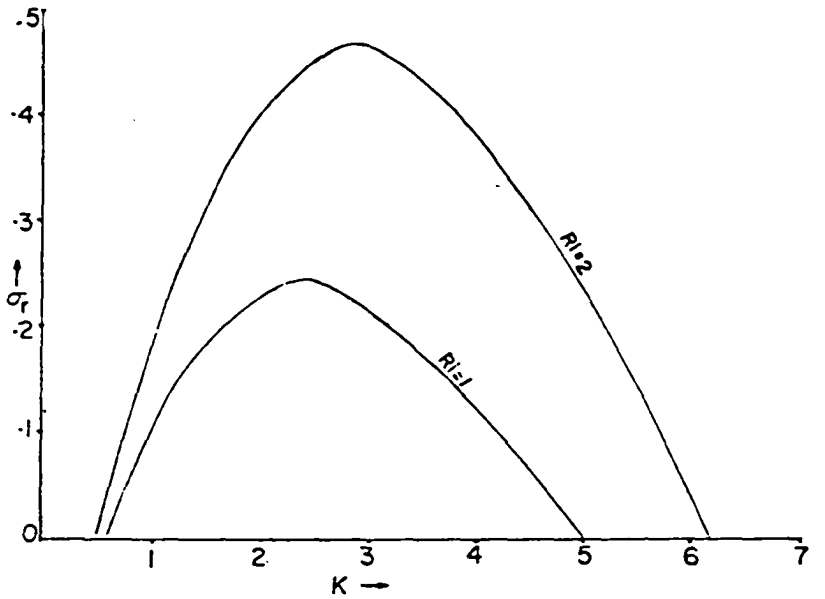

Fig. 4. Amplification rate (σ_r) of unstable modes with different shears (Ri) in the basic current as a function of wave number (k) for the case with no rotation and conducting thermal boundary conditions. In this and in subsequent figures $k_x = k_y$ unless otherwise indicated.

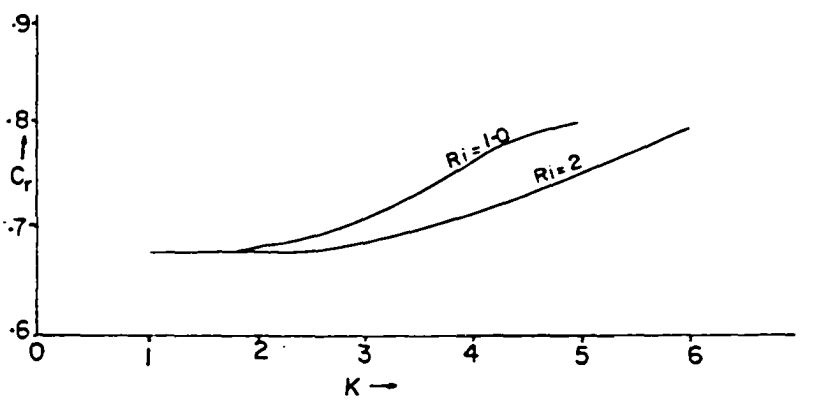

Fig. 4a. Phase velocity (C_r) of unstable modes corresponding to Fig. 4.

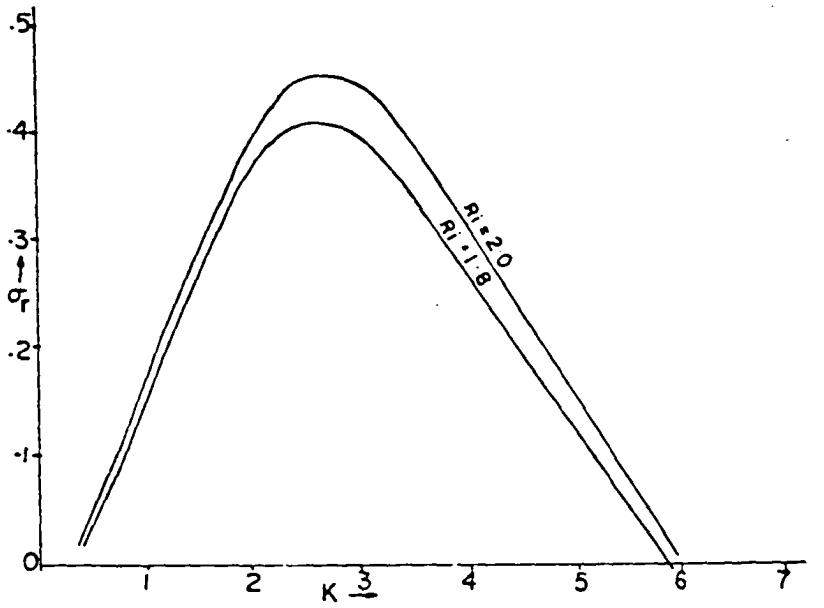

Fig. 5. Amplification rate of unstable perturbation as a function of wave number for different values of Ri with no rotation and constant heat flux thermal boundary conditions.

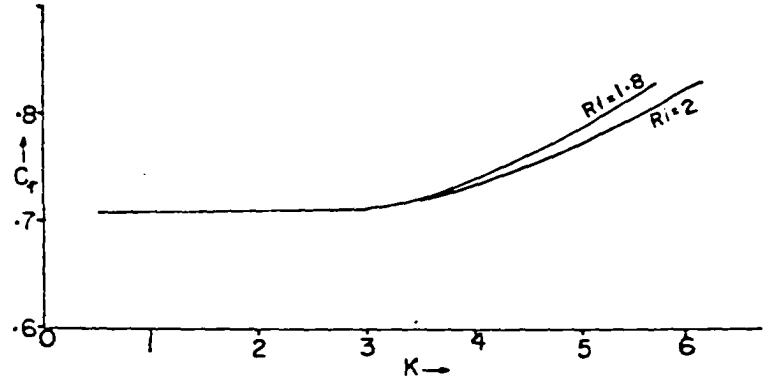

Fig. 5a. Phase velocity of unstable modes corresponding to Fig. 5.

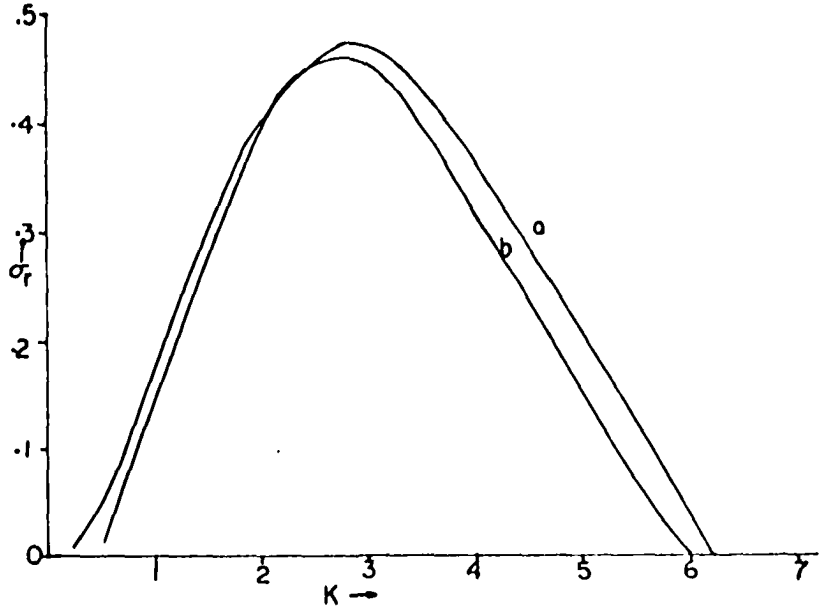

Fig. 6. Comparison of growth rates of unstable perturbations with no rotation and different thermal boundary conditions as a function of k for Ri = 2.0, (a) conducting boundaries and (b) constant heat flux boundaries.

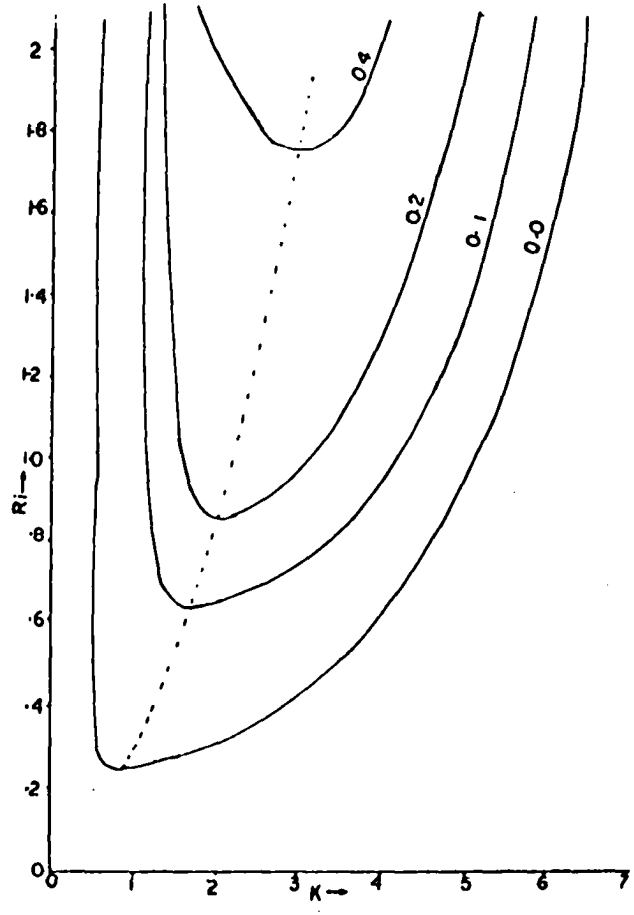

Fig. 7. Stability diagram with conducting boundaries and rotation as a function of Ri and k. The amplification rate is marked on solid lines. The dashed line shows the preferred perturbation at different Ri.

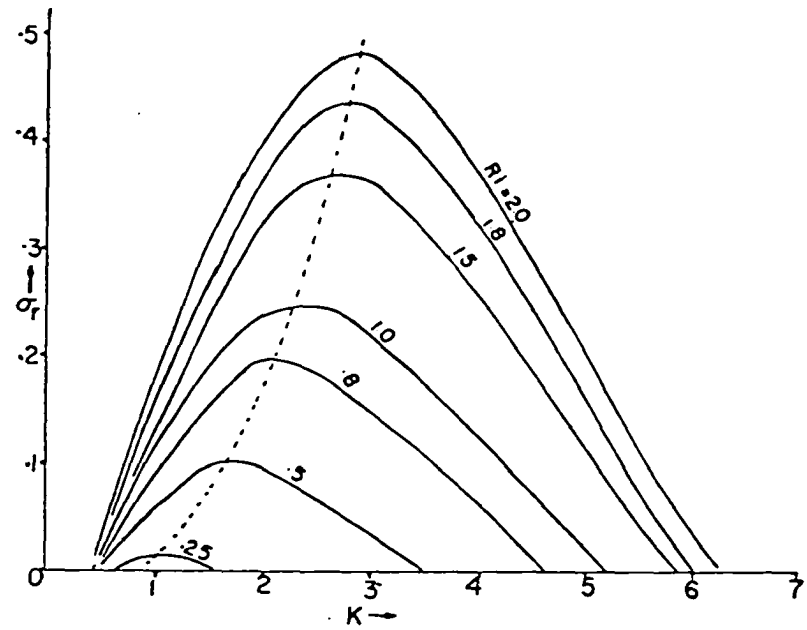

Fig. 8. Variation of amplification rate of perturbation as a function of k at different Ri. The perturbations with maximum growth rate are indicated by the dashed line.

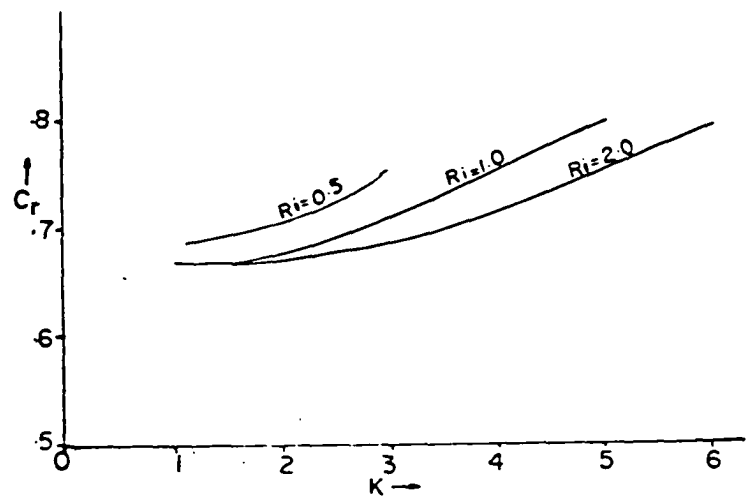

Fig. 9. Phase velocity of unstable modes corresponding to Fig. 8 as a function of k and Ri.

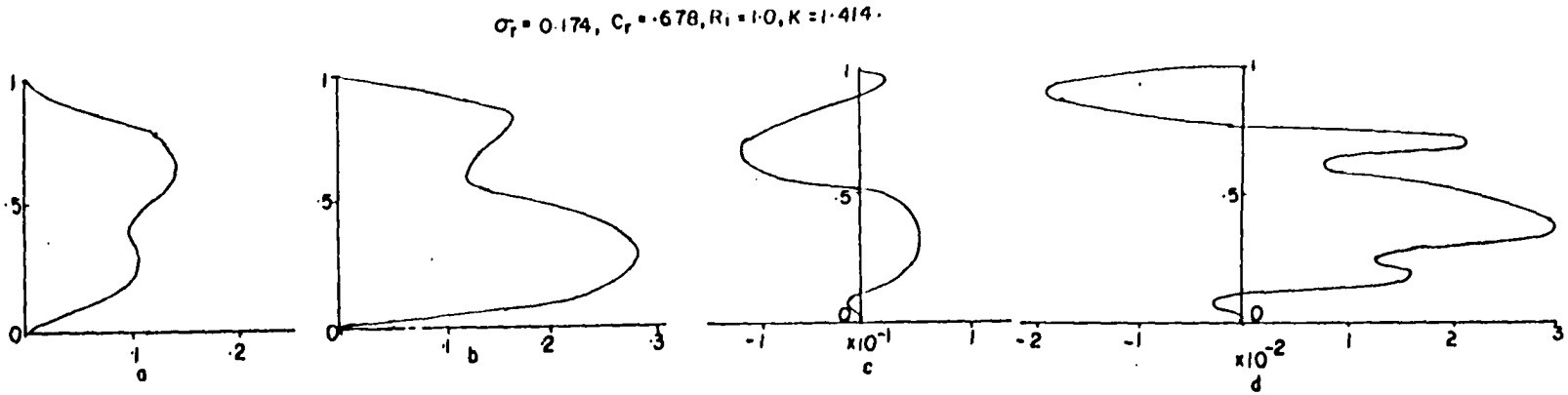

Fig. 10. Vertical profiles of the amplitudes of (a) vertical velocity (w), (b) temperature (θ), transport of, (c) horizontal momentum (uw) and (d) heat (θw) for Ri = 1.0, k = 1.414 with rotation and conducting boundary conditions. In this and in subsequent vertical profiles the ordinate is the height of the convective layer while the magnitude is shown on the abscissa.

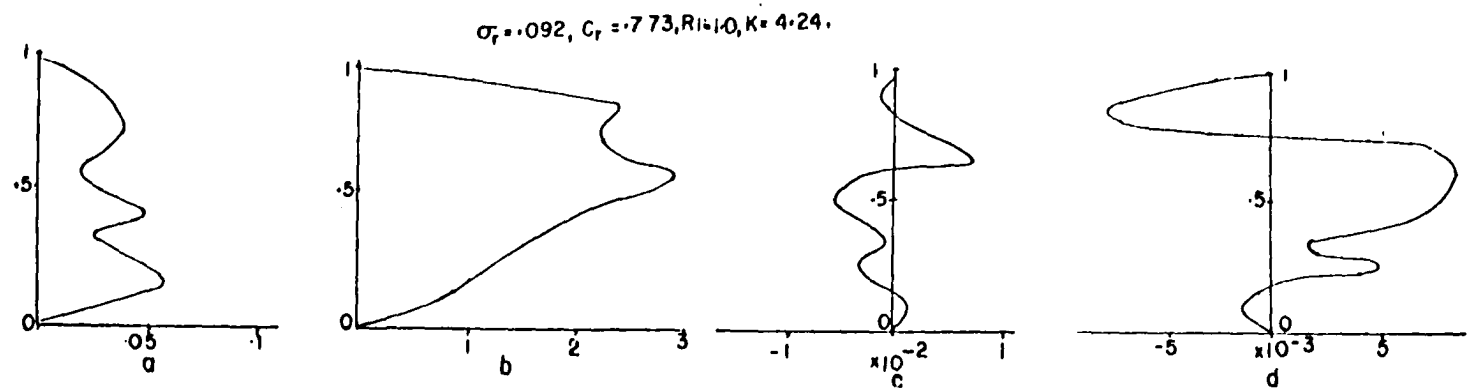

Fig. 11. Same as Fig. 10 except k = 4.24 (short wavelength perturbation).

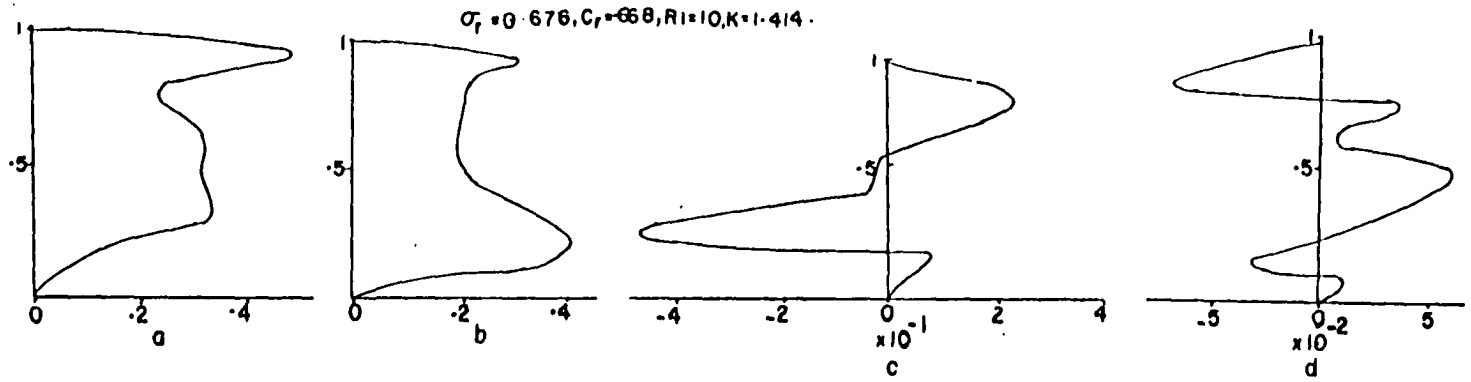

Fig. 12. Same as Fig. 10 except Ri = 10.0 (lower shear).

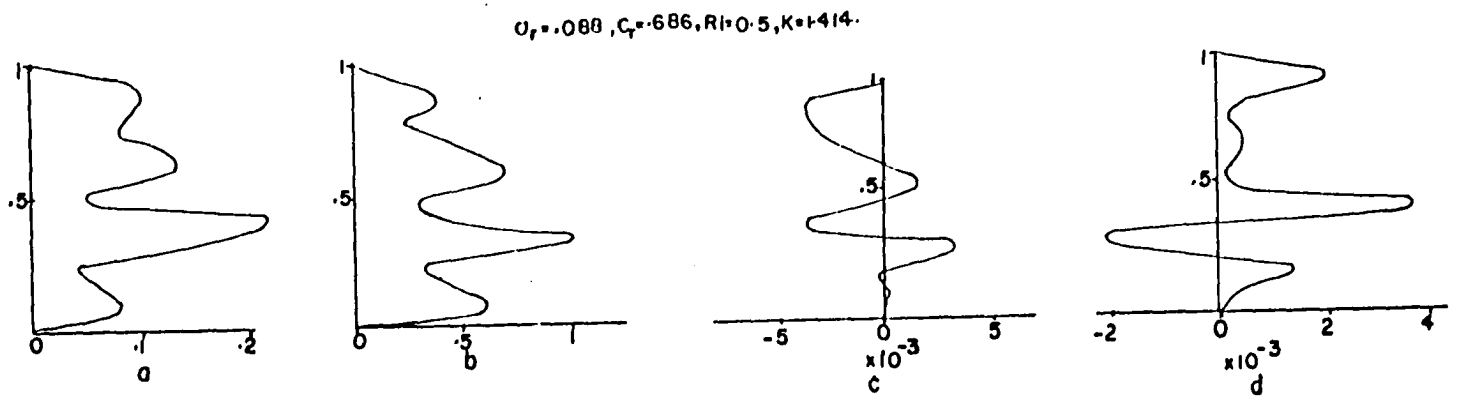

Fig. 13. Same as Fig. 10 except Ri = 0.5 (high shear).

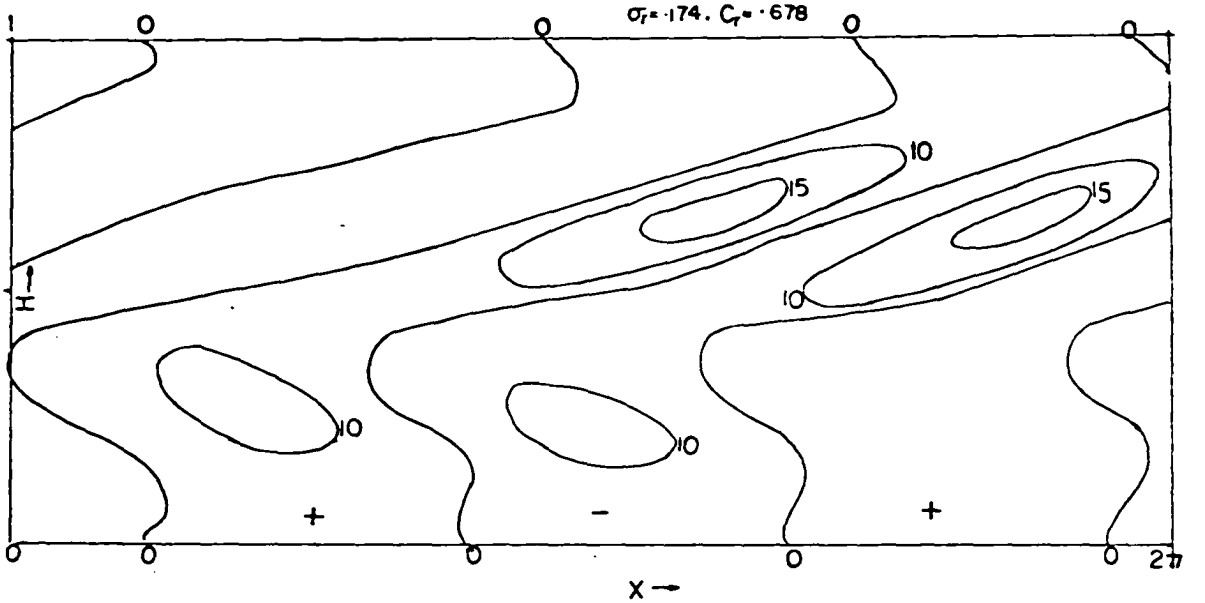

Fig. 14a. Structure of vertical velocity (w) of unstable mode with rotation and conducting boundaries for Ri = 1.0, k = 1.414. In this and in subsequent structure diagrams the ordinate represents the dimensionless height of the convective layer while the abscissa represents one full wavelength of the perturbations. The velocities are scaled with respect to free stream velocity (U_*) and temperatures with respect to imposed temperature difference (τ^*).

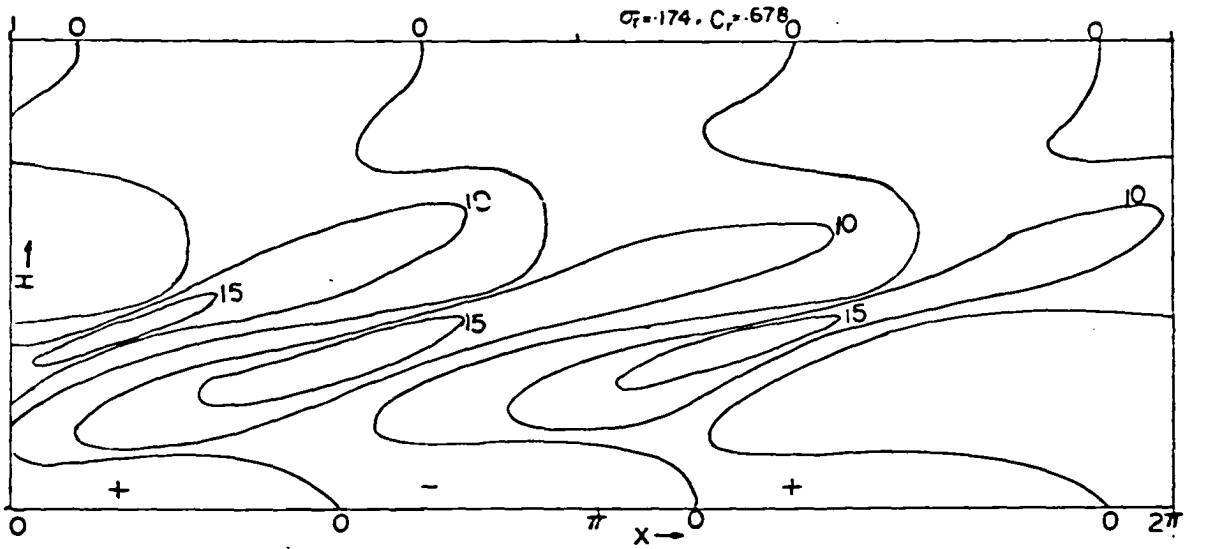

Fig. 14b. Structure for temperature perturbations for the same conditions as shown in Fig. 14a.

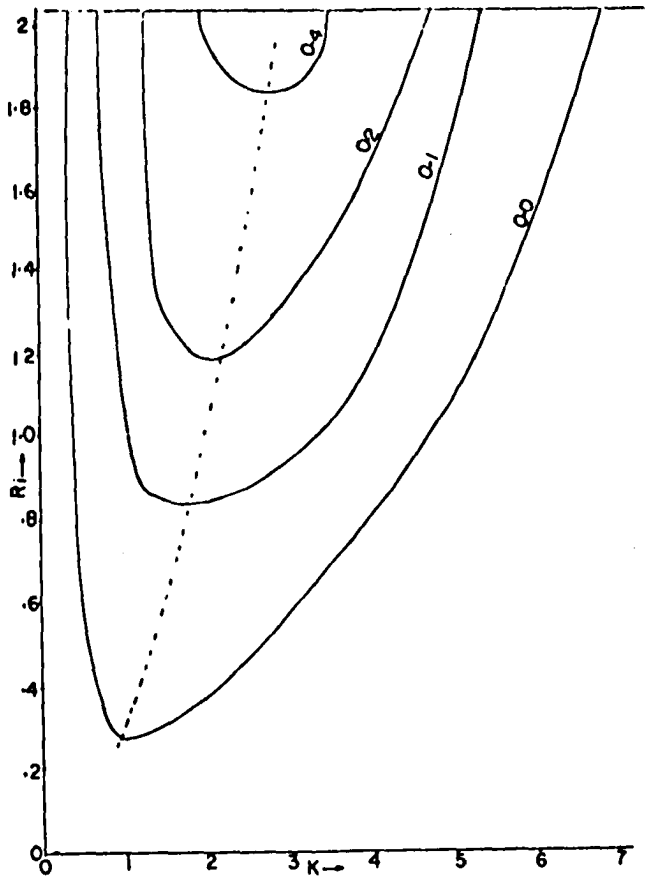

Fig. 15. Stability diagram for the case with rotation and constant heat flux boundaries as a function of Ri and k. Solid lines denote the amplification rate of unstable perturbations; the dashed line shows the preferred perturbation at each Ri. The curve representing zero amplification rate separates the stable and unstable domains.

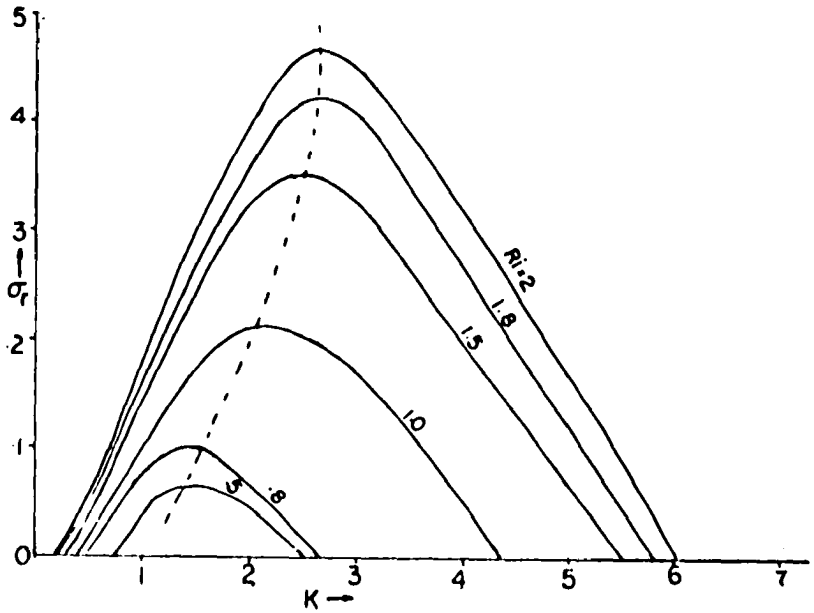

Fig. 16. Variation of amplification rate of unstable perturbations with k for different values of Ri; same as in Fig. 15.

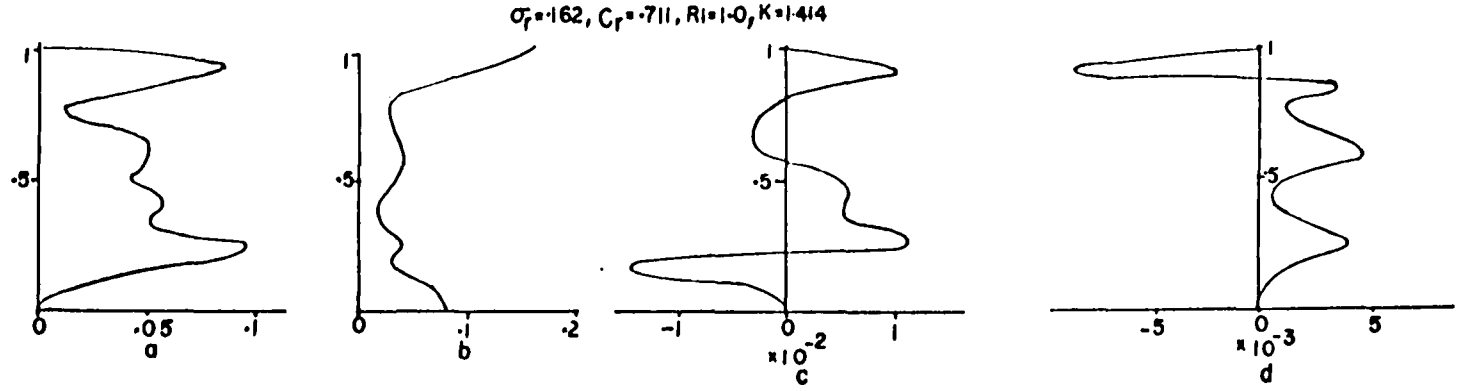

Fig. 17. Vertical profiles of the amplitudes of (a) vertical velocity (w), (b) temperature, and transport of, (c) horizontal momentum (Uw), and (d) heat flux (θw). This diagram is for Ri = 1.0, k = 1.414 with constant heat flux boundaries.

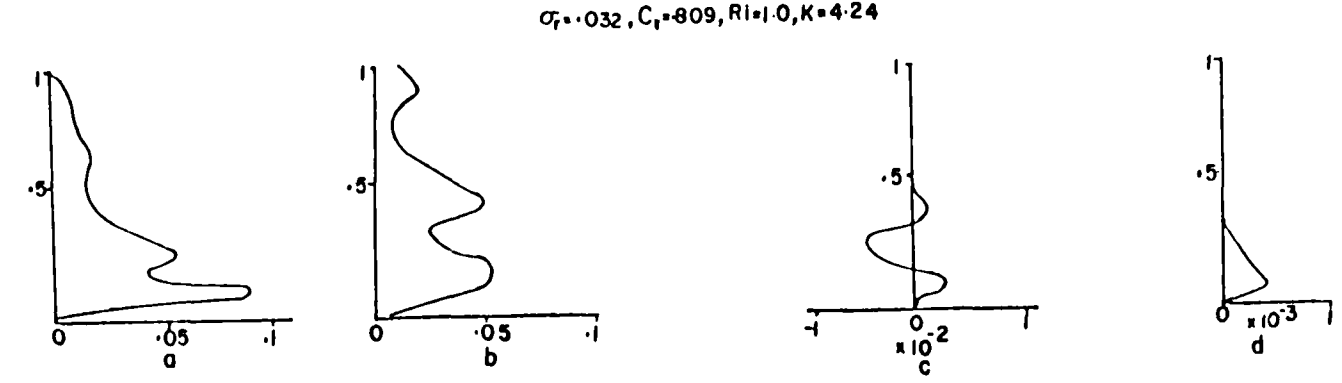

Fig. 18. Same as Fig. 17, except k = 4.24.

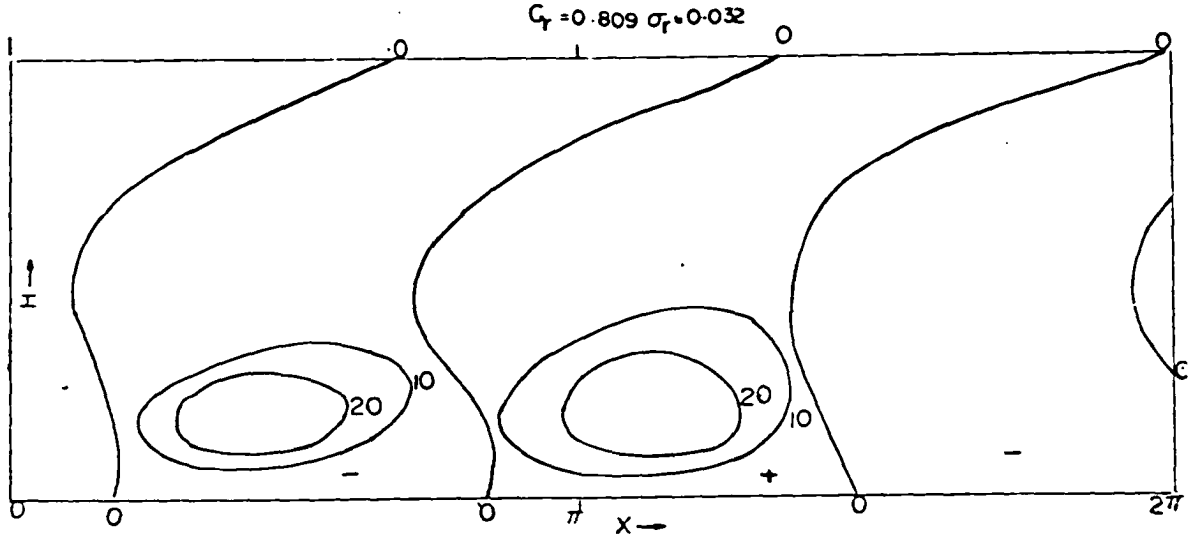

Fig. 19a. Structure of vertical velocity (W) perturbations for k = 4.24 with Ri = 1,0 and constant heat flux boundaries.

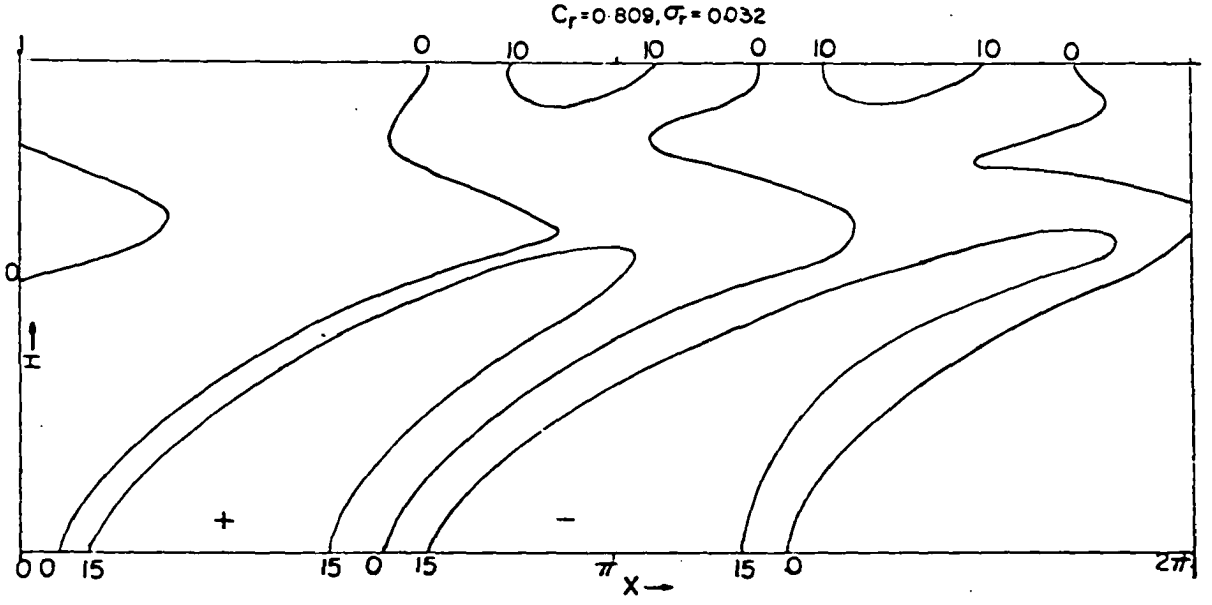

Fig. 19b. Same as Fig. 19a except this diagram is for temperature perturbations.

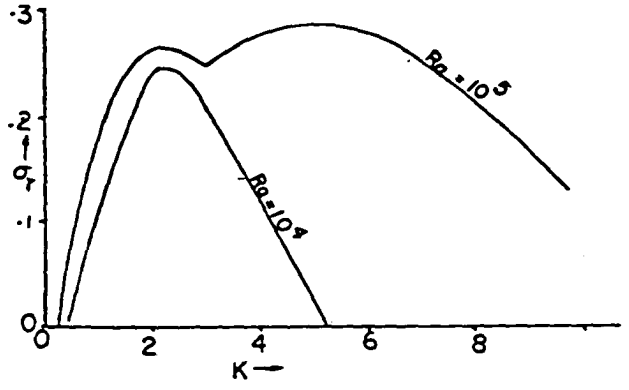

Fig. 20. Variation of amplification rate with rotation and conducting boundaries as a function of wave number for different Ra.

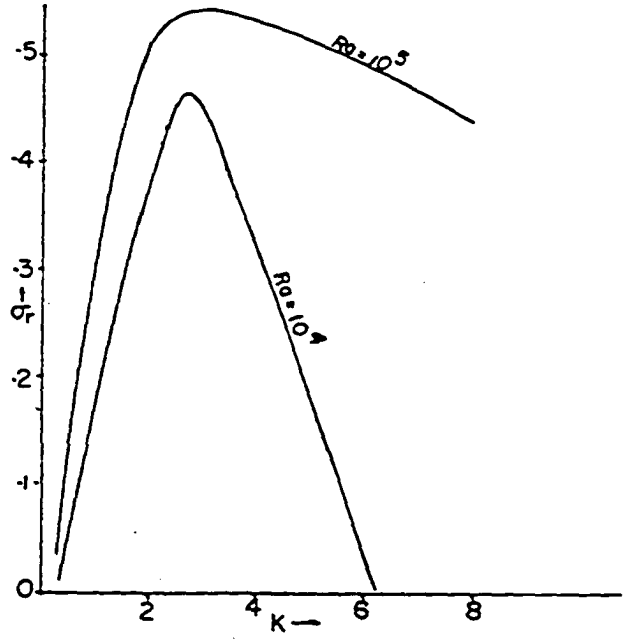

Fig. 20a. Same as Fig. 20 except the thermal boundary conditions correspond to that of constant heat flux.

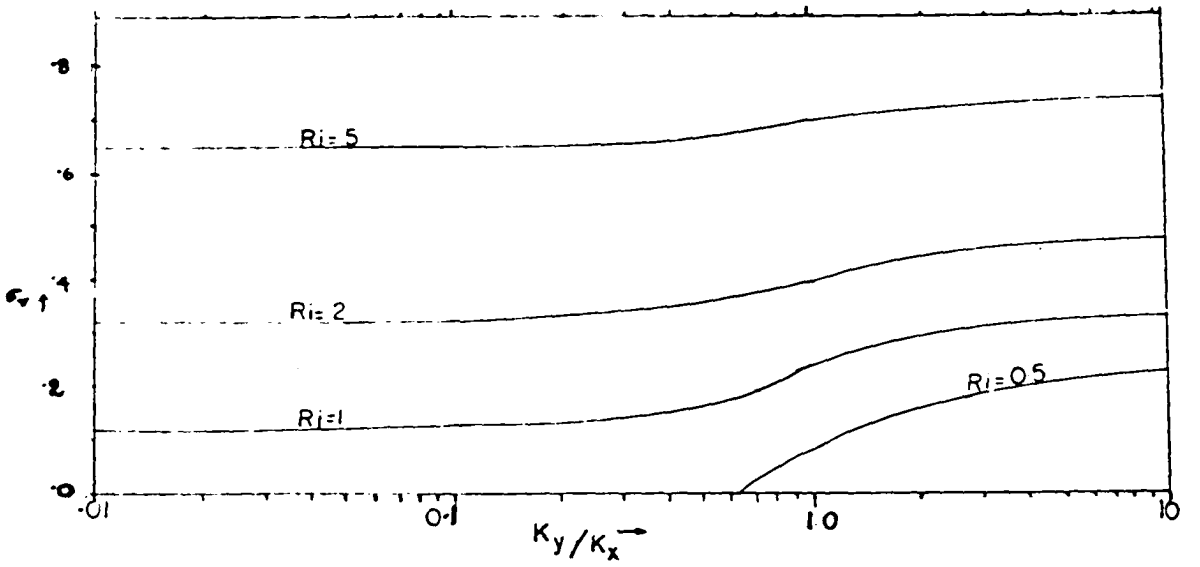

Fig. 21. Variation of growth rate of the unstable modes with rotation and constant temperature boundaries as a function of wave number ratio k_y/k_x for different values of Ri. $k_y/k_x \gtrless 1$ specifies longitudinal, square, and transverse modes, respectively.

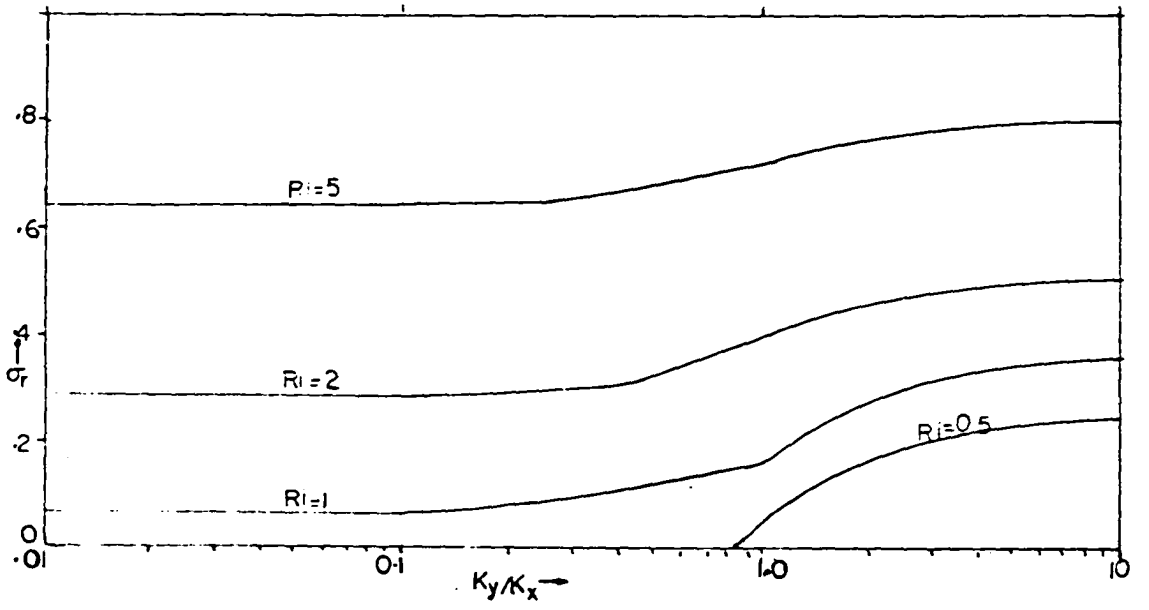

Fig. 22. Same as Fig. 21, except the constant heat flux boundary condition is specified.

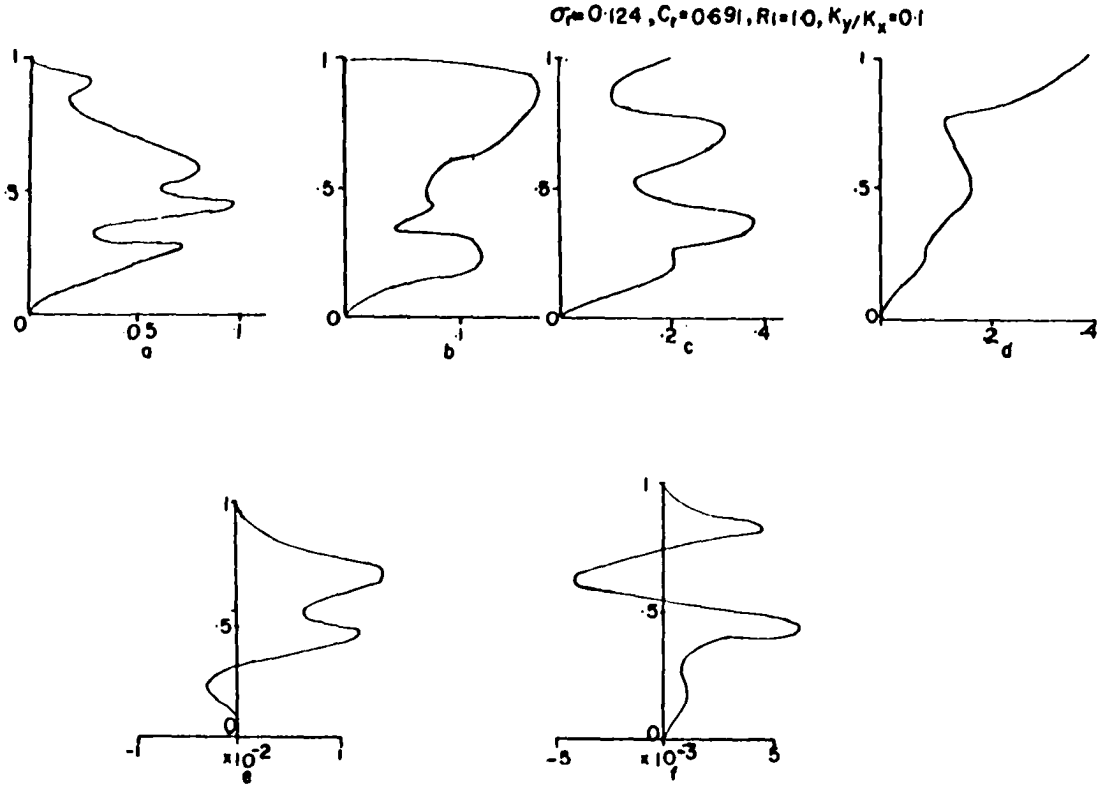

Fig. 23. Transverse mode - vertical profiles of (a) vertical velocity (w), (b) temperature (θ), and (c) and (d) horizontal velocity components (u) and (v). The vertical fluxes of horizontal momentum (uw) and heat (θw) are given by diagrams (e) and (f), respectively. These profiles are with conducting boundaries for k = 2.0 and Ri = 1.0.

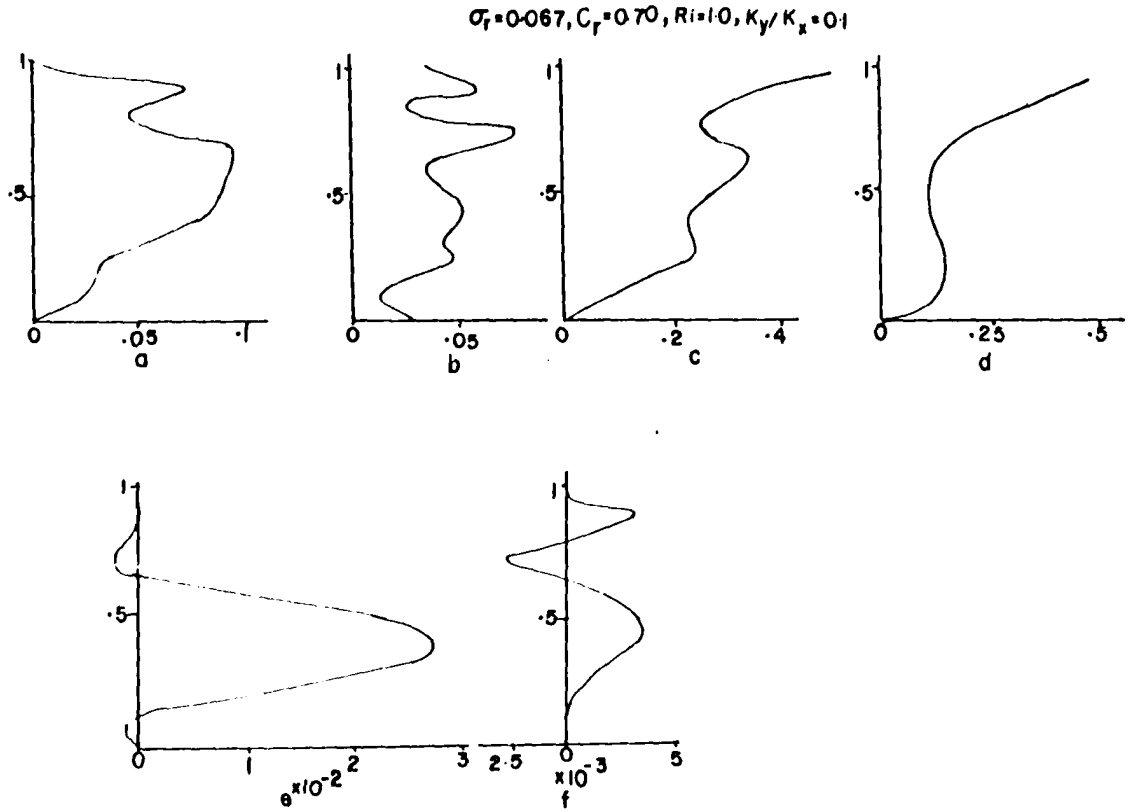

Fig. 24. Same as Fig. 23, except with constant flux boundary conditions.

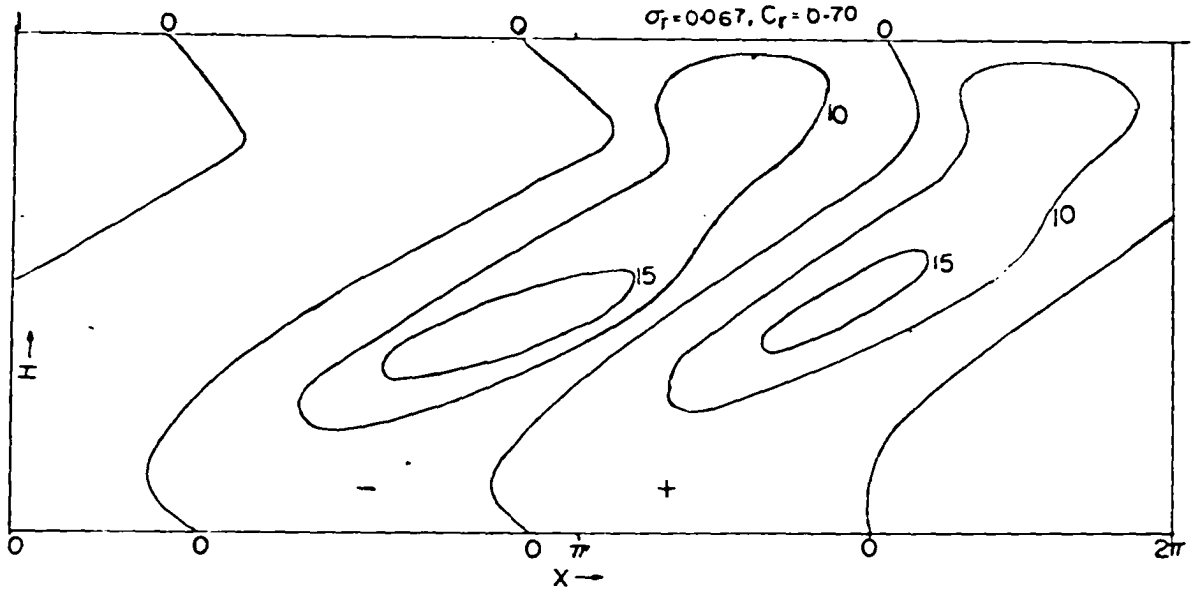

Fig. 25a. Typical structure of w-perturbations of transverse mode for Ri = 1.0, k = 2.0, with constant heat flux boundaries.

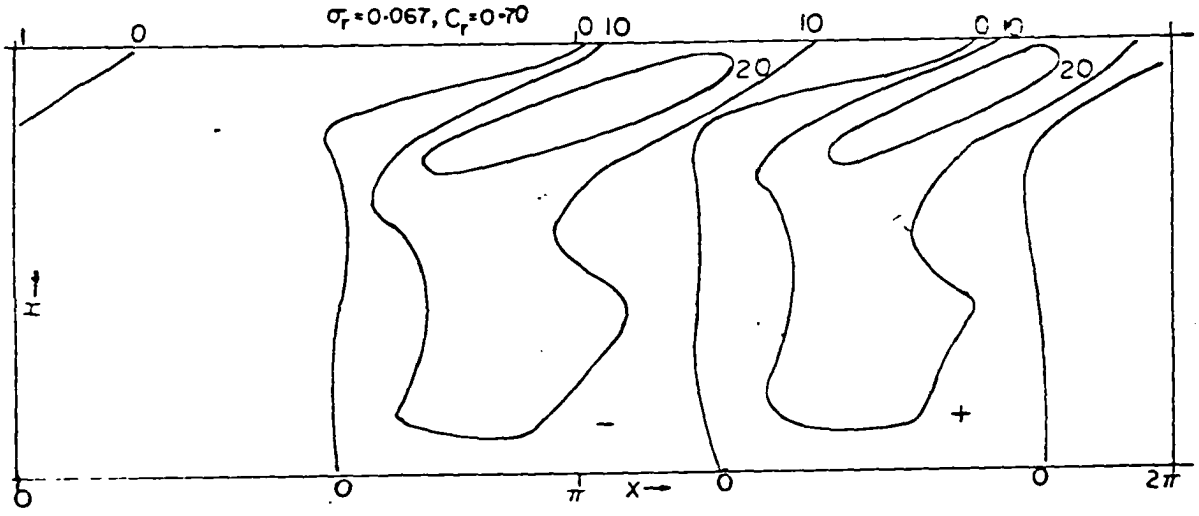

Fig. 25b. Same as above for temperature perturbations.

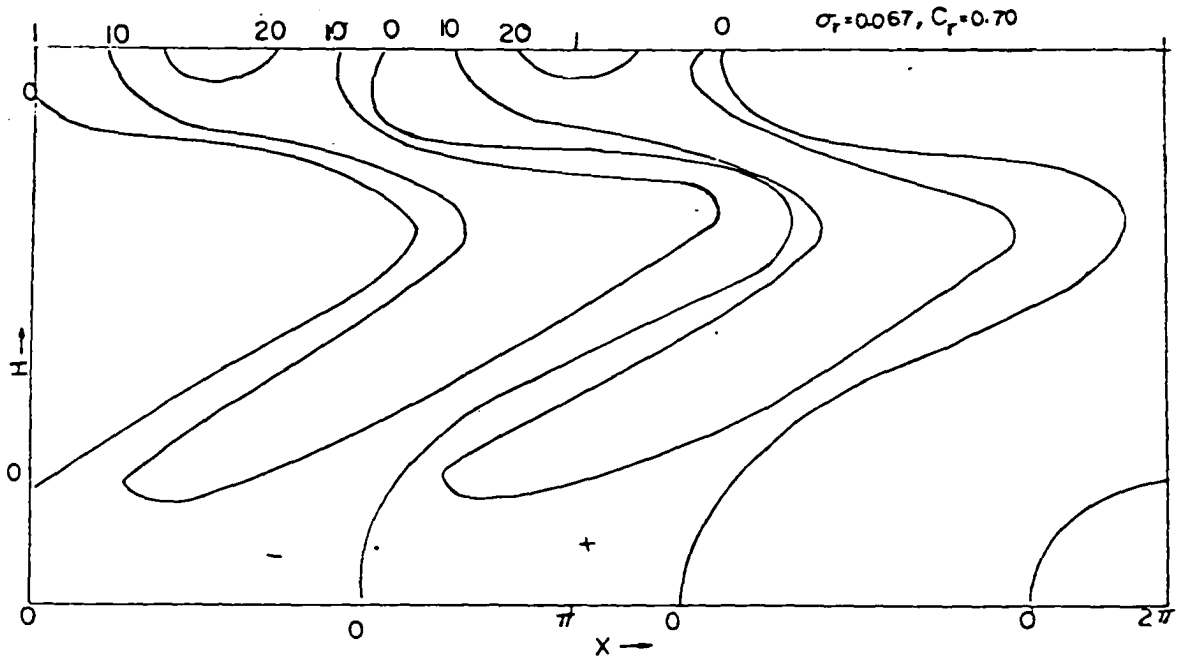

Fig. 25c. Same as Fig. 25a for horizontal u-component of perturbations.

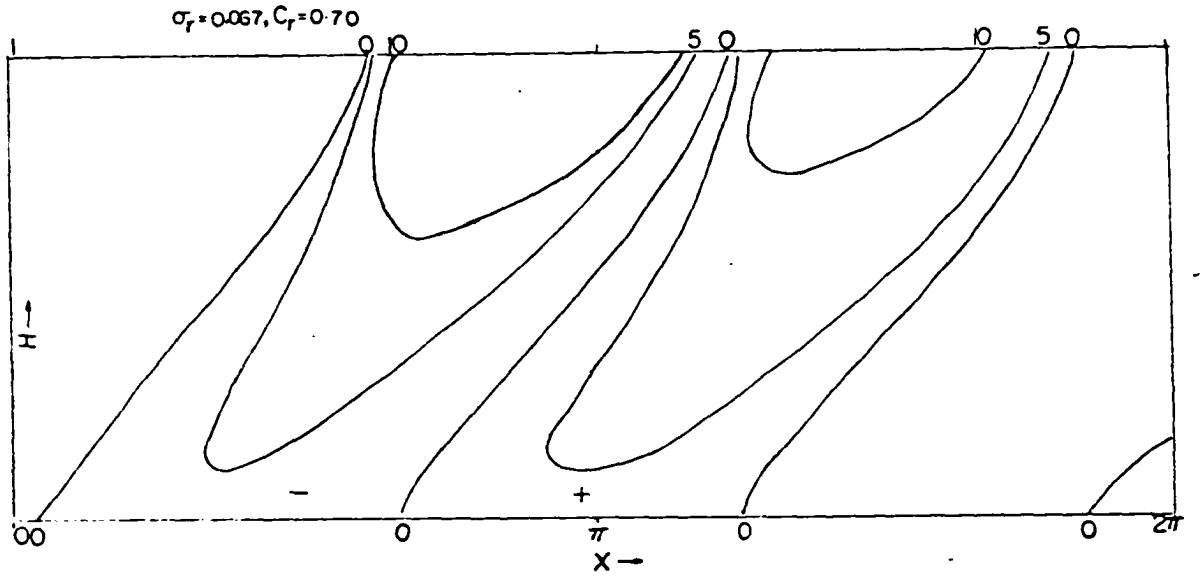

Fig. 25d. Same as above for v-component of perturbations.

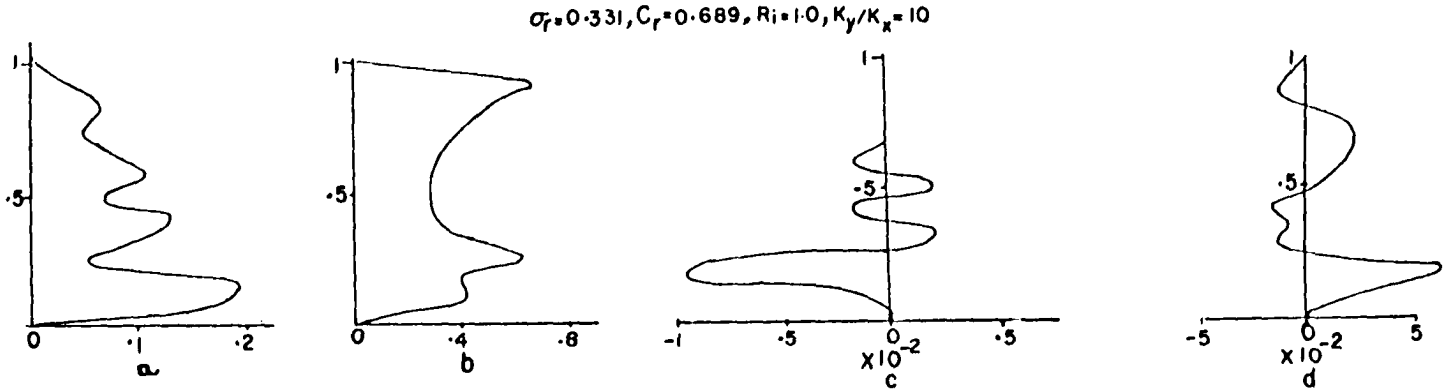

Fig. 26. Vertical profiles of amplitude of (a) vertical velocity (w), (b) temperature (θ), (c) transport of horizontal momentum (uw), and (d) heat (θw) for longitudinal mode with conducting boundaries.

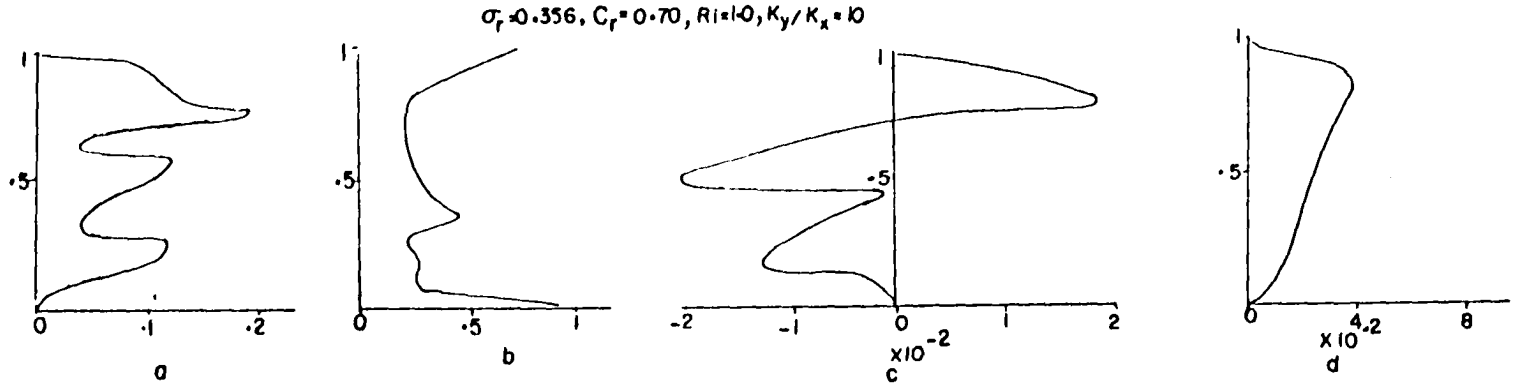

Fig. 27. Same as Fig. 26 with constant heat flux boundaries.

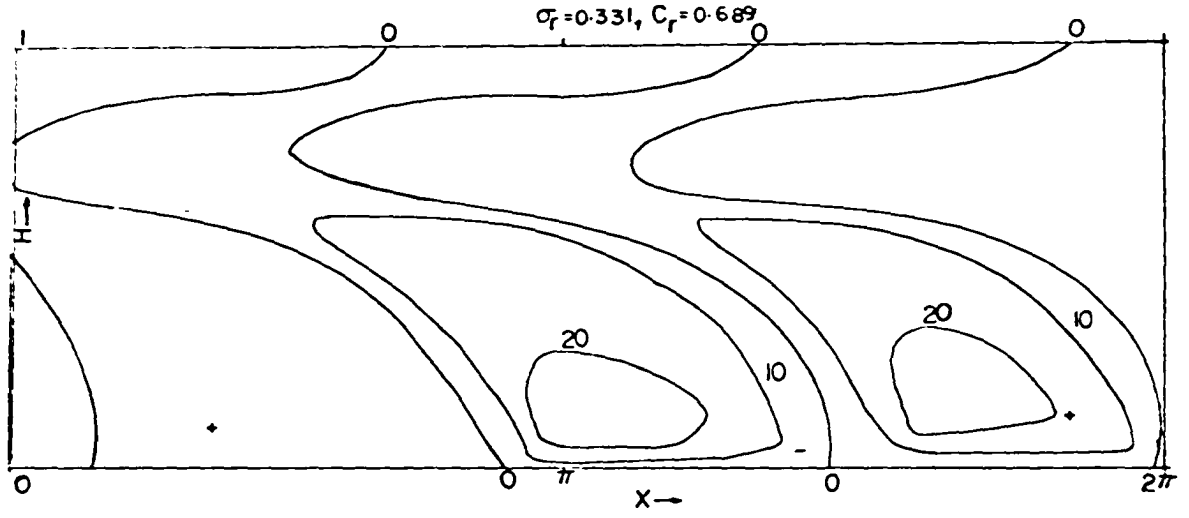

Fig. 28a. Typical structure of vertical velocity (W) perturbations for longitudinal mode with Ri = 1.0, k = 2.0 and conducting boundaries.

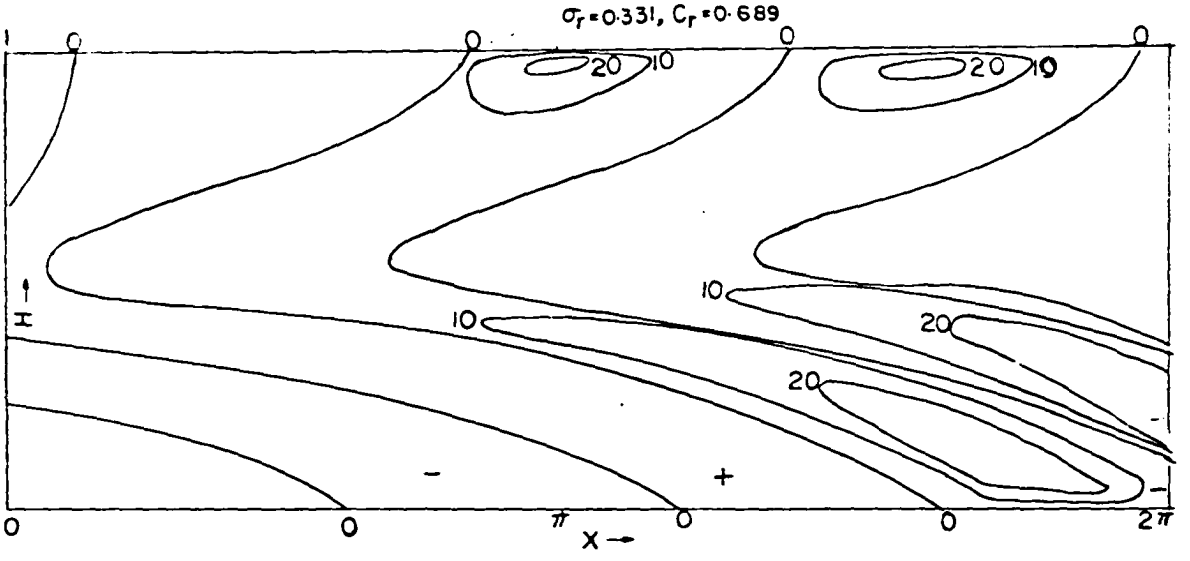

Fig. 28b. Same as Fig. 28a for temperature perturbations.

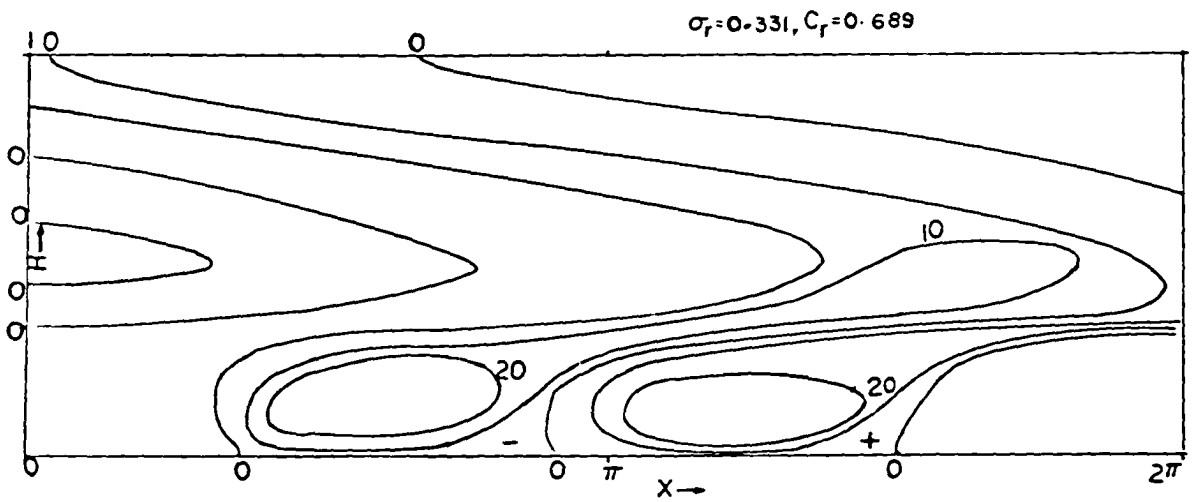

Fig. 28c. Same as Fig. 28a for the horizontal component of velocity u.